TETHER DYNAMICS SOFTWARE REVIEW

HIGH RESOLUTION TETHER DYNAMICS STUDIES

ADVANCED TETHER APPLICATIONS

INVESTIGATION OF ELECTRODYNAMIC STABILIZATION AND CONTROL OF LONG ORBITING TETHERS

Contract NAS8-35036

Final Report

For the period 13 September 1982 through 12 September 1983

Principal Investigator

Dr. Giuseppe Colombo
SAO Visiting Scientist, University of Padova
Padova, Italy

Co-Investigator

Mr. David Arnold

January 1984

Prepared for

National Aeronautics and Space Administration
George C. Marshall Space Flight Center
Marshall Space Flight Center, Alabama 35812

Smithsonian Institution
Astrophysical Observatory
Cambridge, Massachusetts 02138

The Smithsonian Astrophysical Observatory
is a member of the
Harvard-Smithsonian Center for Astrophysics

(NASA-CR-170972) INVESTIGATION OF ELECTRODYNAMIC STABILIZATION AND CONTROL OF LONG ORBITING TETHERS Final Report, 13 Sep. 1982 - 12 Sep. 1983 (Smithsonian Astrophysical Observatory) 159 p

N84-17251

Unclas
G3/18 18373

TETHER DYNAMICS SOFTWARE REVIEW

HIGH RESOLUTION TETHER DYNAMICS STUDIES

ADVANCED TETHER APPLICATIONS

INVESTIGATION OF ELECTRODYNAMIC STABILIZATION AND CONTROL OF LONG ORBITING TETHERS

Contract NAS8-35036

Final Report

For the period 13 September 1982 through 12 September 1983

Principal Investigator

Dr. Giuseppe Colombo
SAO Visiting Scientist, University of Padova
Padova, Italy

Co-Investigator

Mr. David Arnold

January 1984

Prepared for

National Aeronautics and Space Administration
George C. Marshall Space Flight Center
Marshall Space Flight Center, Alabama 35812

Smithsonian Institution
Astrophysical Observatory
Cambridge, Massachusetts 02138

Table of Contents

TABLE OF CONTENTS

ABSTRACT

This is the final report submitted by SAO under contract NAS8-35036, "Investigation of Electrodynamic Stabilization and Control of Long Orbiting Tethers," and covers the period 13 September 1982 through 12 September 1983. It details the results of research undertaken by SAO on three topics under the general area of the dynamics of spaceborne tethers:

1) SAO reviewed existing dynamics models and software and made recommendations for future software development.

2) SAO developed a computationally efficient high-resolution tether model and performed studies of the dynamic behavior of a broken tether.

3) SAO studied three advanced applications of the tether:
   a) Damping of longitudinal tether oscillations by means of a reel motor control algorithm and use of the technique in a payload orbital transfer problem,
   b) Payload acquisition by a Space Station,
   c) Orbital pumping.

The authors of this report are Dr. Giuseppe Colombo, Principal Investigator; Mr. David A. Arnold and Dr. Gordon E. Gullahorn, Analysts; and Mr. Richard S. Taylor, Program Manager. Mr. Arnold was also a Co-Investigator.

Dr. Colombo is a Visiting Scientist at SAO from the University of Padova, Italy.

LIST OF FIGURES

Figure 4-7. The final configurations of three separate runs are plotted side-by-side. The physical situation modeled in each run is the same (as in Figure 4-4). The tether is divided into 30 segments in each case. Each run is for 60 seconds. The three cases differ only in that after an initial partition of the tether was computed, the individual segment lengths were varied by small random amounts in the range -2% to 2%. The lengths were then normalized to give the same total length in all cases: (a) shows the configurations after 40 seconds; and (b) shows the configurations after the full 60 seconds. See the remarks in the text for cautions on the interpretation of detail in the figures.

Figure 4-8. Part (a) shows the evolution of one of the cases used in Figure 4-7, while (b) shows a similar case in which the tether was more evenly segmented resulting in less resolution near the boom tip. Note the distinctly different behavior of the two cases. In (a), a travelling wave was generated, while (b) exhibited no such wave. This same distinction is seen between Figures 4-5(a) and (b) and Figures 4-5 (c), (d), and (e). The finer resolution results are more consistent among themselves and probably closer to the real behavior of the tether.

Figure 5-1. Behavior of the roots of the characteristic equation for fixed values of $\tilde{\kappa}$. Note that we plot the negative of the real part of each root (pairs of complex roots are indicated by a dashed line) and that for $\tilde{\kappa}, \tilde{\beta} > 0$ all roots have negative real parts (i.e. the system is stable). The quantity of greatest interest is the lower line at each value of $\tilde{\beta}$. This root governs the solution which decays least rapidly, and we want to choose parameters $\tilde{\kappa}, \tilde{\beta}$ to optimize this worst solution. In choosing actual parameters $\tilde{\kappa}, \tilde{\beta}$ we may not achieve the desired dimensionless parameters, so there is the additional constraint of robustness; slight errors in the parameters should not lead to large decreases in performance.

Figure 5-2. Tension vs. time for a release study (100-ton Shuttle, 9.5-ton payload, 0.5-ton teleoperator, and an 80-km length of 0.3-cm Kevlar tether) in which the tether is reeled out first to relieve tension. The maneuver is given by (deployed length) = 80 km + A[1-cos(2πt/P)], with amplitude A = -650 meters, period P = 209 sec. After 1/2 period, the deployed length is held constant. The payload is released at 85 seconds.

Figure 5-3. Tension vs. time for a release study in which all parameters are the same as in Figure 5-2 except that at t = 100 sec the sinusoidal maneuver is terminated (held constant) and the active damping control law is initiated (parameters $T_0 = 1.8 \times 10^5$ dynes; $\kappa = 1.6 \times 10^{-5}$ cm-sec^{-1} dynes^{-1}; $\beta = 0.041$ sec^{-1}).

Figure 5-4. Tension oscillations after payload release, with no damping. A reel-in/reel-out sine-law maneuver was used prior to release with amplitude 176 meters, period 114 seconds, phase offset $-\pi/2$. The maneuver terminated at 114 seconds and release was at 117 seconds. We plot only from t = 105 seconds. System: 80-km tether of 0.3-cm Kevlar; 100-metric-ton Shuttle; 9.5-ton payload; 0.5-ton remaining teleoperator.

Figure 5-5. Tension oscillations after release, with active damping. The system and pre-release maneuver are the same as for Figure 5-4, and the damper started at release, t = 117 seconds. Damper parameters: $T_o = 2.86 \times 10^7 \times 10^8$ dynes, $K = 1.6 \times 10^{-5}$ cm sec^{-1} dyne^{-1}, $\beta = 0.041$ sec^{-1}.

Figure 5-6. The same as Figure 5-5, except that the damper parameter K and β are 75% greater. The response is not significantly altered.

Figure 5-7. The same as Figure 5-5, except that the damper's nominal tension T_o is 63% of that used in Figure 5-5. This figure and Figure 5-6 above illustrate the robustness of the damper algorithm; its success does not depend on choosing optimized parameters.

Figure 5-8. Tension variation with a pure reel-out pre-release maneuver and active damping after release. Note that the initial tension increase is avoided. The system configuration is as in Figure 5-4. The pre-release sine-law maneuver had an amplitude of 406 meters, a period of 200 seconds, and a phase offset of $-\pi/2$. Release is at 70 seconds, and the maneuver terminates at 100 seconds ($P/2$). Active damping begins at release with parameters $T_o = 2.86 \times 10^7$ dynes, $K = 1.6 \times 10^{-5}$ cm sec^{-1} dynes^{-1}, $\beta = 0.041$ sec^{-1}.

Figure 5-9. Tether deployed length as a function of time. Components due to sinusoid reel-out maneuver and active damping response shown separately.

Figure 5-10. Reel velocity as a function of time. Components due to the sinusoid reel-out maneuver and active damping response shown separately.

Figure 5-11. Tether tension from the initially deployed configuration (t = 0) through the release and damping (t =1441) until t = 2000 seconds. The detailed mission profile is described in the text.

Figure 5-12. For the case in Figure 5-11, the side-view (in-plane vs. radial components) of the system is plotted at 10-second intervals. Each view is arbitrarily displaced in the in-plane direction to avoid overlap, the earliest configurations being at the left. The components are relative to the Shuttle, and uniformly spaced constant vectors have been subtracted from each mass's position (effectively "cutting out" a portion of tether) to expand the resolution in the radial direction.

Figure 5-13. The tether tension is plotted near the time of release, with an expanded time scale. The pre-release maneuver and active damping are more readily seen.

Figure 5-14. A schematic view of the various orbits discussed in the text. The heavily drawn portions represent actual trajectories.

Figure 5-15. λ vs. δ. λ is computed from the equation $[1-\lambda]^3[1-(\lambda+\delta)/2]=1-\delta$ for the parameter δ with range 0 to 1. λ is the scaled tether length (L/R) and δ is the similarly scaled difference in height between the station orbit and the payload parking orbit. The ratio of the actual solution λ to the first-order approximation $\delta/7$ is plotted.

Figure 5-16. Tether tension vs. time for a case in which the payload is acquired with no other maneuver or damping. The system (1000-metric-ton Space Station, 0.5-ton teleoperator, 44 km of 0.3-cm diameter Kevlar tether) was initially in equilibrium in a 500-km circular orbit, with the tether deployed downward. A 9.5-ton payload was acquired with zero relative velocity (payload delivery orbit, 200 to 456 km) at t = 10 sec. Note the oscillation with period about 185 sec.

Figure 5-17. Tension vs. time for a case similar to Figure 5-16, except that the active damping mechanism is turned on at acquisition. Damping parameters: $T_{o1} = 1.6 \times 10^8$ dynes, $K = 2.66 \times 10^{-6}$ cm dynes^{-1} sec^{-1}, $\beta = 0.012$ sec^{-1}.

Figure 5-18. Tension vs. time and radial vs. in-plane behavior for the case shown in Figure 5-17, plotted with an expanded time scale for comparison with future runs and with an acquisition time of t = 10 sec. (a) Tension vs. time. (b) A series of radial vs. in-plane plots of the tether system. The successive plots are at two-second intervals, the same as the plotted points in (a), and the station position is arbitrarily shifted to the right at each interval so that the horizontal axis is also, effectively, a time axis with the same scale as (a). A constant (in time) vector is subtracted from the position of each mass to emphasize the displacements. The vectors (one for each mass) are such that at t = 0 the spacing between masses is 1/2 km.

Figure 5-19. Post-acquisition tension variations are reduced by turning on the active damper at t = 0 and delaying acquisition until t = 9 seconds.

Figure 5-20. Tension vs. time when the payload is not acquired until 20 seconds after the damper is started (at t = 5 seconds). The tension had already begun to decrease when acquisition occurred and went slack at t = 31 seconds. (Note the expanded time scale in this plot.)

Figure 5-21. Plots, for the case in Figure 5-18, but with acquisition occurring with a 3 meter/sec relative velocity in the in-plane direction along the orbit. (a) Tension vs. time. (b) Radial vs. in-plane behavior.

Figure 5-22. As for Figure 5-21, except that the velocity is in the out-of-orbit plane direction. (a) Tension vs. time. (b) Radial vs. in-plane behavior. (c) Radial vs. out-of-plane behavior.

Figure 5-23. As for Figure 5-21, except that the velocity is radial, directed away from the station (downward). (a) Tension vs. time, note the tension variation is greater than the other cases. (b) Radial vs. in-plane behavior.

Figure 5-24. As for Figure 5-21, except that the velocity is radial, directed toward the station (upward). (a) Tension vs. time. Note that the tether segment nearest the payload goes briefly slack. This may be an artifact of the lumped-mass model. (b) Radial vs. in-plane behavior, the dashed lines indicate slack tether segments.

Figure 5-25. Co-ordinate relationship in dumbbell configuration used in orbital pumping study.

Figure 5-26. A rough plannar sketch of the orientation of Mercury's axis of minimum moment of inertia, at different points along its orbit, given that the rotational period is two-thirds of the orbital period and that this axis is aligned with the Sun-planet vector at perihelion.

Figure 5-27. Orbital transfer from GEO to LEO of a dumbbell OTV. Initially, the system may synchronize in a 9:1 resonance due to spin orbital coupling as shown. During the decay, or even from the beginning if the characteristics of the dumbbell and initial conditions are correct, the dumbbell may low order resonances - 8.5:1, 8:1,-------1:1. It will finally synchronize in the 1:1 spin orbital coupling in the final LEO orbit where the retrieval to compact configuration will be performed.

Figure 5-28. Vector relationships.

Figure 5-29. Spacecraft configurations for orbital pumping.

Figure 5-30. Eccentricity of the center-of-mass orbit vs. the orbital phase (true anomaly/2π). A critically damped dumbbell configuration, with oscillatory frequency tuned to the orbit, is allowed to evolve, converting orbital energy to internal (e.g. thermal) energy, circularizing the orbit. The numerical simulation was made with SKYHOOK.

Figure 5-31(a). Tether length vs. orbital phase for one particular orbit of the study shown in Figure 5-30. (b) The derivative of the curve shown in (a), together with the gravity gradient forcing function. These are nearly in phase and their product (the work done by the orbit on the dumbbell) is nearly maximal. (c) A plot similar to (b) for a case with zero time lag in tether response. The work is shown as well, and obviously integrates to zero over an orbit.

1.0 INTRODUCTION

The work carried out under this contract covered a diverse group of topics under the general heading of the study of the dynamics of spaceborne tethers. SAO has been working in this area for almost ten years under internal and NASA sponsorship. This effort was directed at identifying the state-of-the-art in tether modelling among participants in the Tethered Satellite System (TSS) Program, extending the state-of-the-art to model the slack tether and study its behavior, and studying certain advanced applications of the tether to problems in orbital mechanics.

This report was assembled primarily from the monthly reports submitted under this contract, although much new material is included, particularly in the sections on high-resolution modelling of the tether and advanced applications. Section 2.0 summarizes the results of this study.

Section 3.0 encompasses the review of the features and applications of the TSS software set. Software status is as reported to SAO in March 1983.

The dynamics of the tether itself has traditionally been studied by modelling the tether as a series of interacting lumped masses connected by springs and dampers. The resulting equations of motion are integrated using standard software routines such as the Gear integrator used in SKYHOOK. This approach, although mathematically rigorous, is computationally slow and of relatively limited resolution, typically 10-20 mass points. Section 4.0 describes the successful SAO effort to move beyond these limitations by modelling

the slack tether analytically with as many as 50 mass points and the application of this new model to a study of the behavior of a broken tether near the Shuttle.

Longitudinal oscillations can occur in the tether from a variety of causes, including control reel maneuvers and thruster operations. Proper use of the control reel can damp these oscillations efficiently without adding additional hardware to the system. Section 5.1 describes such a reel control algorithm developed by SAO and gives examples of its use, including an example (in Section 5.2) which also demonstrates the use of the tether in transferring a heavy payload from a low-orbiting Shuttle to a high circular orbit.

Capture of a low-orbiting payload by a Space Station in high circular orbit is described in Section 5.3.

Finally, we show that in some cases it is possible seemingly to "pull oneself up by one's own bootstraps." Section 5.4 shows how energy transfers within a "dumbbell"-type spacecraft by cyclical reeling operations or gravitational effects on the natural elasticity of the connecting tether can circularize the orbit of the spacecraft.

2.0 SUMMARY CONCLUSION AND RESULTS

One-page summaries of conclusions and results are presented in this section for each study topic covered by this report.

2.1 Review of Tether Dynamics Software

19 different tether models are in use; 7 using angle variables 12 using a finite element approach.

Little commonality of hardware and software was found among the models although modelling approaches are often similar.

Angle variable models are used for long term studies, such as control law development; finite element models address the dynamics of the tether itself.

Only TETHER REEL (MMC), "Tethered Satellite" (CDC), and SKYHOOK (SAO) model, the dynamic behavior of the entire Subsatellite/Tether/Shuttle System.

Only SKYHOOK models the dynamic behavior of entire tether system, including its electrodynamic and thermal behavior.

Improvements in software computational efficiency, particularly in modelling the slack tether, will be necessary to meet anticipated real-time simulation and safety study requirements.

New software should be developed with transferability in mind, although there is no compelling reason all software need be transferable.

2.2 Hi-Resolution Study of Tether Behavior Near Orbiter

An efficient two-dimensional analytic model of the slack tether called "SLACK2" was developed under this contract with 50+ mass point resolution.

SLACK2 includes a realistic deployment boom model and the major external forces, the gravity gradient force, air drag, and the Coriolis force. It runs about 100 times faster than SKYHOOK under similar conditions.

The tether break study yielded results similar to SKYHOOK runs, but the higher (2-3m) resolution provided new insight into the behavior of a broken tether.

Deployment boom oscillations add energy and oscillations to tether motion after break.

2.3 Study of Advanced Uses of the Tether

2.3.1 Algorithm for Damping Tether Longitudinal Oscillations

Operation depends only upon measurement of tether tension and deployed length.

"Damper" fully controls tension oscillations within a few cycles after release of a heavy payload using reel-in/reel-out deployment maneuver.

Algorithm is "robust" with regard to parameter sensitivity.

Algorithm allows deployment of payload using a pure reel-out maneuver which limits tether tension to pre-release value.

2.3 Study of Advanced Uses of the Tether

2.3.2 Payload Transfer to Circular Orbit

A 9.5-ton payload was deployed from a 100 ton Shuttle using a 61-km tether of 3-mm Kevlar and the reel-out maneuver and algorithm described in Section 5.1.

Initial Orbit

Perigee: 199km

Apogee: 519 km

Eccentricity: 0.0237

Final Payload Orbit

Altitude: 575 km

Eccentricity: 0.00017

Final Shuttle Orbit

Perigee: 165 km

Apogee: 514 km

Tether tension was always less than stable deployment tension and never zero.

2.3 Study of Advanced Uses of the Tether

2.3.3 Payload Acquisition by a Tether Deployed from a Space Station

A 9.5-ton payload was acquired by a 100-ton Space Station using a 44-km length of 3-mm Kevlar and the damping algorithm of Section 5.1.

Initial Space Station Orbit

Aititude: 500 km Circular

Initial Payload Orbit

Perigee: 220 km

Apogee: 456 km

Acquisition is stable and relatively insensitive to velocity mismatch between payload and tethered teleoperator.

2.3 Study of Advanced Uses of the Tether

2.3.4 Orbital Pumping

Dumbbell-type tethered spacecraft placed in elliptical orbits will self-circularize the orbit due to tidal forces acting on the spacecraft and or due to deliberate reeling operations on the tether.

Applications of this pumping technique include self-circularization of an OTV orbit at low altitude and geostationary capture of a satellite from a high-eccentricity orbit.

Energy may actually be recovered as electrical power in transferring a spacecraft from LEO to GEO using tides developed in the spacecraft system by the Earth's gravity gradient.

3.0 REVIEW OF TETHER DYNAMICS SOFTWARE

3.1 Method of Software Review

SAO solicited data from Tethered Satellite System (TSS) program participants on their tether dynamics models, programming languages, computers, displays, and non-standard support software requirements.

Responses were received from all program participants: Aeritalia (AIT), Torino, Italy; Control Dynamics Company (CDC), Huntsville, AL; Johnson Space Center (JSC),Houston, TX; Martin Marietta Corporation (MMC), Denver, CO; Marshall Space Flight Center (MSFC), Huntsville, AL; University of Padova, Padova, Italy; and Smithsonian Astrophysical Observatory (SAO), Cambridge, MA. These were reviewed by SAO and the results of the review and summarized in an applications matrix and in the text below. We also comment on the issue of software compatibility, outline potential tether dynamics study topics, and make recommendations for software development.

3.2 Summary Descriptions of Tether Dynamics Software

Appendix I contains the completed questionnaires as received by SAO and a complete list of the respondees. Here the features of each of the models is summarized from data provided on the questionnaires.

3.2.1 Aeritalia Tether Dynamics Software

Aeritalia runs three tether dynamics programs: ASSETTO, POSI, and BALLAST. All model the three-dimensional behavior of the tether; ASSETTO adds the three Euler angles of the subsatellite. All assume that the Shuttle has infinite mass and that the tether is straight and

inelastic with distributed mass. Atmospheric drag is modelled, Shuttle out-of-plane delta-V can be applied, and arbitrary control laws can be used. Orbits can be circular or low eccentric. Tether and subsatellite mass variations can be accommodated.

POSI models the subsatellite and Shuttle as point masses and includes a movable boom. The three second-order differential equations in the model are numerically integrated by a fourth order Runge-Kutta integrator with variable step size or by a predictor/corrector integrator. In the case of rate tether control laws, the equations related to tether speed and acceleration are removed and the remaining equations are integrated. All effects related to the elasticity and flexibility of the tether are neglected and the Shuttle orbit is unperturbed in the analysis.

ASSETTO adds to POSI the three Euler angles of the subsatellite to model its rigid body rotation. It also includes the diagonal inertial tensor of the subsatellite and can handle misaligned subsatellite thrusters. The subsatellite attitude does not affect the position of the tether, an acceptable assumption for subsatellite diameters small in relation to the length of the tether.

BALLAST is a double pendulum model (equivalent to a three-mass model) which allows four different physical systems to be simulated: double tethers (satellite deployed from the subsatellite), two-section tethers, a subsatellite with variable attitude, and a tether/subsatellite system with a moveable boom. Two different mathematical models are used. The first allows control of the primary tether; the second, control of the secondary tether. The systems are

first solved with respect to the second derivatives then numerically integrated. Instantaneous control of only one tether at a time is possible. Transverse and longitudinal wave propagation effects were neglected.

3.2.2 Computer Dynamics Company (CDC) Tether Dynamics Software

CDC uses a modal representation of the wire and models the Shuttle and subsatellite as point end masses. The disturbances modelled include: 1) Gravity terms using a non-spherical earth model and third-body perturbations; 2) Aerodynamic terms using various optional density models, including the Jacchia model; 3) Solar radiation pressure; 4)Tether bending stiffness; and 5) Thrust maneuvers by either end body. The dynamics of the tether is modelled by partial differential equations which are solved by conversion to finite difference equations with a selectable number of nodes. The equations are integrated using a 7(8) Runge-Kutta-Felberg variable-step size scheme. Rigid body motion of the Shuttle and/or the subsatellite are not currently included. Only open loop thrust maneuvers are allowed. No deployment boom or mechanism is modelled at present. Modifications to correct these deficiencies are expected to be complete by the end of May 1983.

3.2.3 Johnson Space Center Computer Dynamics Software

PMG (Plasma Motor-Generator) models the tether as a continuous cable with mass and internal moments of inertia. The D1 (PMG-D1) version currently in use is a preliminary version. Two-dimensional dynamics are provided using a constant (specified) length tether operating under variable I X B forces with constant (specified) values

for the magnetic field, gravity, and an arbitrary net force vector which is the vector sum of any other force terms such as atmospheric drag, radiation pressure, and induced electric forces. Specified terms may be varied from an external program to match an assumed or calculated reference orbit, to include unique conditions, or to include thrust or drag current inputs. The dynamic model is developed for application on a hybrid (digital/analog) computer system. The current (interim) version is discretized for a finite element solution on a digital system using a backward Euler integration package by Hindmarsh. This version is cumbersome for changes to the input values and is restricted to constant length and in-plane (2D) dynamics.

3.2.4 Martin Marietta Corporation Tether Dynamics Software

Martin Marietta runs three tether dynamics programs: TSSONE, TETHR, and REEL.

TSSONE models the subsatellite as a point mass connected to the Shuttle by a straight, inextensionable tether. The Shuttle and deployment boom are considered as point masses constrained to the defined orbit plane. Numerical integration is used with prescribed initial conditions to develop time histories of motion of the subsatellite and other data. The model includes atmospheric drag effects, gravity gradient torques, and may include in-line, in-plane, and out-of-plane thruster effects. Numerical integration is via the Runge technique. The Gauss quadrature approach is used to establish atmospheric drag effects.

TETHR models the three-dimensional motion of the system using a lumped mass model ("bead" model in MMC terms). The co-ordinate system rotates with the orbit. Integration is by a relaxation method in which mass point positions are propagated independently relative to the center-of-gravity of the Shuttle-Tether-Subsatellite system in short time steps; they are not simultaneously integrated. This approach relies on damping within the tether to achieve stability. If the damping is too low, the integration "blows up." In exchange for the damping requirement, relatively fast integration times are achieved. Inherent in the relaxation method is that it works better with a more elastic tether, worse with a stiff tether. The integration time step must be decreased as as stiffness increases. For typical values of stiffness, a fairly large (on the order of seconds) time step may be used. Typical run times with six mass points on the CDC Cyber 750 computer were 100 times faster than real time. TETHR uses a spherical gravity model although a non-spherical model could be easily added. It includes an elastic tether representation with hysteresis data derived from tether test data. Air drag, including angle-of-attack, can be modelled. It handles tether "breaks" but not rotation of the end masses.

REEL is a development of TETHR. In addition to the features of TETHR, this model simulates tether reel-in and reel-out and allows input of a control law to regulate the reeling process. This program was not fully verified at the time of writing although reel-in/reel-out had been successfully achieved. For reel-in/reel-out, the mass points are "restrung" at appropriate intervals to maintain accuracy. Re-stringing and tether cut are

mutually exclusive in a given run.

3.2.5 Marshall Space Flight Center Tether Dynamics Software

Marshall Space Flight Center presently runs four tether dynamics programs: TETHER, TETHER-PD, SKYHOOK (Formation Flying), and SKYHOOK (Tether Configurations). The two SKYHOOK programs are derivatives of the SAO SKYHOOK program discussed further on in this section of the report.

TETHER simulates the system with the satellite considered as a point mass connected to the Shuttle by a tether which has mass and which is extensible. Disturbances modelled include the spherical gravitational field, aerodynamic drag with an exponential rotating atmosphere, and longitudinal vibration of the tether. Numerical integration of the differential equations is by a fourth-order fixed step size Runge-Kutta integrator. The current version does not include modelling of a deployment boom nor satellite thrusters. Changes to incorporate these features are expected in the near future.

TETHER-PD is a two-mass-point model which simulates subsatellite trajectories in three dimensions. It assumes a circular orbit and incorporates a deployment boom oriented along the local vertical. The tether is modelled as a massless inelastic wire; no end mass rotation nor atmospheric drag is included in the simulation. Retrieval of the subsatellite is modelled by a control law which includes a tether retrieval rate limit, tether angle and angle rate thruster control law, and which has the tension control gain adjusted for short tethers. Integration of the equations of motion is by a fixed step size trapezoidal integrator. MSFC describes this program as a fast,

simple simulator of satellite trajectories which is the work horse for studying control laws , satellite impulse requirements, and gross system characteristics.

SKYHOOK (Formation Flying) uses the same environmental model as SAO SKYHOOK which is described below. The tether model was changed to permit individual mass elements (subsatellites) to be in separate orbits with state vectors referenced to a main spacecraft (i.e., a Space Station). Additional program changes were made to allow the program to run on a UNIVAC computer.

SKYHOOK (Constellation) is the same as SAO SKYHOOK with minor changes to update tether system configuration and control laws. It too has been adapted to run on a UNIVAC machine.

3.2.6 University of Padova (Italy) Tether Dynamics Software

The University of Padova runs the original version of SAO SKYHOOK modified to provide polar coordinate output and to accept Shuttle orbital element variations. It does not include the SAO electrodynamics package.

3.2.7 Smithsonian Astrophysical Observatory Tether Dynamics Software

SAO runs a variety of general purpose and specialized tether dynamics models, integrators, data processors, and display programs.

SKYHOOK models the tether as an N-mass point system where N is at most twenty in the present software. A ten mass point model runs in approximately real time. Each mass point has the physical

characteristics of a finite length tether segment and mass point interactions are determined by a set of coupled differential equations which are numerically integrated to determine the behavior of the system. There are no restrictions on mechanical, thermal, electrical, or bulk characteristics of any tether segment nor are there any restrictions on the initial conditions representing eccentricity or orientation of the Shuttle orbit. SKYHOOK models all potential physical and dynamical effects on the tether/subsatellite/Shuttle system. The numerical integration is done in Cartesian co-ordinates. Rotation of the subsatellite was added in a recent upgrading of the software.

DUMBEL models the tether system as a massless elastic wire with two end masses. It includes position, velocity, and rotation of the subsatellite in the integration variables. Numerical integration is done in Cartesian co-ordinates. DUMBEL also computes initial state vectors as a function of orbital and tether system parameters. Wire mass points, and their initial conditions, can also be generated along the wire to set up initial conditions for SKYHOOK.

STABLE models the tether as a rigid massless rod. It assumes that the Shuttle is in a circular orbit and integrates the in-plane angle, out-of-plane angle, distance to the subsatellite, and the rate of change of each as a function of time. The velocity of the subsatellite can be replaced by a rate control law.

WAVES is a "many" mass point model of the tether which integrates only the radial variable with no gravity field and, hence, runs very quickly even with large numbers of mass points. It has been run with

as many as 40 mass points and is typically used in special case studies to verify or to form a basis for studies with other software.

SLACK2 is a multi-mass point free-space model of the tether for studying the behavior of a slack tether with exceptionally high resolution and with high computational speed. Mass points can be arbitrarily distributed along the wire and concentrated in areas of interest. As many as 50 mass points have been used in recent studies with this model but expansion to 100 or more mass points appear to be straightforward. It runs 50 to 100 times faster than SKYHOOK in equivalent simulations. The model assumes that the center of mass of the tethered system is in circular orbit and that the co-ordinate system rotates with it. Gravity gradient, Coriolis, and air drag forces are included. It is presently written in two-dimensions; extension to the third dimension is not difficult. Forcing equations have been linearized (expanded in the first order in the small quantities x/R and y/R where x and y are the co-ordinates of the orbit center and R is the orbital radius.

GRAPH, PLOTFIL, PLOTFIL2, INIT, CRUNCH7, and CRUNCH9 are routines used with each of the SAO tether dynamics programs to process and display data.

3.3 Tether Dynamics Software Applications Matrix

3.3.1 Tether Dynamics Software Applications Areas

Potential applications of the tether dynamics software set are listed across the top of the Applications Matrix (Figure 3-1). The matrix identifies those application areas considered most suitable by SAO for each program described in the questionnaires. Topics of interest within each of these areas are described below.

Safety Studies:

The behavior of tether after a break, reel jam, or various control system failure modes, as well as the development of methods for dealing with such situations, are included in this category. Among the results of such studies would be appropriate Shuttle avoidance maneuvers, the specification of tether oscillation damping algorithms for the control reel, the design of tension wave shock dampers for the subsatellite, and the development of "safe operating area" curves for the deployment, retrieval, and station-keeping mission phases. Such curves would identify the safe limits of tether velocity and departure angles as a function of orbital altitude, tether break strength, tether deployed length, subsatellite mass, subsatellite thruster activity, STS mission safety requirements, and other such applicable parameters and requirements.

ORGANIZATION	PROGRAM NAME	PROGRAM TYPE: ANGLE VARIABLES	PROGRAM TYPE: FINITE ELEMENT	SAFETY STUDIES	ORBITER DYNAMICS	SUBSATELLITE STUDIES: DYNAMICS	SUBSATELLITE STUDIES: ATTITUDE CONTROL	SUBSATELLITE STUDIES: DYNAMIC NOISE	SUBSATELLITE STUDIES: DEEP ATMOSPHERE	CONTROL LAWS	TETHER MATERIALS STUDIES	ELECTRODYNAMIC STUDIES
AIT	POSI	✓		X	X	X	X	X	X	✓	X	X
	ASSETO	✓		X	X	✓	✓	X	✓	✓	X	X
	BALLAST	✓		X	X	✓	✓	X	✓	✓	X	X
CDC	TETHERED SATELLITE PROGRAM		✓	✓	✓	X	X	X	X	✓	✓	X
JSC	PLASMA MOTOR GENERATOR		✓	X	X	X	X	X	X	X	X	✓
MMC	TSSONE	✓		X	X	X	X	X	X	✓	X	X
	TETHER		✓	✓	✓	X	X	X	X	X	✓	X
	REEL		✓	✓	✓	X	X	X	X	✓	✓	X
MSFC	TETHER	✓		X	X	X	X	X	X	✓	X	X
	TETHER-PD	✓		X	X	X	X	X	X	✓	X	X
	SKYHOOK FORMATION FLYING		✓	X	X	X	X	X	X	X	X	X
	SKYHOOK TETHER CONFIGURATIONS		✓	X	X	X	X	X	X	X	X	X
PADOVA	SKYHOOK ORIGINAL VERSION		✓	✓	✓	X	X	X	X	✓	✓	X
SAO	SKYHOOK		✓	✓	✓	✓	✓	✓	✓	✓	✓	✓
	STABLE	✓		X	X	X	X	X	X	✓	X	✓
	WAVES		✓	✓	X	X	X	X	X	X	✓	X
	ZETAO		✓	X	X	X	X	X	X	X	X	X
	DUMBEL		✓	X	X	X	X	X	X	X	X	X
	SLACK2		✓	✓	X	X	X	X	X	X	✓	X

Figure 3-1. Tether Dynamics Software Applications Matrix

Orbiter Dynamics:

The Shuttle center-of-mass moves off its normal position as the tether is deployed, remains so during station keeping, and returns to its normal position as the tether is retrieved. The behavior of the Shuttle/Tether system must be accurately modelled under each of these conditions to determine the effects of Shuttle and subsatellite thruster firings and tether control operations on the behavior of the combined system and to evaluate contingency maneuvers in tether failure situations.

Subsatellite Dynamics:

Detailed study of the motion of the subsatellite while it is deployed is essential to baselining its performance as an experiment platform. These studies would determine the behavior of the deployed subsatellite under dynamic inputs from the Shuttle, tether, atmospheric drag, and the action of its own thrusters. Attitude control requirements and performance specifications could also be determined by means of these studies. The behavior of the subsatellite in the deep atmosphere is of particular interest because of the high drag level and potentially high thermal load anticipated in such a mission.

Control Law Optimization and Verification:

Control law optimization will continue to be an area of interest as the overall Shuttle/Tether system dynamics are further studied and evaluated. This area also includes passive and active retrieval studies (retrieval of a subsatellite with a failed in-line thruster is

one potential study), stabilization of the system during station keeping, and deployment and retrieval time minimization.

Tether Material Studies:

Tension wave propagation and elastic and damping properties of tether materials fall in this area of study. Modelling of real tether characteristics will be an important part of verifying the true dynamics of the tether system.

3.3.2 Comments on the Dynamic Model Set

Computer programs for studying the dynamics of tethered satellite systems fall into two main categories. In one, the Shuttle is assumed to be in a fixed orbit and the equations of motion of the subsatellite relative to the Shuttle are used to integrate the motion of the system. The position of the subsatellite is specified in a spherical coordinate system by two angles and a radius vector. The angles are the in-plane and out-of-plane deviations of the subsatellite. Since the motion of the Shuttle and the dynamics of the tether are not considered, these computer programs are computationally efficient and can be used to study the behavior over long time periods. The primary application of such programs is the study of deployment, retrieval, and station keeping. Control algorithms for the reel motor or thrusters can be developed and tested to optimize processes such as the retrieval of the subsatellite. Rigid body rotations of the Shuttle or subsatellite may also be included in the models to study attitude control. This type includes the Aeritalia and MSFC models, and TSSONE used at Martin-Marietta.

In the other approach, the tether system is represented by a discrete set of masses or segments. The motion of the discrete elements is then integrated as a function of time. This approach is more general but relatively more expensive in terms of computational time in proportion to some power (2.0 to 2.5) of the number of elements used to represent the system. It has the advantage, however, of allowing the orbital motion and dynamics of the tether itself to be studied and is the most accurate representation of the actual system. Rotation of the Shuttle or subsatellite may also be included to study attitude control. A variation of this approach is to use normal modes to describe the tether dynamics. The detail achieved depends upon how many modes are integrated. Deployment and retrieval can be studied with all these models by including control laws and a method of handling the variation in tether length. Models of this type are SKYHOOK and the CDC tethered satellite program. Program TETHR written at MMC dispenses with the matrix inversion usually required by the integration routines to achieve fast integration. However, this method is stable only if sufficient damping is included in the model, although this is only a minor constraint in many modelling situations.

Only TETHR/REEL (MMC), "Tethered Satellite" (CDC), and SKYHOOK (SAO) are capable of addressing the dynamic behavior of the tethered satellite system as a whole. Only SKYHOOK can integrate the dynamic behavior of the entire system with its electrodynamic and thermal behavior, including all potential dynamic inputs.

3.3.3 Comments on Hardware and Software Compatibility

There are few points of hardware and software commonality among tethered satellite dynamics model users and developers (See Figure 3-2). REEL (MMC), TETHER-PD (MSFC), and SKYHOOK (SAO) were specifically designed for transportability, but even these were written in two different languages, ALGOL68 and FORTRAN IV, and run on three different machines: CDC Cyber NOS-1, UNIVAC 1100, and the DEC VAX. FORTRAN IV is the most common language used; other versions of FORTRAN are next most common. Only JSC and MMC use the same computer, the UNIVAC 1100. There is no commonality among display systems. All users can handle magnetic tape for transfer of data and programs, however. Even the programs which were designed for transportability would require support from the developer to get them running elsewhere, since some reprogramming would be required to meet the requirements of different computer and display systems. SKYHOOK was successfully transferred to MSFC and the University of Padova in this manner. A SKYHOOK tape has also been sent to JSC and should be running there shortly.

Figure 3-2. Tether Dynamics Software Computer Facilities and Languages in use.

	AIT	CDC	JSC	MMC	MSFC	Padova	SAO
1. Operating Systems	Honeywell DPS-8	IBM PDP-11/23 Sigma V	UNIVAC 1100/61	CDC Cyber 750 & NOS1	Honeywell Sigma V UNIVAC 1100	CDC Cyber76	DEC VAX
2. Primary Source Code Others Used	FORTRAN 77 FORTRAN IV	FORTRAN IV	FORTRAN 77	FORTRAN V ALGOL 68	FORTRAN IV,V & ASCII	FORTRAN IV	FORTRAN IV
3. Precision Required	15 Digits Maximum	64 Bit Double Precision	7 Digits	15 Digits Maximum	64 Bit Double Precision	14 Digits	15 Digits
4. Batch or Interactive	Both	N/S	N/S	Both	Both	Both	Both
5. Data Transfer Format	Magnetic Tape	Magnetic Tape	Magnetic Tape	Magnetic Tape Punch Cards	Magnetic Tape Punch Cards	Magnetic Tape	Magnetic Tape
6. Peripherals Required	Standard Tape & Disc, TI Graphics	Terminal & Disc Drive, TI Graphics	N/S	Plotter, Stereo Graphics Plotter	Terminal	Disc Drives, Calcomp Plotter	Tape & Disc Drives, Terminal, Versatec Plotter
7. Required Pre- and Postprocessors	None	None	N/S	None	None	DUMBEL	DUMBEL
8. Other Software Required-Standard	Honeywell & IBM Math Library	FORTRAN Library	N/S	FORTRAN & ALGOL 68 Math Sets	Standard FORTRAN Routines	Standard FORTRAN Routines	DEC Math Library
-Unique	Interactive I/O Program	None	N/S	MMC/FORMA	Plotter Software	None	None
9. Optional Software	DYFSIS Integrator, Interactive Display Program	Graphics Routines	N/S	Graphics Routines	Plotter Software	N/S	None
10. Software Designed for Transportability?	No	No	No	No- (FORTRAN V) Yes- (ALGOL68)	Yes (TETHER-PD)	Yes	Yes

4.0 HIGH RESOLUTION STUDY OF TETHER BEHAVIOR NEAR ORBITER

4.1 Model Development

Under a prior contract (NAS8-33691), studies were done on the behavior of the tether under various failure modes such as jamming of the reel motor during deployment and a break at some point along the tether. Various analytic and numerical techniques were used to study the behavior under these extreme conditions. The analytic study modelling the tether as a single lump suggested that the recoil velocity after a break is independent of tether length. This result was confirmed by numerical integration under the assumption that the recoil is purely elastic with no damping losses. The numerical method used the SKYHOOK program which models the three-dimensional orbital motion of the tether by breaking it up into a series of discrete segments. The discretization procedure makes it possible to model a slack tether, however, the numerical integration becomes much slower. In order to obtain good resolution, it is necessary to have as many mass points as possible. Unfortunately the amount of computer time required rises rapidly as the number of mass points increases. The increase is partly due to the higher frequencies that exist when the wire is modelled in smaller sections. Damping can be used to eliminate the high frequencies and obtain faster integration using methods designed for stiff systems. Of course, damping suppresses all longitudinal modes along the wire and cannot be used to study longitudinal motions if the behavior is nearly elastic.

Since high resolution and high computational speed are necessary for efficient study of such failure modes, alternative methods were sought to these standard approaches. For very short pieces of wire, the motion after a break is nearly one dimensional and force free, if Coriolis and gravity gradient effects are neglected. Therefore, a one-dimensional program called WAVES was written under the previous contract to allow more economical integration with a larger number of mass points. The program was used with 40 points and the results were presented in the Interim Report to contract NAS8-33691 dated March 1982. The one-dimensional program was particularly useful in studying stress propagation and recoil velocity effects as the wire goes slack both under purely elastic conditions and with various levels of damping. Once the wire goes slack, the points representing the masses are in free flight most of the time, coming into tension only when the distance between mass points becomes equal to the natural length of the wire segments joining the masses. Each time a segment goes in or out of tension it causes a discontinuity in the numerical integration. With a large number of masses the integrator is continually encountering discontinuities. The time at which the discontinuity occurs must be found by trial and error and the polynomials used for extrapolation must be rebuilt past the discontinuity.

The awkward manner in which WAVES dealt with discontinuities led us to develop another approach in which each bounce is treated as a point event and in which both the free flight and the bounce are handled by analytic techniques. This development led ultimately to SLACK2, the model used in this study.

Initially, the program was written in one dimension only to compute the force-free motion of the section of wire next to the Shuttle. The program used the same main routine used in WAVES to take advantage of the input and output facilities already developed, but used a new analytic subroutine written to have the same main program interface as the integrator. The main routine computes the recoil velocity analytically from the system parameters and assigns this initial velocity to each wire mass point. The subroutine then computes the relative velocity between each pair of mass points and the time required for the points to separate by a distance equal to the natural length of the segment of wire connecting the points. The pair of points having the smallest time to the next bounce is determined and all the positions updated to that time. The subroutine then returns a linear polynomial giving the position of each mass vs. time.

Initial test runs done with this analytic program showed a large percentage of simultaneous bounces, an unexpected and almost certainly non-physical result. When two bounces are simultaneous, the order in which the bounces are treated in the program can be determined either by convention (depending on how the computer code is written) or by roundoff error (where numbers cannot be represented exactly by a finite number of digits).

As detailed in Monthly Reports 5 and 6 to this contract, a set of rules was developed for handling these bounces in a way which led to results in this model consistent with normal integration techniques. A more general two-dimensional formulation of the model was then developed which yielded the immediate advantages that the symmetries

leading to simultaneous bounces (and the related difficulties) in the earlier model were broken, that a tether deployment boom offset from the local vertical could be included, and that the influence of gravity gradient, Coriolis, and air-drag forces was readily modelled and interpreted.

4.2 The SLACK2 Model

4.2.1 Model Description

SLACK2 is a "lumped mass" model, in which the physical tether is divided into segments. The properties of each segment are mapped onto a spring with a mass at the end away from the point of attachment. The point of attachment to the Shuttle or tether boom is modelled separately.

The model allows the tether to be divided into unequal length segments. It uses a coordinate system rotating with the tether system's orbit center and assumes that the orbit center is in a circular orbit. It is two-dimensional in the plane of the orbit.

The prime characteristic of this model is that it assumes a tether which is slack almost all the time. The springs connecting the masses are never extended past their natural length and when a spring does become taut the masses on its ends rebound instantaneously. The rebound is computed in the center-of-mass system for the two masses as a reversal of the momentum components along the line joining the masses. Damping has been included by allowing the velocity to be reduced by a constant percentage at each rebound.

The reason for restricting this model to a slack-with-bounces case is computational simplicity. It leads to equations of motion for the masses which are strictly decoupled between rebounds. The solution for the motion of each point then becomes straightforward as described in Section 4.2.2, below.

Initial conditions in the present model are for a tether deployed vertically upward, with a uniform recoil velocity toward the Shuttle such that the elastic energy of the stretched tether before the break is converted to kinetic energy. Simulations with the full SKYHOOK program described in previous reports show that this is a good approximation to the state at the moment when the broken tether goes slack. The program is modular, and these initial conditions could easily be generalized. The segments are of unequal length to break the symmetry leading to simultaneous bounces.

SLACK2 includes a flexible deployment boom as the point of attachment. More general boom models, e.g. damped or rotating, could be added easily. The present boom model is purely kinematic, with no allowance for the influence of the tether on the boom/Shuttle system. The governing equations for the motion of the boom were derived under the assumption that the boom, which had been bent by the tether and was in equilibrium before the break, is released suddenly at the moment integration begins and oscillates with no damping. Relaxation of these restrictions must await a more complete tether model allowing the computation to proceed from the initial break. The Shuttle is assumed to be an infinite mass at the origin in the co-ordinate system of the model. The boom characteristics were as provided by MSFC:

length: 849 inches, weight: 104.2 lbs., bending stiffness: (EI) 1.3 x 10^8 lb. x in^2.

This model also includes the external forces: air-drag, Coriolis, and gravity gradient. These forces, in the approximations used, all result in linear differential equations for the coordinates of each mass; the masses remain uncoupled. The drag is modelled as a balloon attached to each mass point. This choice, rather than the SKYHOOK model of a taut segment between adjacent masses, was made to decouple the equations of different masses. For the slack case, it is believed to be also physically more realistic.

For display purposes SLACK2 creates a file in the same format as the SKYHOOK plot file so that the existing post-processor can be used to generate plots in the familiar side-view (radial vs. in-plane) format.

Two distinct though related concerns of utmost importance are the robustness of the computational model and the stability of the actual physical system (in the sense that minor changes in the initial state do not lead to drastically different states at later times). These issues are discussed below along with a review of the mathematical basis for the model.

4.2.2 Details of Mass Point Motion

The forces acting on the mass points which simulate the tether are linear approximations. Coriolis and gravity gradient forces are given by the first-order terms of expansions in x/R and y/R, where x and y are coordinates in a Shuttle-centered system and R is the orbit

radius. Drag force is modelled using a constant atmospheric density with a streaming velocity much greater than the tether's internal velocity. The acceleration produced by drag, as well as by gravitational forces, does not depend on the segment length modelled by a given mass in this model. The cross-sectional area, hence the force, is proportional to the length, and therefore, in proportion to the mass. The acceleration due to drag is computed as

$$\tilde{D} = (1/2)F\ C_D\ A\rho_a\ v^2/m$$

where A = (diameter) x (length) is the segment's cross-sectional area; F = 0.75 is a factor to account for projection; $C_D = 2$ is the coefficient of drag; ρ_a is the atmosphere density; v is the streaming velocity; and m is the mass of the tether segment. We used $\rho_a = 1.55 \times 10^{-13}$ gm cm^{-3}, the value given by Jacchia (1971) for a 1000° exosphere at 220-km altitude.

The coordinates x and y are defined relative to the Shuttle (or the orbit center of the system if the Shuttle is finite mass), x is the outward radial direction, and y is in the forward along-orbit direction. Motion perpendicular to the orbit plane is decoupled from in-plane motion and is ignored. The equations of motion are then:

$$\ddot{x} = 3\Omega^2 x + 2\Omega\dot{y}$$

$$\ddot{y} = -2\Omega\dot{x} - \tilde{D} \qquad (1)$$

We scale the time by defining $\tau = \Omega t$, where $\Omega = (GM/R^3)^{1/2}$ is the orbital angular velocity and then,

$$x'' = 3x + 2y'$$

$$y'' = -2x' - D \tag{2}$$

where $( )' = d( )/d\tau$ and $D = \tilde{D}/\Omega^2$. We may re-write this as

$$p' = Q\,p - d \tag{3}$$

where $p(\tau) = [x,\ x',\ y,\ y']^T$, Q is a constant matrix

$$\begin{bmatrix} 0 & 1 & 0 & 0 \\ 3 & 0 & 0 & 2 \\ 0 & 0 & 0 & 1 \\ 0 & -2 & 0 & 0 \end{bmatrix}$$

and $d = [0,\ 0,\ 0,\ D]^T$. Equation (3) is our fundamental equation.

This is an in-homogeneous linear system of first-order differential equations with constant coefficients and is soluble by standard techniques (e.g., Boyce and DiPrima, 1977, Chapter 7). In outline, one finds a <u>particular solution</u> $p_d(\tau)$ to Equation (3), and then any other solution may be written

$$p(\tau) = p_d(\tau) + p_h(\tau) \tag{4}$$

where $p_h(\tau)$ solves the <u>homogeneous system</u>

$$p'_h = Q\,p_h \tag{5}$$

Note that <u>any</u> particular solution p_d may be used. By inspection,

$$p_d(\tau) = [-2D\tau,\ -2D,\ 1.5\ D\tau^2,\ 3D\tau]^T \qquad (6)$$

To find all solutions of (5), which is fourth-order, we need four independent solutions, $p_1(\tau)$, $p_2(\tau)$, $p_3(\tau)$, $p_4(\tau)$; then any solution may be written $p_h(\tau) = a_1\ p_1(\tau) + a_2\ p_2(\tau) + a_3\ p_3(\tau) + a_4\ p_4(\tau)$, with constants a_i depending on the initial conditions. To find the p_i, attempt solutions of the form $p(\tau) = r\ e^{\lambda\tau}$, where the constant λ and the constant vector r are to be found. This leads to the requirement

$$Q\ r = \lambda\ r \qquad (7)$$

i.e. λ and r form an eigenvalue-vector pair of the matrix Q.

Q has eigenvalues 0, 0, + i, and - i: the multiple eigenvalues lead to a somewhat more complex form of the corresponding solution (see Boyce and DiPrima, Section 7.8) and the complex exponentials corresponding to + i and - i may be combined to give real solutions with sin(τ) and cos(τ) terms. The end result is:

$$p_1(\tau) = [0,\ 0,\ 1,\ 0]^T$$
$$p_2(\tau) = [0,\ 0,\ 1,\ 0]^T\ \tau + [-2/3,\ 0,\ 0,\ 1]^T$$
$$p_3(\tau) = [0,\ 1,\ 2,\ 0]^T\ \cos(\tau) + [1,\ 0,\ 0,\ -2]^T$$
$$p_4(\tau) = [-1,\ 0,\ 0,\ 2]^T\ \cos(\tau) + [0,\ 1,\ 2,\ 0]^T \qquad (8)$$

Combining (4), (6) and (8), we see that the general solution is of the form

$$p(\tau) = a + b\tau + c\tau^2 + d\cos(\tau) + e\sin(\tau) \qquad (9)$$

where a, b, c, d, e are vectors determined by the initial conditions and the drag. These coefficient vectors are computed as follows. First, given the initial conditions x_o, x_o', y_o, y_o', compute a vector α (of length 5):

$$\alpha = \begin{bmatrix} 0 & -2 & 1 & 0 & -4 \\ -6 & 0 & 0 & -3 & 0 \\ 0 & 1 & 0 & 0 & 2 \\ 3 & 0 & 0 & 2 & 0 \\ 0 & 0 & 0 & 0 & 1 \end{bmatrix} \begin{bmatrix} x_o \\ x_o' \\ y_o \\ y_o' \\ D \end{bmatrix} \qquad (10)$$

and then use α to get the coefficients:

$$a = \begin{bmatrix} 0 & -2/3 & 0 & 0 & 0 \\ 0 & 0 & 0 & 0 & -2 \\ 1 & 0 & 0 & 0 & 0 \\ 0 & 1 & 0 & 0 & 0 \end{bmatrix} \alpha \qquad (11a)$$

$$b = \begin{bmatrix} 0 & 0 & 0 & 0 & -2 \\ 0 & 0 & 0 & 0 & 0 \\ 0 & 1 & 0 & 0 & 0 \\ 0 & 0 & 0 & 0 & 3 \end{bmatrix} \alpha \qquad (11b)$$

$$c = \begin{bmatrix} 0 & 0 & 0 & 0 & 0 \\ 0 & 0 & 0 & 0 & 0 \\ 0 & 0 & 0 & 0 & 3/2 \\ 0 & 0 & 0 & 0 & 0 \end{bmatrix} \alpha \qquad (11c)$$

$$d = \begin{bmatrix} 0 & 0 & 0 & -1 & 0 \\ 0 & 0 & 1 & 0 & 0 \\ 0 & 0 & 2 & 0 & 0 \\ 0 & 0 & 0 & 2 & 0 \end{bmatrix} a \qquad (11d)$$

$$e = \begin{bmatrix} 0 & 0 & 1 & 0 & 0 \\ 0 & 0 & 0 & 1 & 0 \\ 0 & 0 & 0 & 2 & 0 \\ 0 & 0 & -2 & 0 & 0 \end{bmatrix} a \qquad (11e)$$

In practice it proves convenient to form one matrix with these vectors as columns:

$$U = [a : b : c : d : e] \qquad (12)$$

and compute the state vector as

$$p(\tau) = U \begin{bmatrix} 1 \\ \tau \\ \tau^2 \\ \cos(\tau) \\ \sin(\tau) \end{bmatrix} \qquad (13)$$

(Note that U is mostly filled, having only four zero elements.)

Routines which compute the mass point position using the above formulation were tested by comparing a sample run (followed for about 20,000 seconds) with a direct numerical integration of (2) using a fourth-order Runge-Kutta method.

4.3 Modelling Results

4.3.1 Comparison of SLACK2 with SKYHOOK

For studying SLACK2 a case which had previously been run using the SKYHOOK program was used. The results of the SKYHOOK run are shown in Figure 4-1. Here, 100 km of 0.2-cm Kevlar tether with a 300-kg subsatellite was initially deployed upward. It was cut 200 meters from the Shuttle and the run is started with a uniform tension of 12 kg on the tether which quickly (0.03 seconds) leads to a recoil velocity of about 3.8 m/sec. The recoil was followed for 66 seconds.

Figure 4-2 shows a simulation of a similar case using SLACK2. SLACK2 includes a deployment boom which is vertical in this example and hence does not oscillate laterally upon release. SLACK2 begins the simulation with the tether already slack and recoiling. The recoil velocity is calculated by assuming that the stored elastic energy is converted uniformly to kinetic energy, leading to

$$V_{rec} \approx (1 + M_T/2M_{SS})(3\Omega^2 L M_{SS})/(A\sqrt{\rho E})$$

where M_T is the tether mass (before the break), M_{SS} the subsatellite mass, L the original length, A the area, ρ(=1.5) the density, and E (=0.7 x 10^{12}) the elastic modulus. To reproduce the results of Figure 4-1, we were forced to set $M_T = 0$. In computing the initial tension for the SKYHOOK run, the mass of the tether was neglected.

Figure 4-3 shows a run with the tether divided into 40 segments, but otherwise the same as in Figure 4-2 (with $M_T = 0$). The gross behavior is similar, but comparison clearly shows that the point-to-point structure seen in Figure 4-2 (and presumably that in

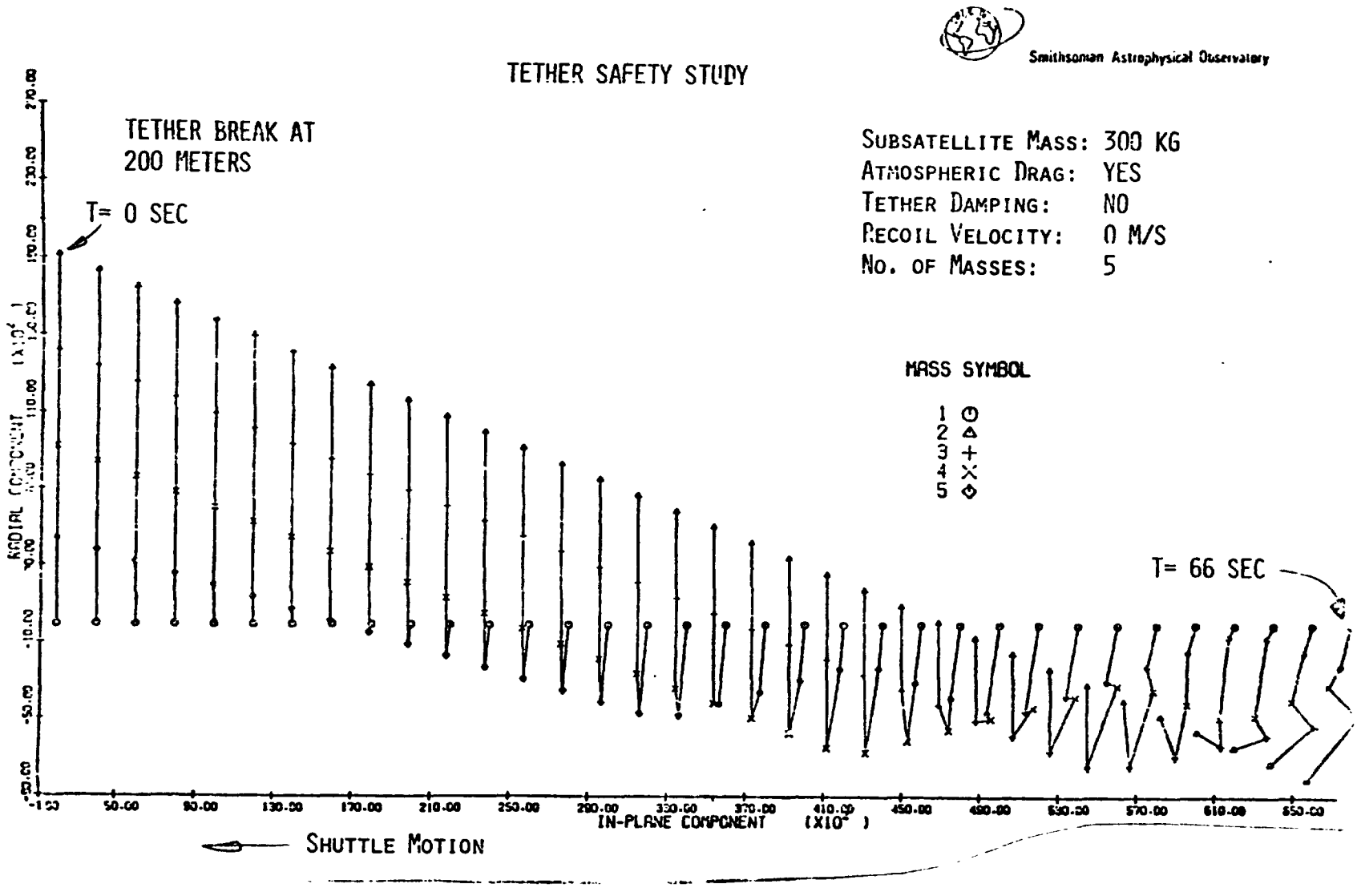

ORIGINAL PAGE IS
OF POOR QUALITY

Figure 4-1. A SKYHOOK run showing tether recoil after a break at 200 meters of a 100-km tether of 0.2-cm Kevlar with a 300-kg subsatellite. The figure is in the familiar side-view form. The in-plane component is forward (in the direction of Shuttle motion) to the left. Configurations are plotted at 2-second intervals, as they are in Figure 4-2 to Figure 4-5.

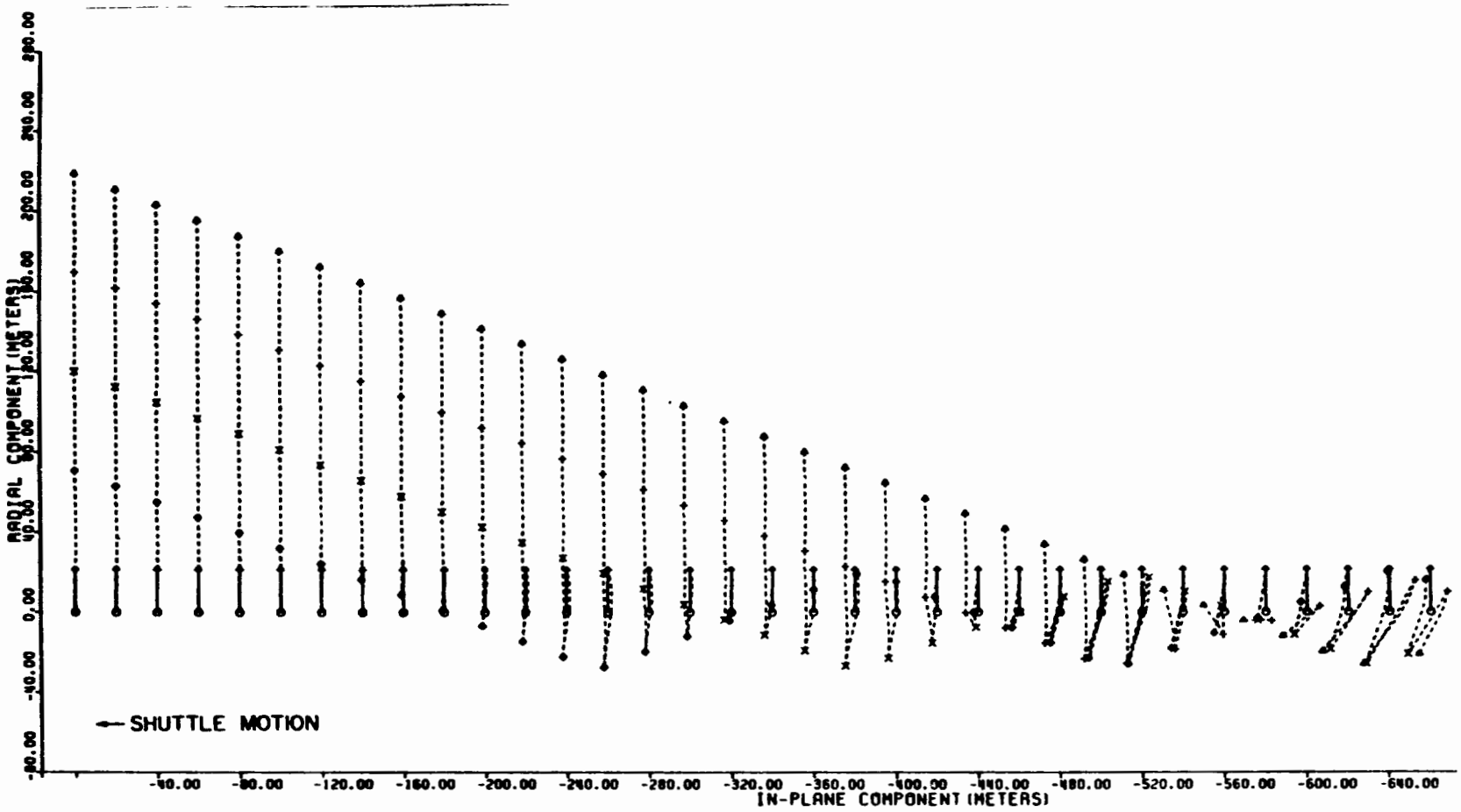

Figure 4-2. SLACK2 was used to run a close analog of the case in Figure 4-1. The tether was divided into four segments. Note the boom (solid line) deployed straight up, with the boom tip as "mass 6." The curvature in some dashed lines is an artifact of the plotting process. The vertical scale is not quite the same as Figure 4-1. In computing the recoil velocity, the tether mass was set to zero (see text).

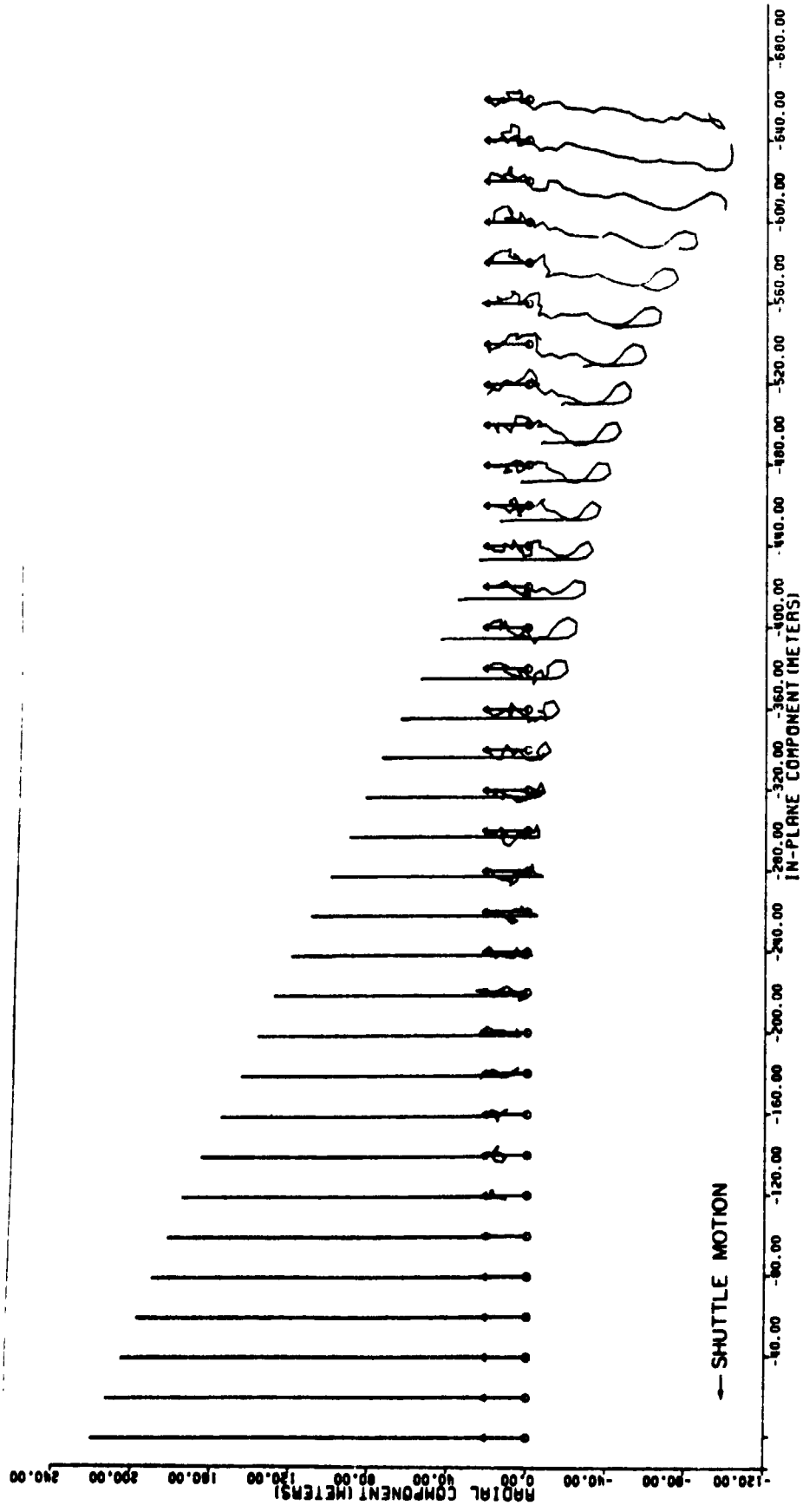

Figure 4-3. As in Figure 4-2, with 40 tether segments. For large numbers of segments, the plotting program was modified to omit plotting the "mass points" other than the boom tip and Shuttle.

4-1) is largely spurious. This situation likely occurs at all levels, and is probably a feature of the bouncing mass model rather than its particular realization in SLACK2.

There is overall agreement between Figures 4-1 and 4-2, that is, between SKYHOOK and SLACK2. However, there is considerable difference in detail. The two simulations should be investigated further to determine what is causing the difference. Oddly enough, though the four segment SLACK2 run should approximate the SKYHOOK run, the 40-segment run exhibits behavior much closer to SKYHOOK.

Figure 4-4 shows the results of a run in which the tether mass was included in the computation of the recoil velocity; the boom is deployed 30° forward of vertical, but otherwise the physical situation is the same as above. Thirty tether segments were used and the run proceeded for 240 seconds. Note the quasi-periodic motion (the time between peaks is actually decreasing) and the appearance of damping. It is not clear if energy is actually being lost (to air-drag or the boom) or if the motions are simply becoming less ordered.

4.3.2 Running Time Considerations

The four-segment run (see Figure 4-2) took 3.3 seconds of CPU time, including setup and output. The analogous SKYHOOK run (Figure 4-1) took several hundred seconds. This time is due to the very discontinuous nature of the tether forces in when the tether is slack, which causes the numerical integrator to search for each discontinuity and restart once it is found. The advantages of this new approach to running fundamentally the same physical model are obvious. The 40-segment run (Figure 4-3) took nearly 20 times the physical time

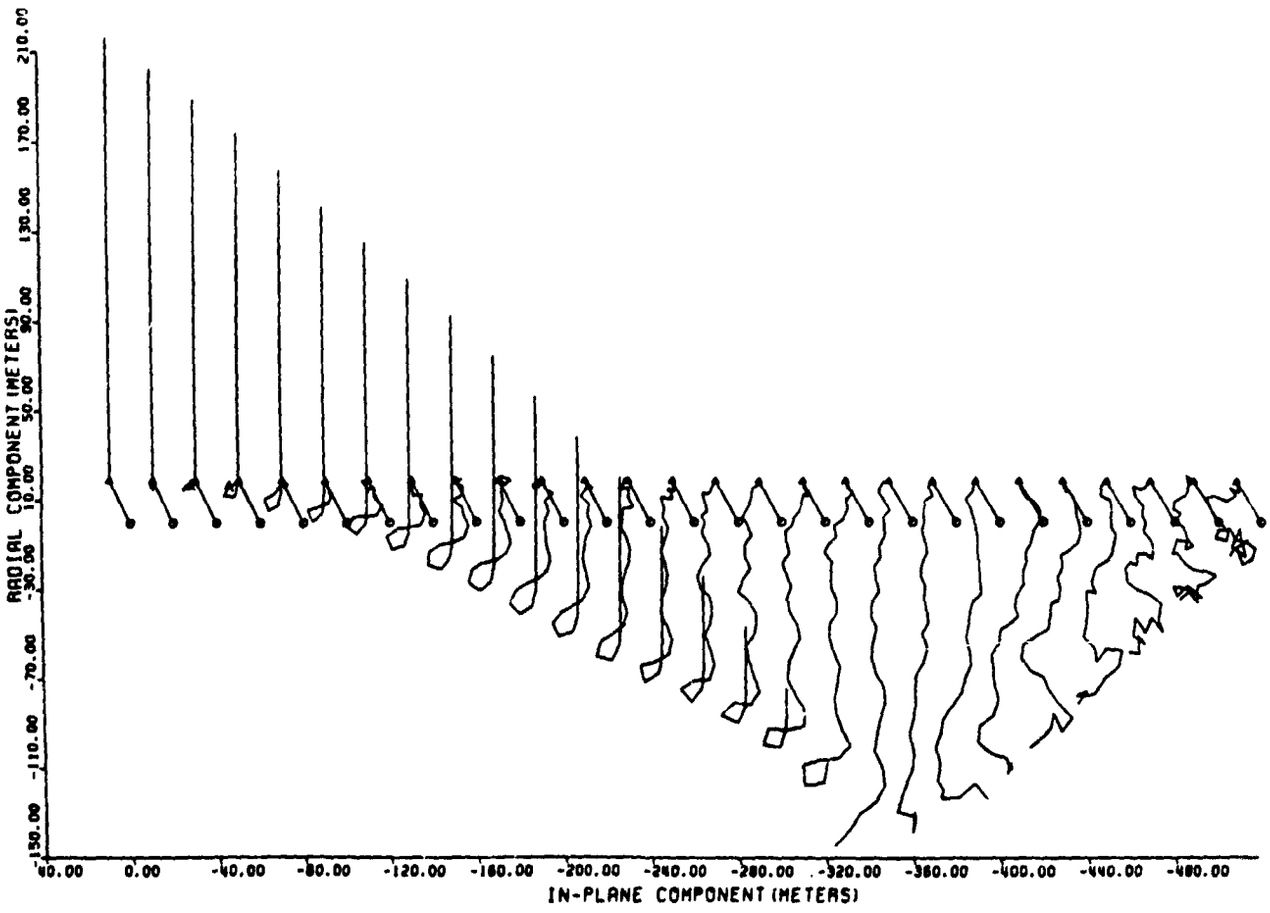

Figure 4-4. In plane vs. radial behavior of the tether plotted every two seconds for a total period of 240 seconds after a break for the situation modelled in Figure 4-2 and Figure 4-3 except that tether mass is included in computing the initial recoil velocity and the boom is deployed 30° forward of the local vertical. The first 52 seconds of the run is shown above (a); the entire run is shown on the next page (b). Note the tether oscillations induced by the motion of the boom and the overall behavior similar to damped oscillations.

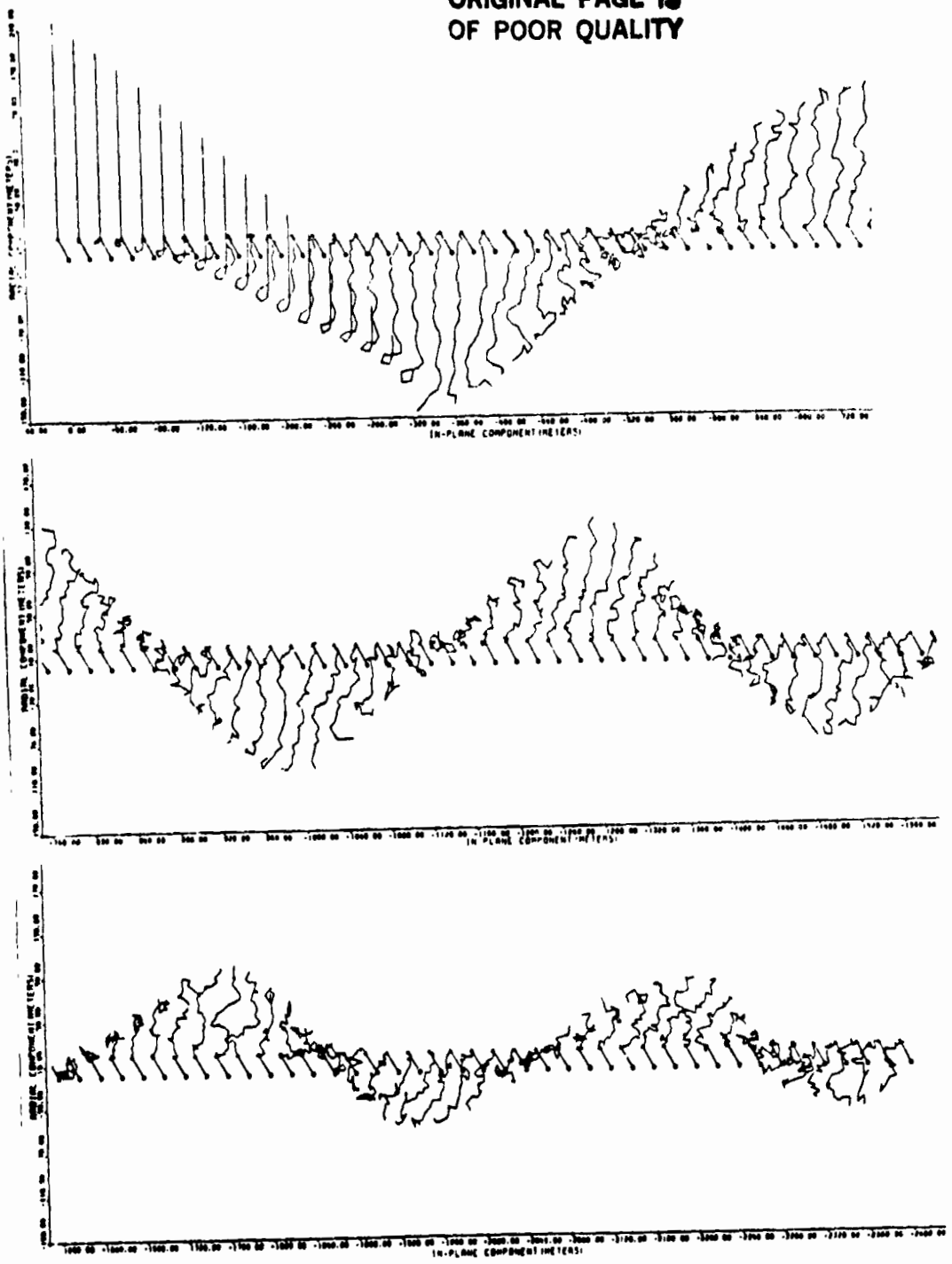

Figure 4-4(b)

modelled, but such high resolution could not be achieved by SKYHOOK under any conceivable computation budget.

To study the dependence of computation time on the number of segments the same physical case with 20-, 30-, 40- and 50-tether segments was run. These results are shown in Figure 4-5. The timing results are plotted in Figure 4-6 where (a) shows the CPU time divided by the physical time modelled and (b), shows the number of bounces per physical second and the CPU time per bounce. The computational cost increases rapidly, about CPU=(# segments)^4, but Figure 4-6(b) demonstrates that almost all of this increase is due to an increasing number of bounces. The time to compute each bounce is a very weak function of the number of segments.

The computation time depends on more than simply the physical time modelled. The discretization used appears to effect the running time, even for the same number of segments. As the resolution near the boom is made finer, the computational cost uses.

Another factor which effects the computation time is the initial recoil velocity. A series of precisely comparable runs is not available but the ratio of CPU to physical time seems roughly proportional to this velocity as might be expected. The time taken to reach a particular tether configuration is roughly inversely proportional to the initial velocity. The number of bounces is a function not of a unit of time, but of a unit of "action."

It should be noted that the program could be made to run moderately faster. Efficiency in programmer time was emphasized in developing SLACK2 and there are numerous places where changes could improve the computational speed. Some immediately obvious ones are

(a)

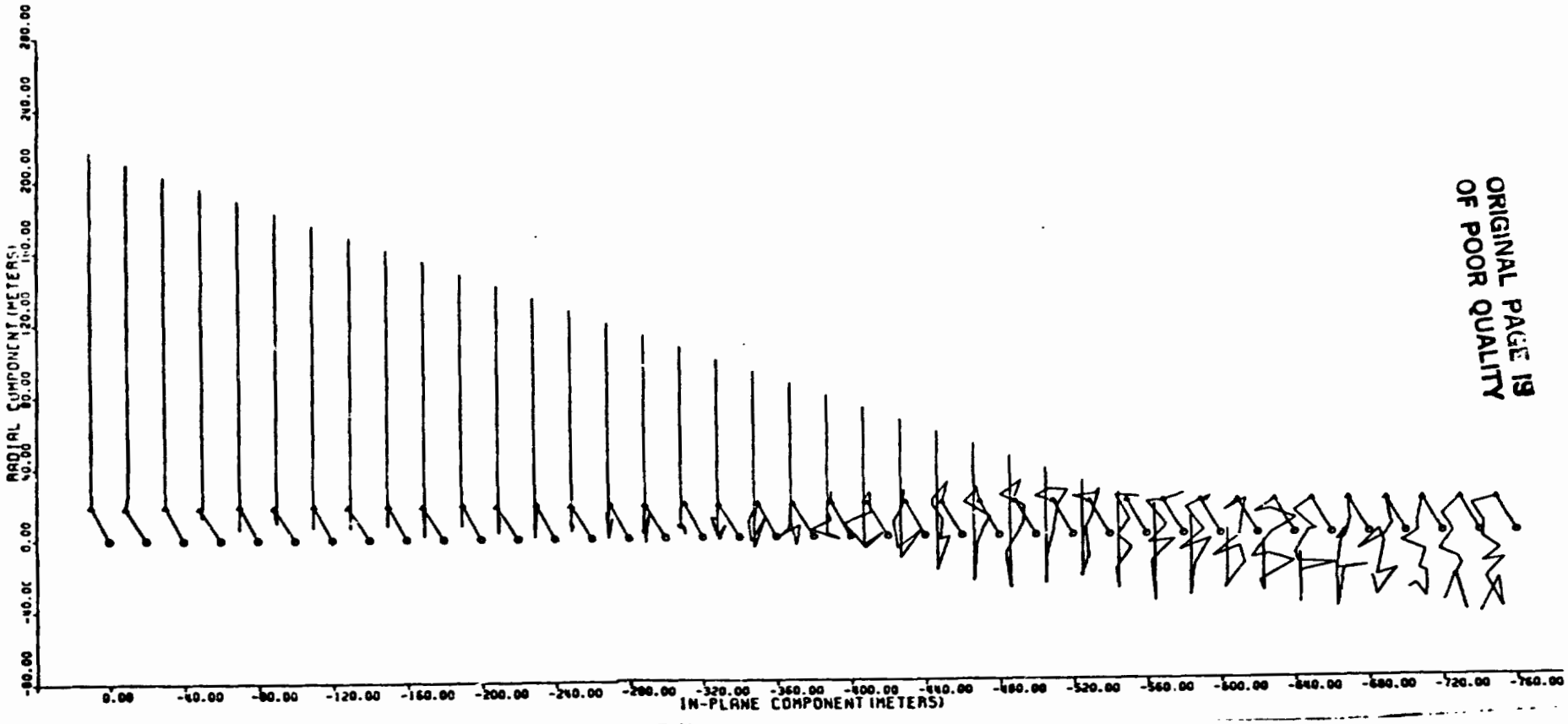

Figure 4-5. A series of runs for the same case as in Figure 4-4, with 10-, 20-, 30-, 40- and 50-tether segments. All runs are for 38 seconds with output at 1-second intervals. Note the qualitatively different results obtained with 10 and 20 segments in (a) and (b) from those with 30, 40 and 50 segments in (c) through (e).

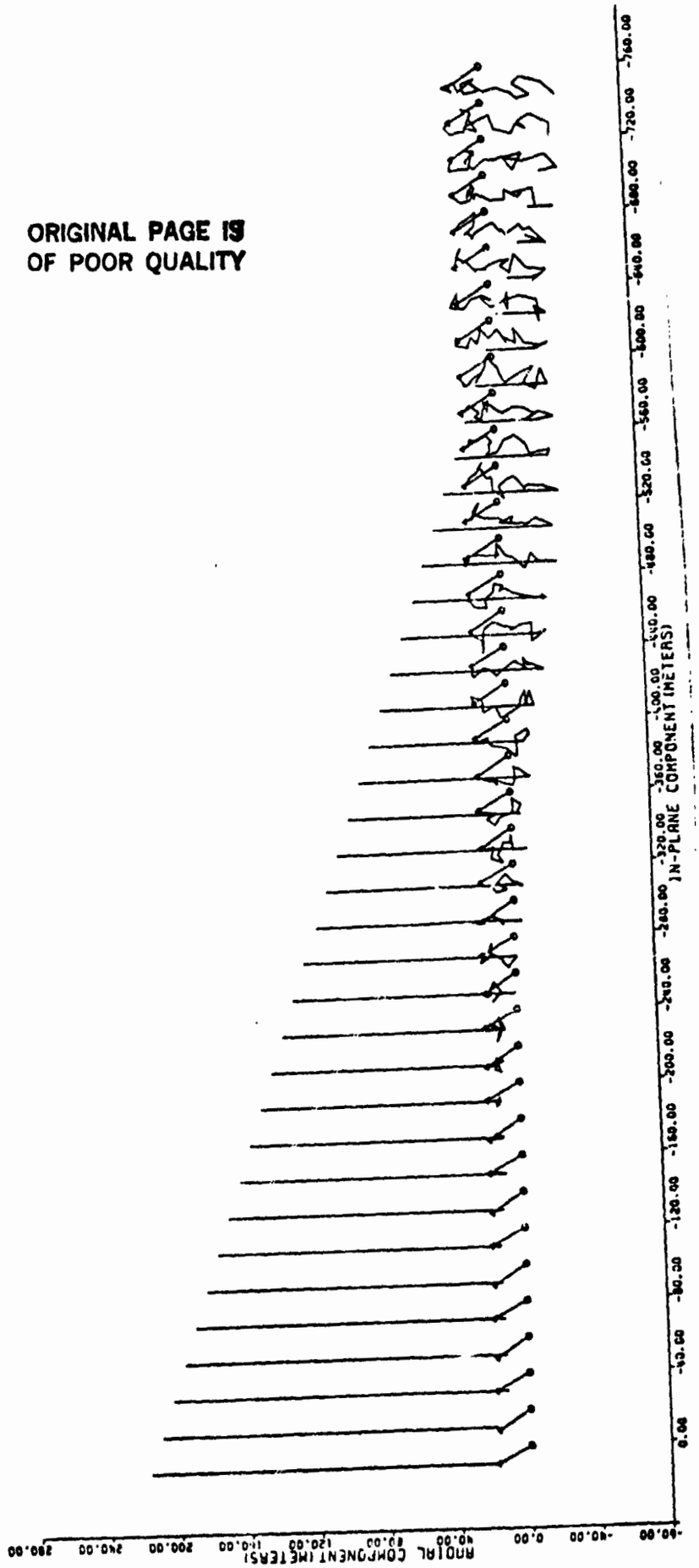

Figure 4-5 (b)

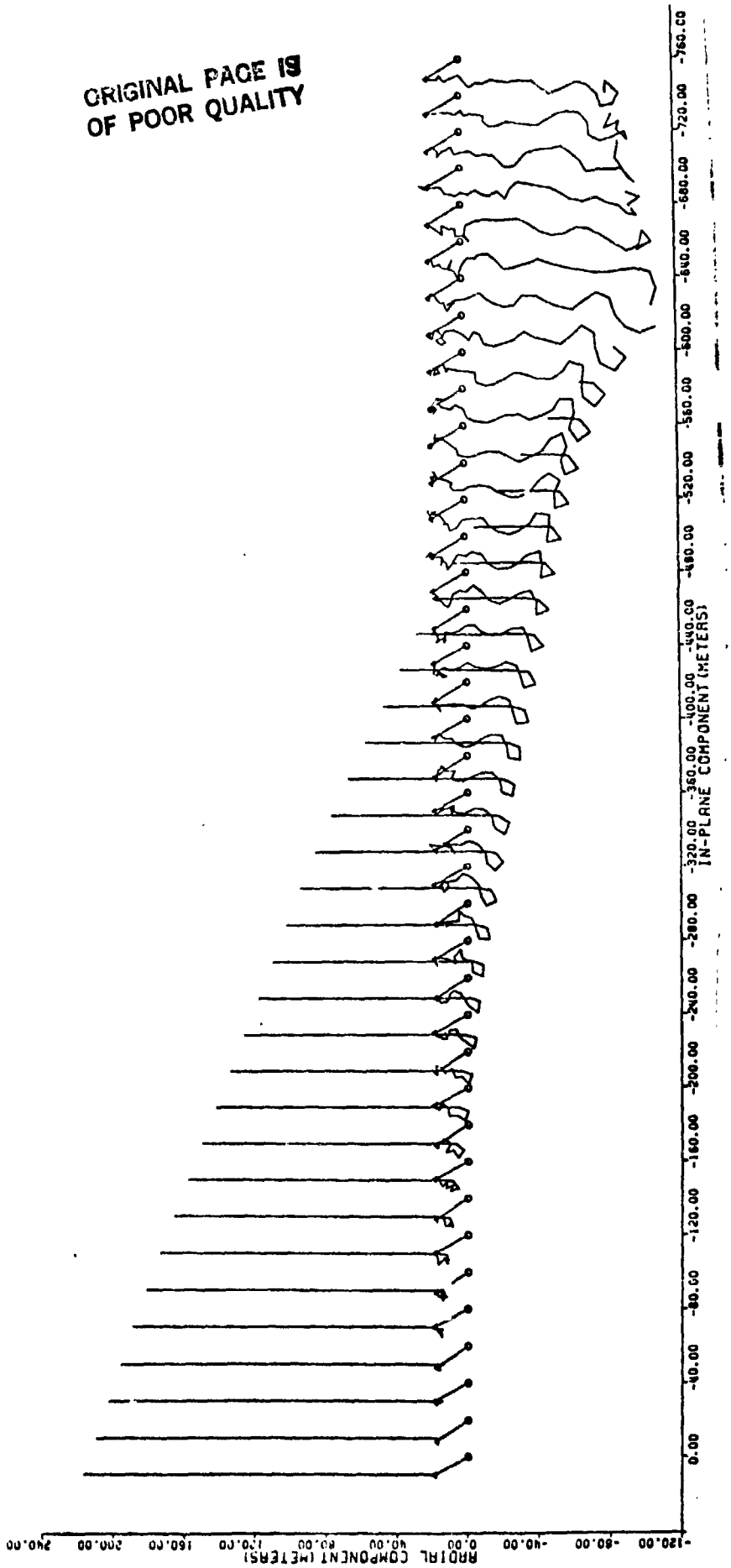

Figure 4-5 (c)

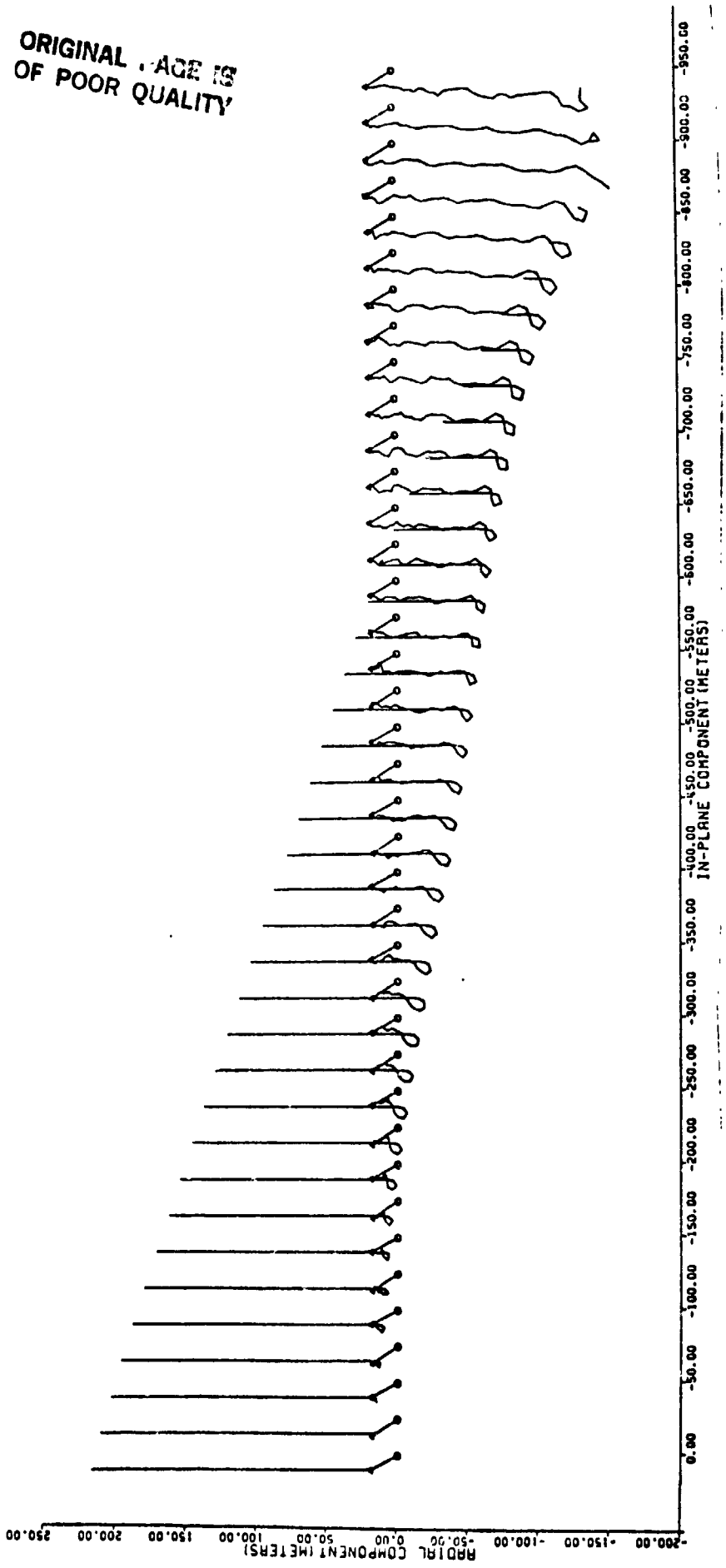

Figure 4-5 (d)

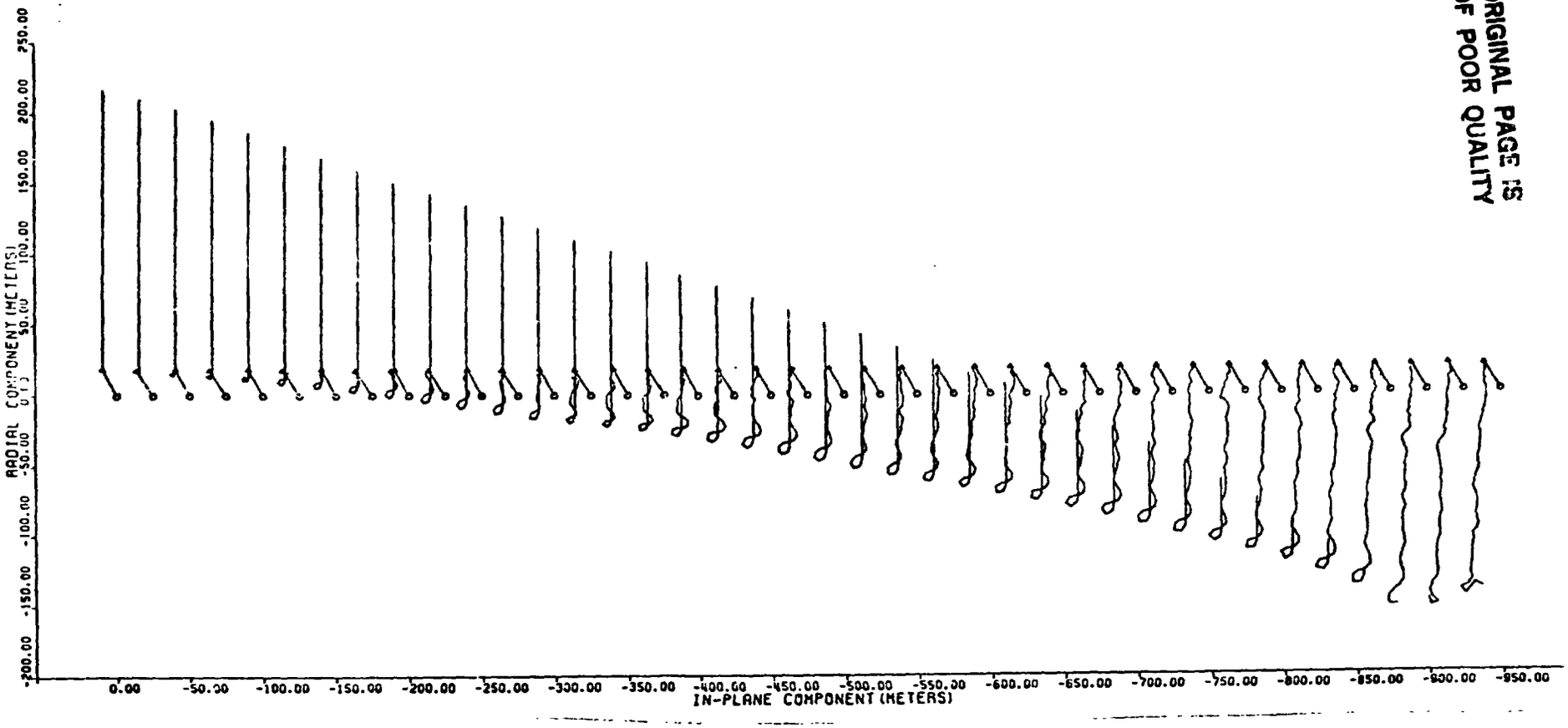

Figure 4-5 (e)

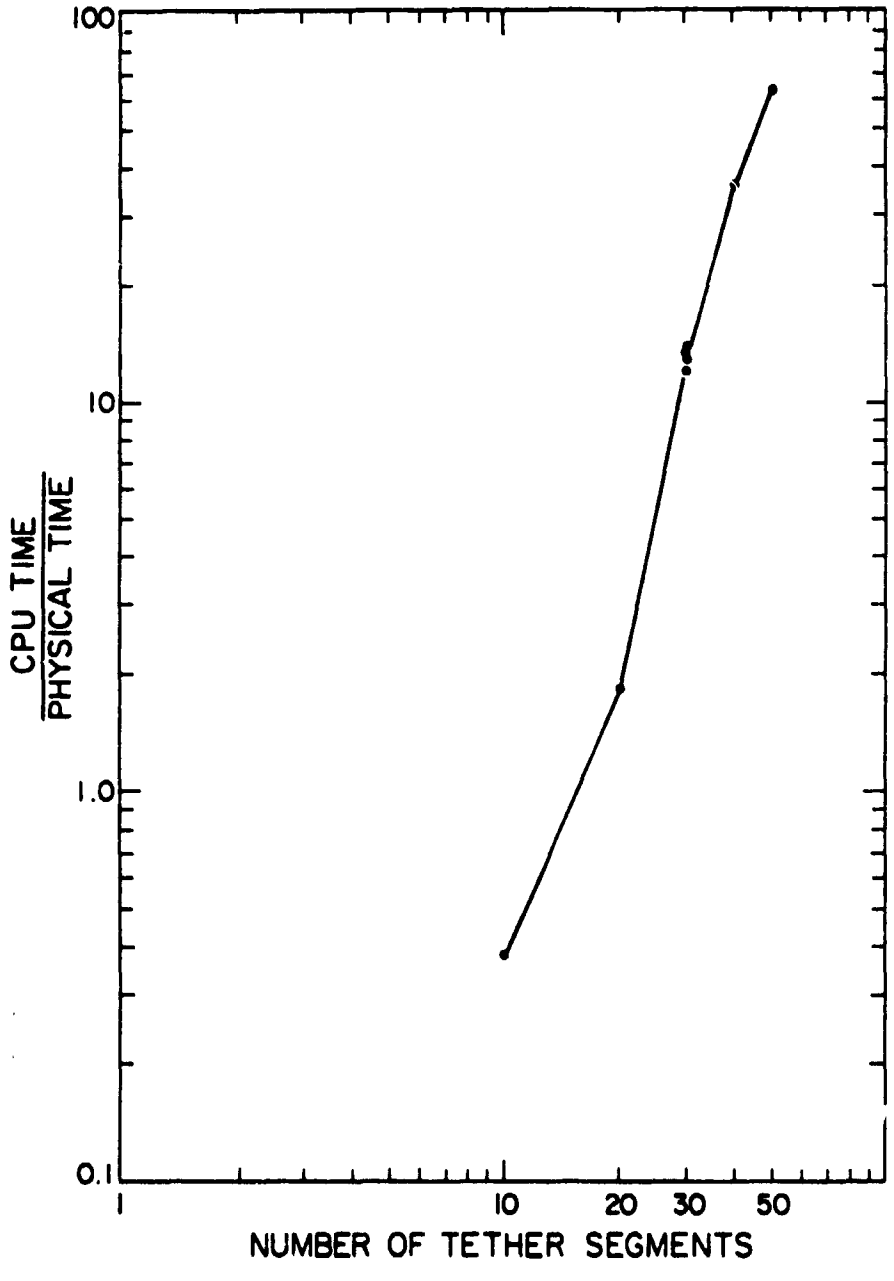

Figure 4-6. Timing results for the four runs shown in Figure 4-5, plotted as cumulative results for the full 38 seconds of each run: (a) The ratio of the computation (CPU) time to the physical time modelled; log-log plot vs. the number of segments; and, (b) The ratio of the number of bounces to the physical time; log-log plot vs. the number of segments. Also plotted in (b) is the CPU time taken to compute the average bounce, which is seen to increase much more slowly with increasing resolution.

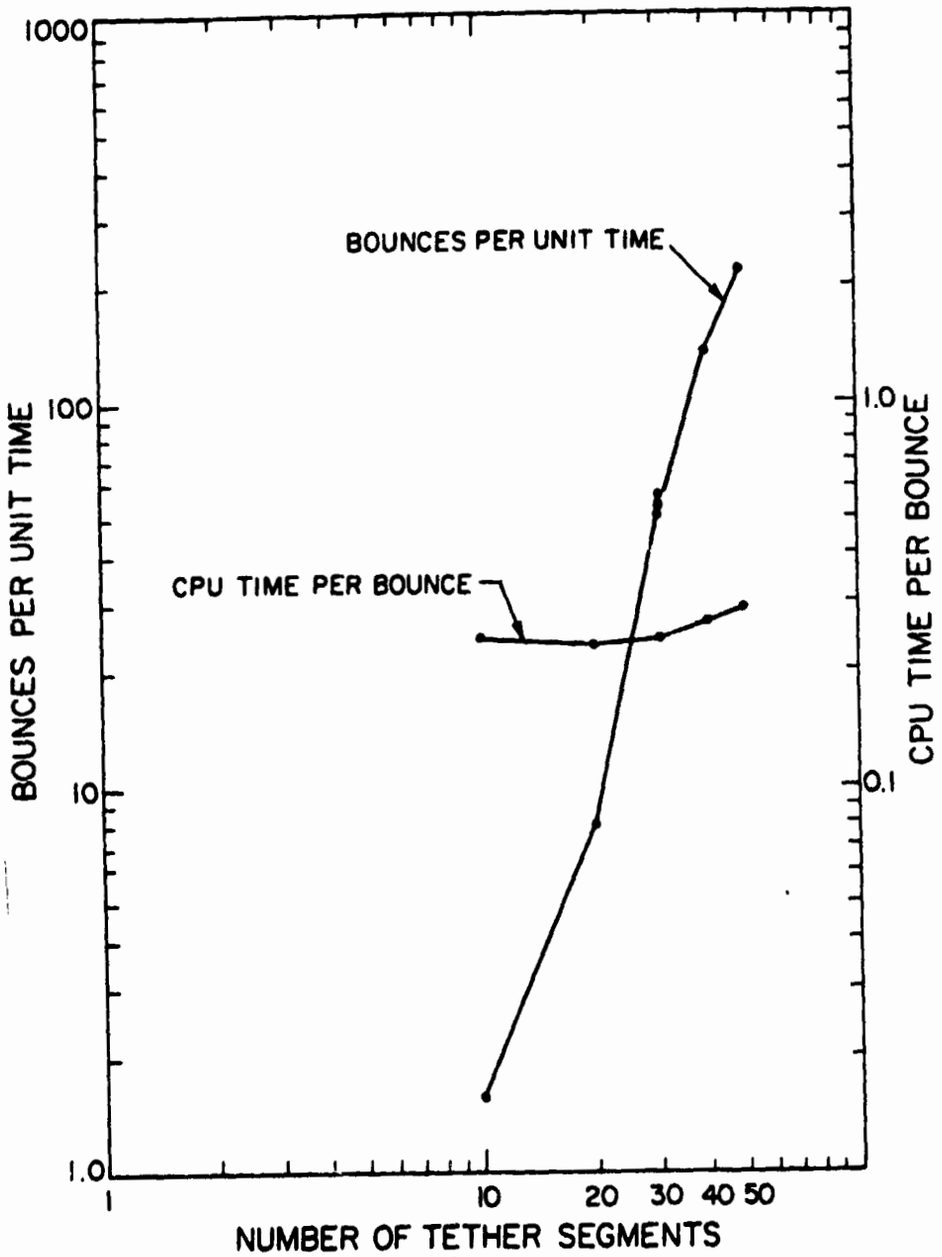

Figure 4-6(b)

not computing the full state vector when only x and y are needed (which would halve the cost of these operations); optimizing the present foolproof and simple, but relatively slow, subroutine which refines root positions; and using a more sophisticated algorithm for calculating the earliest bounce with boom tip. Cutting the computational time by a factor of two would allow the use of 30% more mass points at the same computational expense.

4.3.3 Stability of the Model System

This section addresses the questions of how well SLACK2 represents the real tether and how predictably the real tether behaves.

On the road to an operating computer program we are led through a series of levels of abstraction. Initially, of course, there is the physical system itself: the length of tether (with all its imperfections introduced in manufacture or handling), the complex sub-systems attached to either end, and the full complement of external forces. Assumptions and approximations (such as uniformity, the laws of solid mechanics, and linear force models) are made and a mathematical model is written. For systems such as the tether, this model consists of coupled sets of differential equations (DE's): partial differential equations (PDE's) for continuous components, and ordinary differential equations (ODE's) for discrete elements. These equations typically cannot be solved exactly and one must approximate the solution. One common method, particularly for complex systems, is to generate a spatially discretized model which will consist only of ODE's. This may be done, for instance, by considering the state of

the continuous components only at a set of discrete points and approximating the spatial derivatives as differences between values at these points. The procedures for (approximate) solutions of ODE's are well enough understood that one now generally proceeds to the numerical model and its realization as a computer program.

The lumped mass model used here differs somewhat from this approach in that the spatial discretization is realized directly on a physical level and we need never write down the PDE's of continuum mechanics. The mathematical model of the lumped mass physical system consists entirely of ODE's which are solved as before.

These stages are not, of course, neatly segmented but interact one with another. Possession of a well-analyzed mathematical model will allow one to determine more clearly which forces and effects may be neglected in proceeding from the physical system. Computational difficulties in programming the lumped mass model may suggest better ways to effect the original physical approximation.

When speaking of the stability of the system it is necessary to be specific about what is meant. The transition from one modelling level to another can either introduce artificial stability (as when a critical force or degree of freedom is not modeled) or convert a stable system into an unstable one (damping might be improperly neglected, or improper discretization can lead to numerical instabilities). Thus, the results of computer simulations must be reviewed carefully before conclusions can be drawn about a physical tether in space.

In the lumped mass model there are two chief areas of concern: (1) How predictable is the behavior of the actual, physical system? That is, if we were to conduct actual experiments, would the state of the tether after some reasonable time (say after the first rebound) depend strongly on the initial conditions or variations in the tether properties? (2) How well does the (physical) lumped mass model (point masses tied together by massless tether segments) represent the original system?

Intuitively, it would not be unreasonable to find that the system itself may show some instability. Experience shows that the consequences of a sudden release of stress are unpredictable in detail and that the normal response of a cut string is to crumple and move about. However, it is not clear whether this represents an instability in the dynamics of the string or strong variability in the details of the cutting process.

With regard to question (2) above, multiple computer runs were done to explore the stability of the results with respect to variations in the details of the model used. If somewhat different models give closely similar results, then confidence in the model is high. If models varying only slightly in detail give wildly varying results, the model is in some sense suspect. SLACK2 was written so that after generating a particular discretization of the tether, the individual segment lengths could be varied by (1+s) where s is a random number in the range, [-0.02, +0.02] (2% variation); the lengths are then normalized to retain the original total tether length.

Before examining these results, refer to Figure 4-5, which shows simulations for the same physical case modeled with different numbers (10 to 50) of tether segments. Looking at the final configuration for each run (t=36 sec), we note that though the 10- and 20-segment models bear little resemblance to the others, the 30-, 40-, and 50-segment models yield similar results, indeed appear to be converging, an indication of model stability.

A 30-segment model was therefore chosen as a suitable case for the randomized partition study. Thirty segments gave about the same results as 40 or 50 in Figure 4-5 and ran substantially faster. These runs were carried through to t=60 seconds to generate some large-scale structure (tether trailing and level with the boom tip). Figure 4-7 shows the configuration at t=40 and t=60 seconds for three runs with 2% segment length randomization. It should be emphasized that these are intended to represent the same physical tether.

Figure 4-7(a) shows the configuration at a moment when the tether has extended to nearly its full length below the Shuttle and rebounded for a few seconds; Figure 4-7(b) shows the tether after it has rebounded and extended again in its original direction [see Figure 4-8(a)]. In (a), the consistency between the three results is striking; note particularly that the tips in all three simulations are beginning to swing upwards in the same direction. The situation in (b) does not seem so consistent, but we must bear three things in mind: the tether extension is much less than in (a), i.e. the tether is more crumpled; the scale is larger, emphasizing the differences; and, as a matter of general experience, all models and numerical processes subject to initial perturbations will diverge farther from

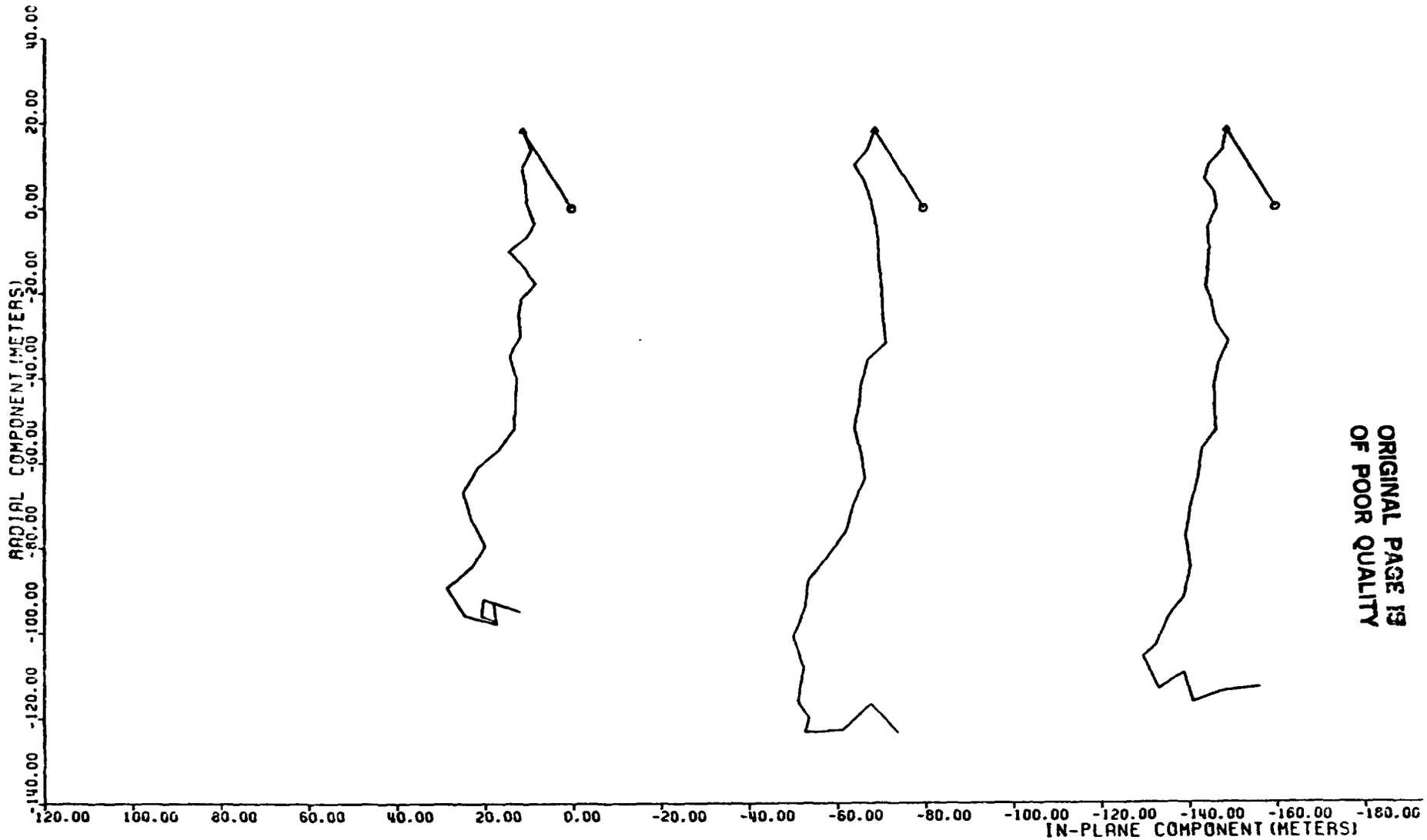

Figure 4-7. The final configurations of three separate runs are plotted side-by-side. The physical situation modeled in each run is the same (as in Figure 4-4). The tether is divided into 30 segments in each case. Each run is for 60 seconds. The three cases differ only in that after an initial partition of the tether was computed the individual segment lengths were varied by small random amounts in the range -2% to 2%; the lengths were then normalized to give the same total length in all cases. (a) shows the configurations after 40 seconds; (b) shows the configurations after the full 60 seconds. See the remarks in the text for cautions on the interpretation of detail in the figures.

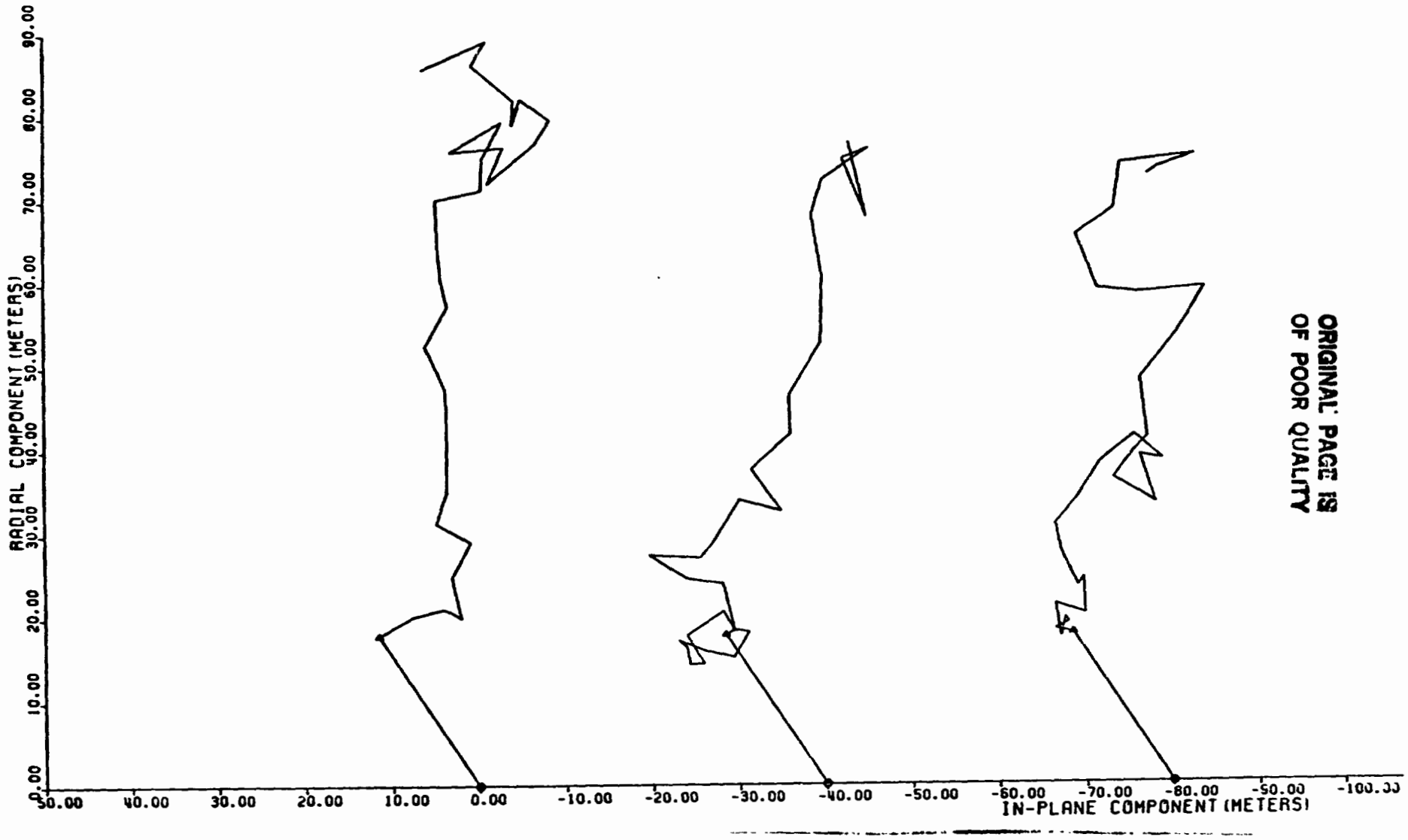

Figure 4-7 (b)

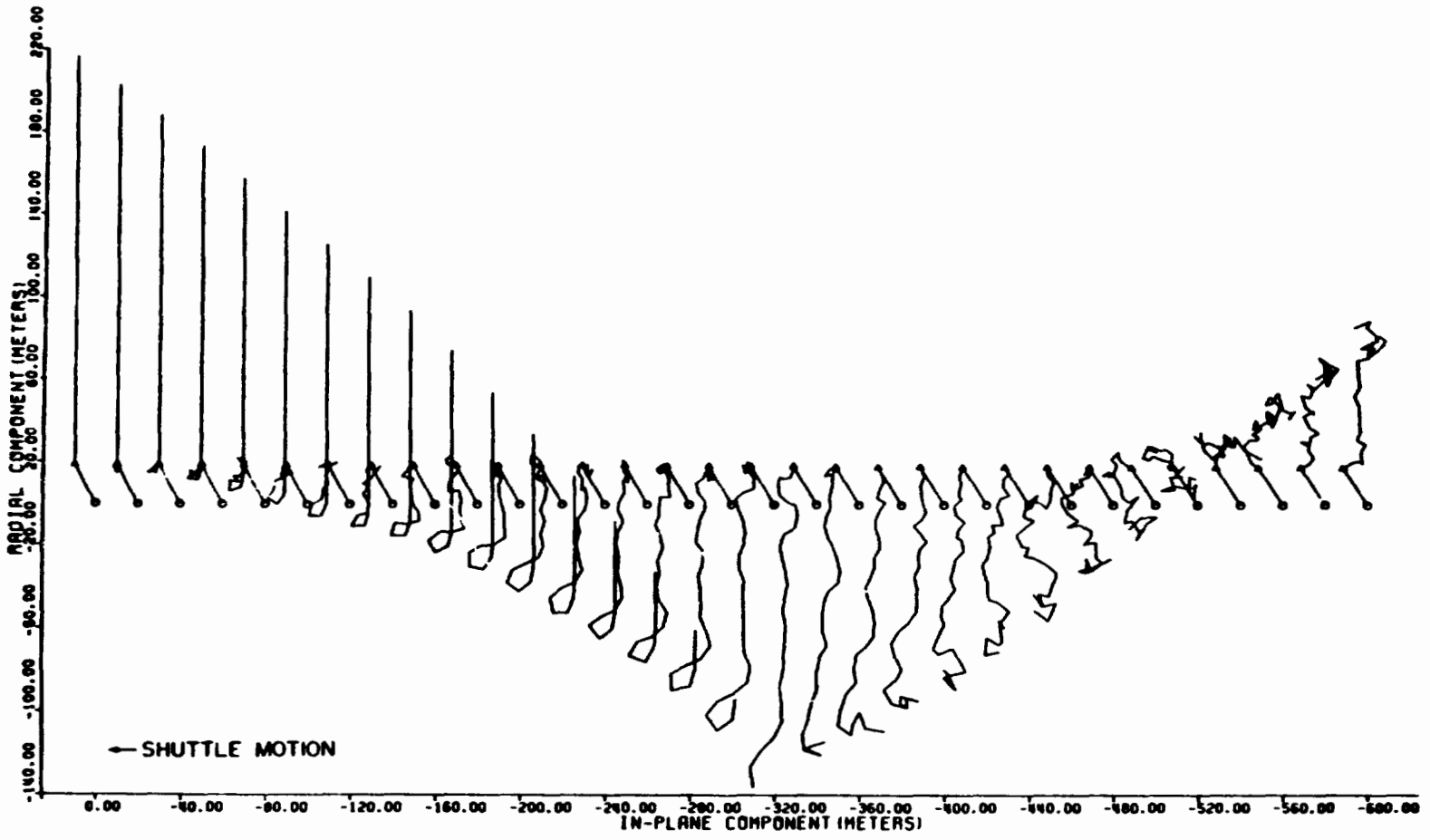

Figure 4-8. Part (a) shows the evolution of one of the cases used in Figure 4-7, while (b) shows a similar case in which the tether was more evenly segmented resulting in less resolution near the boom tip. Note the distinctly different behavior of the two cases. In (a), a travelling wave was generated, while (b) exhibited no such wave. This same distinction is seen between Figures 4-5(a) and (b) and Figures 4-5 (c), (d), and (e). The finer resolution results are more consistent among themselves and probably closer to the real behavior of the tether.

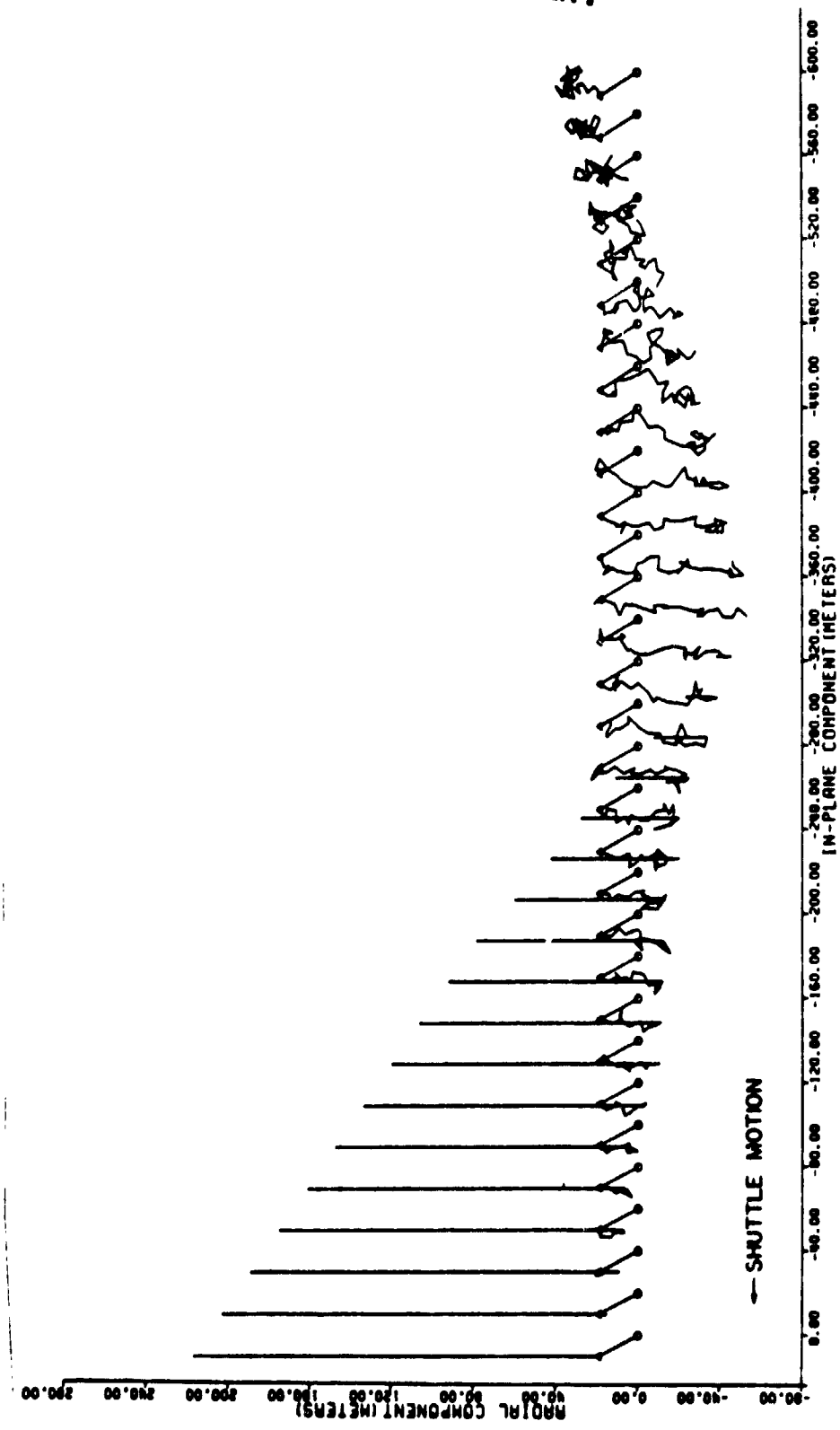

Figure 4-8(b)

the reference model as time increases unless there are special circumstances.

In summary, if we do not expect detailed accuracy of the model on a point-by-point basis (something which seems unlikely considering the discrete bounce nature of the model), the repeatability of the simulations is encouraging.

These plots contain more apparent detail than is strictly justified. In Figure 4-7(b), there are 200 meters of tether crumpled into a space barely 70 meters across. The resolution (segment length) varies from 5 to 9.5 meters and is finer near the attachment point. The discrepancies are therefore only a few segment lengths at most. Finally, the straight segments plotted are misleading. The length of tether between two mass points may be several times their plotted separation and will be crumpled somewhere in an ellipse with the mass points as foci. A more precise rendition of the physical tether would plot the rope between mass points in some way such as a "hazy cloud" representing the uncertain location of the length of slack tether between the mass points. Just as in SKYHOOK, SLACK2 shows where one end of each tether segment is, not the actual tether shape between mass points. Here, of course, the actual resolution is much higher.

4.4 Conclusions and Recommendations

If the physical system itself is unstable then this form of probabilistic cloud mentioned above may be the best prediction one can make about the tether state some time after a break. The results of these comparison studies are varied enough that such a conclusion is suggested. Probabilistic results, though not as clear cut as deterministic solutions, will be about as useful in that, a range of potential behaviors can be derived from the model. This will set limits on the behavior of the real tether; after all, the tether is inherently probabilistic, since it is inhomogenous and subject to non-deterministic forces such as air drag, random break forces, and random attitude control forces. Further study will be necessary to determine just what model conditions automatically yield the most probable behavior of the tether, and what model conditions are appropriate to identifying, say 3σ or 5σ behavior variations.

Another conclusion of interest is that this model, at least in its present form, is sensitive to input parameter variations. The occasional pair of near-simultaneous bounces is usually handled adequately, although there have been cases in which the program gets caught in a tight cycle of bounces (which seem genuine, given the model, and not an artifact of the program). If the entire tether comes into tension at the same time, which may easily happen because of the linearized forces, then multiple simultaneous bounces are possible and cannot be handled adequately in the present model. Further thought must be given to this behavior to ensure it is correctly handled in future simulations.

A major feature of the model behavior, and one that likely applies to all lumped mass models, is the existence of two distinct models. In high-resolution models (large numbers of tether segments), soon after the simulation starts a wave propagates outward from the near-Shuttle region of the tether resulting in increased velocity of the base end. In lower resolution models, this effect does not appear and the overall behavior of the tether is decidedly different, resulting in a more crumpled, "chaotic" configuration.

Considerable work remains to be done before this wave phenomenon is fully described and clearly understood. Experiments with our program should delineate the dependence of the cutoff between the models (and such properties as the wave propagation velocity and the energy transfer) upon factors such as the number of segments, the discretization details, the recoil velocity, the tether length, and other tether properties, such as density and diameter. Other questions to be considered are: Why does the velocity exchanged become directed <u>along</u> the tether? Are there other waves beyond this initial one, perhaps more subtle in their effect?

In summary:

-The true resolution of SLACK2 appears to be a few segment lengths.

-The tether configuration after one recoil depends somehow on the way in which the tether is discretized. However, for large numbers of masses, the final configuration seems to converge.

-Our model, and probably any lumped mass model, fails to find the physically significant wave phenomenon for fewer than 30 to 50 segments. Models with fewer segments also show substantially different gross tether motion and mask this phenomena.

-It is difficult at this point in development of the model to draw conclusions about the stability of the physical system but it appears that at least a probabilistic description of the behavior of the slack tether is attainable.

-The program is computationally efficient, running about 100 times faster than SKYHOOK under similar conditions.

SLACK2 presently models motion within the orbital plane only. It would be simple to add motion in the third dimension and should not increase computational time substantially. This would be useful to study (a) instability to out-of-plane perturbations and (b) effects of a sideways-deployed boom (which might be effective in avoiding tether recoil onto the Shuttle).

Further development would also allow the springs to come into tension and remain taut. Since the extensibility of the tether is small, the spring forces may also be linearized. The model would still have a system of linear differential equations (with constant coefficients) which may be solved exactly under this condition. However, in contrast to the present model, the masses attached to taut springs would generate coupled equations. If a segment is slack it effectively decouples all the masses above and below it, and these problems may be solved separately; but, there is still the potential for 4N coupled equations, where N is the number of tether segments

(masses). The solution of the coupled system is equivalent to solving an eigenvalue/eigenvector problem for the coefficient matrix. Due to the form of the coefficient matrix, SAO believes that a routine can be developed to compute these exact solutions much more efficiently than current library routines allow.

Self-intersection of the tether is ignored in this model. Currently, if two sections of tethers approach they simply pass through each other without interacting, a requirement of the two-dimensional model. Methods of dealing with self-intersection are under consideration for inclusion in a future three-dimensional model.

Development of SLACK2 along these lines is expected to lead to a computationally efficient high resolution (~50 mass point) and complete dynamic model of the tether suitable for a wide variety of simulations and studies. Development of the model from this point would include modelling the dynamics of the boom in reaction to the tether, the influence of a non-circular reference orbit, a finite mass shuttle, and a drag model in which the balloon radius attached to each mass is re-calculated after each bounce with a projected segment area model (this would still leave the equations decoupled between bounces).

5.0 STUDY OF ADVANCED USES OF THE TETHER

5.1 Algorithm for Damping Longitudinal Oscillations in the Tether

An algorithm to control the tether reel on the Shuttle has been devised to damp out longitudinal oscillations of the system. This algorithm depends only on the force (tension) perceived by the reel mechanism and on the deployed length; it specifies changes to be applied to the deployed length. Parameters to the control law require knowledge of the tether properties and subsatellite mass, but no detailed knowledge of the system state is required.

The fundamental scheme is simply:

- When the perceived tension is high relative to some nominal tension, reel out more tether.
- When the tension is low, reel in.

This scheme acts to relieve stress on the tether under high tension and to add stress under low tension. It will also remove energy from any tether oscillations, since a full cycle bringing the length back to some original value will cause the tether to do net work on the reel motor.

Mathematically, we define an applied control length $\Delta(t)$ such that the natural length at time t is given by

$$z_0(t) = \bar{z}_0 + \Delta(t)$$

where z_0 is some nominal or initial natural length and $\Delta(t)$ is given by

$$\dot{\Delta}(t) = K[T(t) - T_0] - \beta\,\Delta(t).$$

Here,

$T(t)$ = perceived tension on the reel at time t,

T_o = a nominal or target tension; this is a parameter chosen, ideally, to be the equilibrium tension.

K, β = control parameters.

The first term represents the fundamental control scheme of reeling in or out in response to tension changes. The second term is required to make the algorithm stable. In the absence of tension variations it would cause the control length to decay exponentially to zero, while if the equilibrium tension is incorrectly estimated, it avoids a secular term in the tether length, which would otherwise increase or decrease without bound.

Although in the cases studied, the parameters K, β, and T_o were held constant (with the control law being turned on sharply), there is no a priori reason why this must be so. For instance, the control law might be phased in more gradually to avoid a sharp disturbance or one might vary the parameters as the system properties vary, as during deployment or retrieval.

A detailed (theoretical) analysis of this control algorithm was made when it operates on a simple system consisting of a mass (the subsatellite) connected to a fixed point (an "infinite mass" shuttle) by a massless spring in a constant gravity field. This study provided a valuable insight into the system behavior as a function of the parameters K and β. A number of factors are left out of this analysis: tether mass, particularly the finite propagation velocities this induces; the fact that the gravity gradient force does not yield

a constant gravity field; Coriolis forces; the Shuttle's finite mass; and air drag, electrodynamic forces, and light pressure. Of these omissions, only the first seems likely to have any significant qualitative effect on the system behavior, at least in the limit of small oscillations.

5.1.1 Results of the Idealized Case Study

The model consists of a spring of natural length $\bar{z}_o$ and spring constant k, fixed at one end with a mass m at the other. It is in a uniform gravity field, g. The damping law given above is applied and we assume Hook's law gives the tension T(t). Let $\omega = \sqrt{(k/m)}$, and use a displacement $L(t) = z(t) - (\bar{z}_o + g/\omega^2)$, as the dependent variable. The equilibrium tension is simply gm, but let us introduce some error ε, so that we use $T_o = g\,m + k\,\varepsilon$. We then have a system

$$\ddot{L} + \omega^2 L = \omega^2 \Delta$$

$$\dot{\Delta} = \mathbb{K}\, k[L - \Delta - \varepsilon] - \beta\Delta$$

After normalization of the time by ω we obtain a linear system whose characteristic equation is

$$\lambda^3 + (\tilde{\mathbb{K}} + \tilde{\beta})\ \lambda^2 + \lambda + \tilde{\beta} = 0$$

with the dimensionless parameters:

$$\tilde{\mathbb{K}} = \mathbb{K}\, k/\omega$$

$$\tilde{\beta} = \beta/\omega$$

The time has been scaled by ω, so the frequencies of the damped system are $\omega\lambda$. Since the solutions of the homogeneous part of the system are sums of terms $\exp(\omega\lambda t)$, stability requires that all roots of the characteristic equation have negative real parts. So long as $\tilde{\beta} \neq 0$,

an inhomogeneous constant term (due to an external force or to an erroneous estimate of the equilibrium tension T_o) leads only to a constant term in the solution. The behavior of the roots as functions of $\tilde{K}$ and $\tilde{\beta}$ was examined by solving the characteristic equation numerically for many combinations of the parameters and is quite complex (see Figure 5-1). The precise quantity of interest- the least negative real part of the set of roots- behaves more predictably: If we fix $\tilde{K}$ and consider this stability determining real part (let us call it simply "the stability") as a function of $\tilde{\beta}$, the stability increases from 0 at $\tilde{\beta} = 0$ and has a cusp at some optimal value, after which it slowly decreases. The cusp is much sharper for $\tilde{\beta}$ below the optimal value than above. We not only wish to obtain rapid damping, which would lead us to choose the optimal $\tilde{\beta}$, but we wish a "robust" damping mechanism, one insensitive to errors in the parameters or in the model used for analysis; thus, it is safer to choose β to give a damping $\tilde{\beta}$ somewhat larger than optimal, since if the optimal value was aimed for but the actual $\tilde{\beta}$ achieved were lower than optimal the stability would be seriously effected. More detailed examination of the roots suggests reasonable parameter values of $\tilde{K} = 1.3$, $\tilde{\beta} = 0.24$; for true $\tilde{K}$ in the range 1.0 to 1.6, the damping will not be seriously degraded from optimal.

5.1.2 Numerical Simulation

The reel control law was implemented in the SKYHOOK program by concatenating the differential equation for the deployed (control) length with the differential equations for the positions and velocities. The control law parameters are read from the input file describing initial conditions, and the control length was then solved

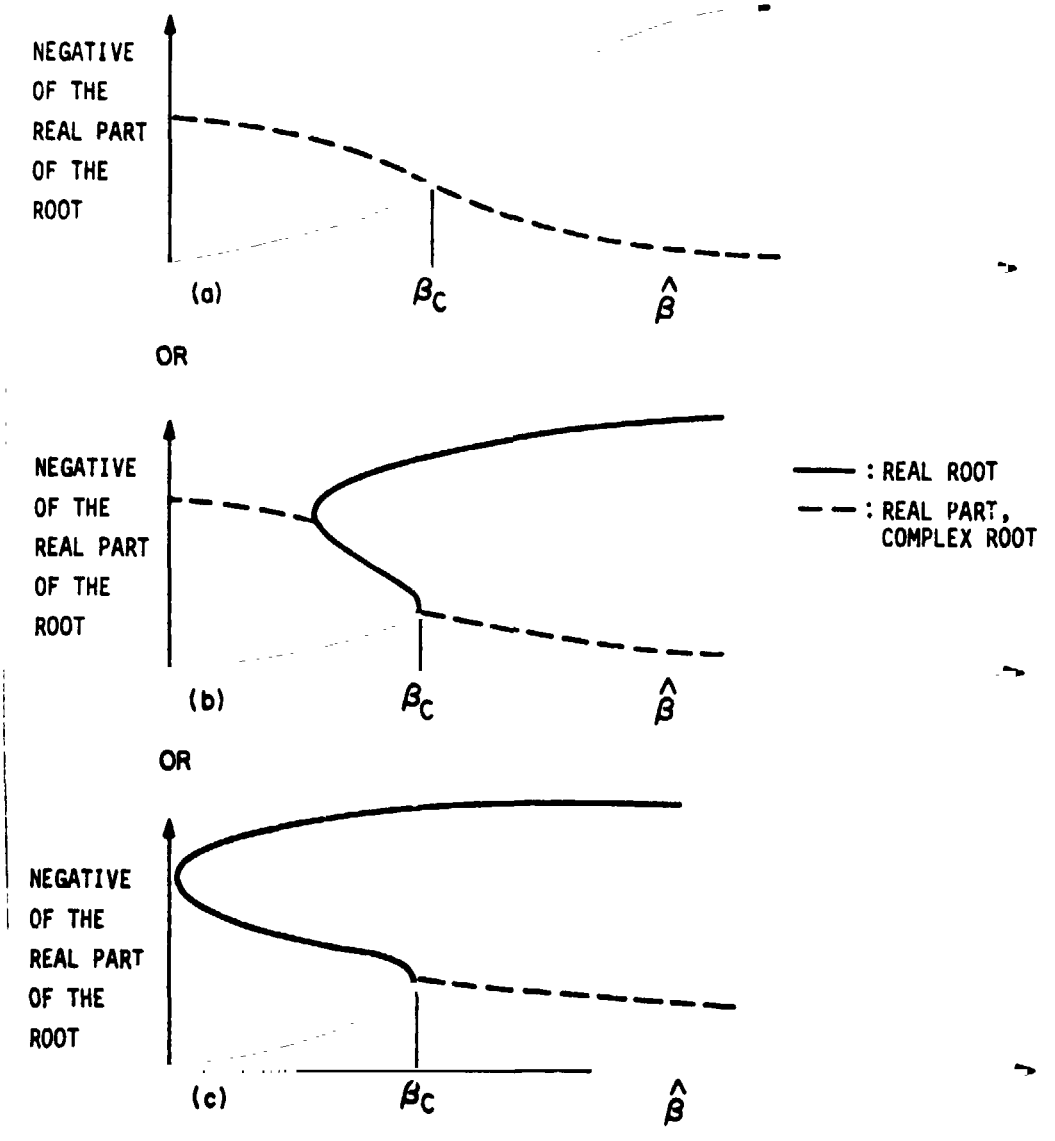

Figure 5-1. Behavior of the roots of the characteristic equation for fixed values of $\bar{K}$. Note that we plot the negative of the real part of each root (pairs of complex roots are indicated by a dashed line) and that for $\bar{K}, \tilde{\beta} > 0$ all roots have negative real parts (i.e. the system is stable). The quantity of greatest interest is the lower line at each value of $\tilde{\beta}$. This root governs the solution which decays least rapidly, and we want to choose parameters $\bar{K}, \tilde{\beta}$ to optimize this worst solution. In choosing actual parameters K, β we may not achieve the desired dimensionless parameters, so there is the additional constraint of robustness; slight errors in the parameters should not lead to large decreases in performance.

along with the other equations using the stiffly stable Gear integrator. The goal was to choose damping parameters which led to a robust damping scheme (one that behaves well in many circumstances if not optimally for the ideally expected case).

Figure 5-2 shows tension variations when a sinusoidal reel maneuver of period 105 sec is applied with release at 85 sec of a 10-ton payload, initially reeling out the tether. This has the advantage over an initial reel-in maneuver in that the tension never increases over the pre-release equilibrium value; however, experiment with the parameters of the simple sinusoidal maneuver being used (see the Final Report, March 1983, Contract NAS8-33691) failed to prevent the tether going slack. Figure 5-3 shows the same case where the active damping control law was initiated at t = 100 sec, at which time the sinusoidal maneuver was terminated. This avoided the slack tether, although tension did get close to zero at one point, and can be seen to be damping the tether oscillations. From the sharp turn in the tether tension curve when the damping started, one suspects that a gradual initiation might be beneficial and later runs bore this observation out.

All simulations used an 80 km initial deployed length of 0.3-cm Kevlar (density 1.5 g/cm^3, E = 0.7 x 10^{-12} dyne/cm^2). The mass of the shuttle was taken as 100 metric tons, that of the payload as 9.5 tons, and the remaining teleoperator as 0.5 tons; the tether mass is 0.85 tons. The system was in a circular orbit of height 200 km.

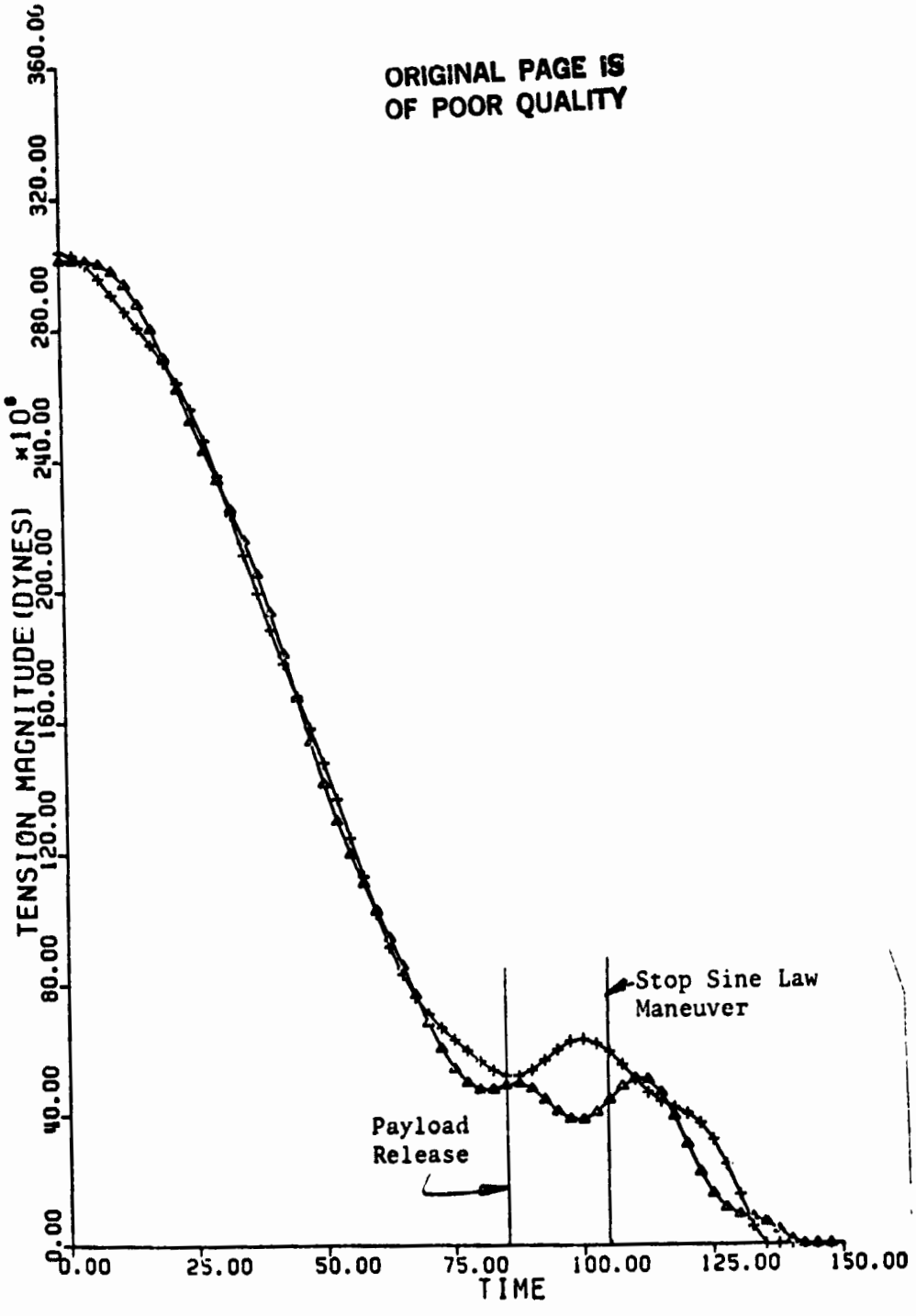

Figure 5-2. Tension vs. time for a release study (100-ton Shuttle, 9.5-ton payload, 0.5-ton teleoperator, and an 80-km length of 0.3-cm Kevlar tether) in which the tether is reeled out first to relieve tension. The maneuver is given by (deployed length) = 80 km + A[1-cos(2πt/P)], with amplitude A = -650 meters, period P = 209 sec. After 1/2 period, the deployed length is held constant. The payload is released at 85 seconds.

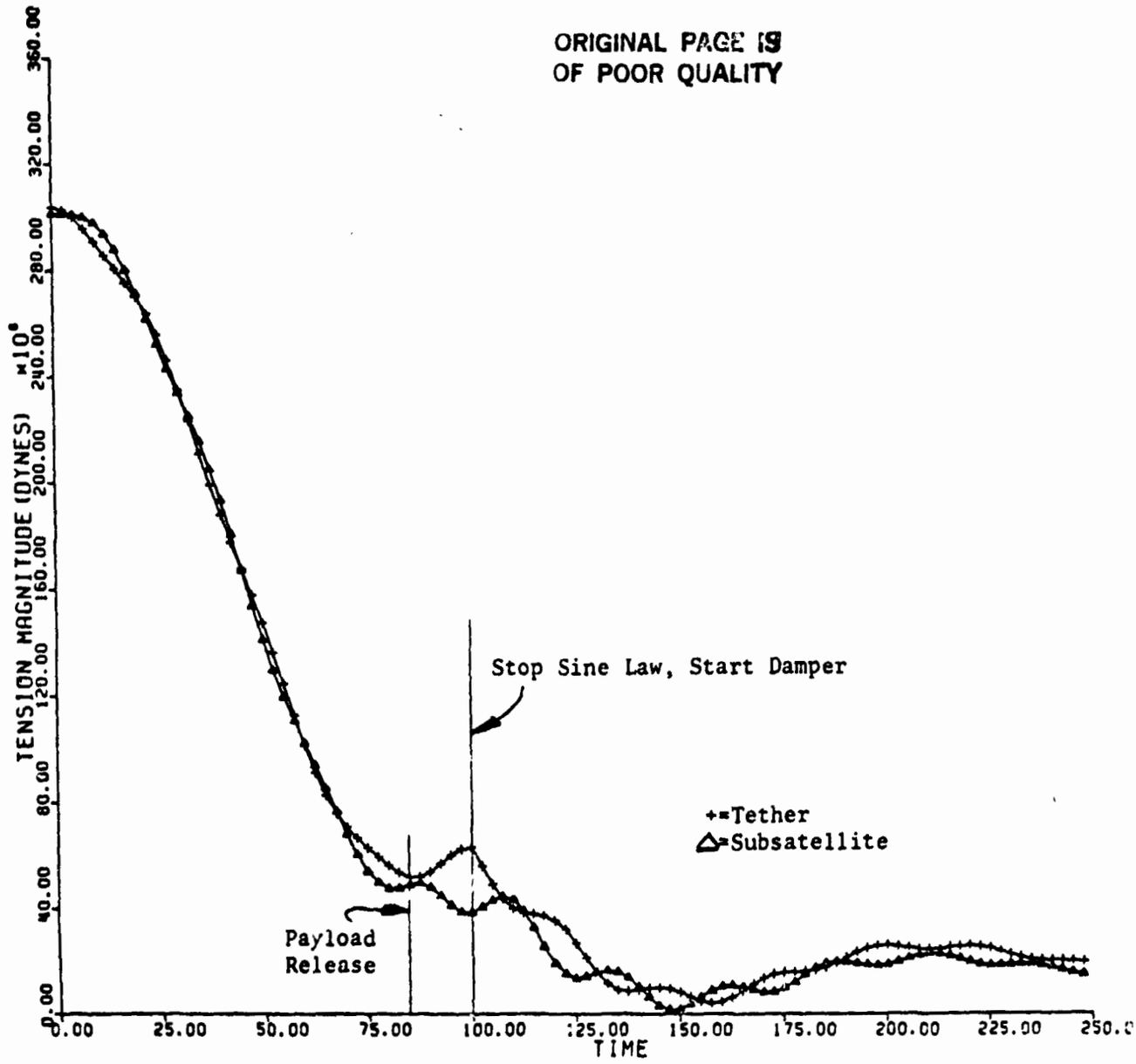

Figure 5-3. Tension vs. time for a release study in which all parameters are the same as in Figure 5-2 except that at t = 100 sec the sinusoidal maneuver is terminated (held constant) and the active damping control law is initiated (parameters T_o = 1.8 x 10^6 dynes; K = 1.6 x 10^{-5} cm-sec^{-1} $dynes^{-1}$; β = 0.041 sec^{-1}).

The fixed pre-release reel maneuver specified an addition to the natural length of $A\sin(2\pi\, t/P + \phi)$ of amplitude A and period P; the phase ϕ was, in the cases studied, $-\pi/2$ so that the maneuver started gradually. A time is also specified at which the maneuver terminates; and, after this time, the natural length remains constant (except as modified by the damping control below). Generally, this stop time is chosen as P/2, so that the maneuver "tails off" gradually as well.

The active damping control law is different in concept from the pre-release maneuver: whereas the maneuver is strictly determined by the parameters A, P, ϕ and the stop time, the active damping algorithm reacts to the state of the tether itself, as well as to parameters input at the start of the simulation; the reel control length specified by the damper of necessity depends on the tether state since the purpose is to modify whatever state is found in the direction of equilibrium.

We first applied the damping scheme to maneuvers in which the tether is reeled in before release (with a possible subsequent reel-out), then we investigated the possibility of simply reeling the tether out to relieve tension. The tension on the tether (at equilibrium) will, of course, be higher with the 9.5 ton payload still attached than with only the 0.5-ton teleoperator (and 0.85 ton of tether). To avoid a rebound of the tether it is thus imperative to reduce the tension to near the final desired equilibrium value before releasing the payload. The reel-in maneuver has the advantage that by manipulating the parameters one can also have the system nearly at rest at the moment of release. This leaves the post-release system close to equilibrium. On the other hand, by initially pulling on the

tether while the heavy payload is still attached, the maximum tension experienced during the maneuver is increased over the equilibrium by about 50%, requiring a stronger tether. If we reel out rather than in, the tension never increases above the equilibrium value; however, experiment with the simple deterministic maneuver always found the tether going slack, seemingly because the system could not be left with a near-zero velocity and oscillated strongly after release.

Our studies of the active damper in combination with a reel-in pre-release maneuver used as a starting point the case shown in Figure 4-5 of the NAS8-33691 Final Report (Colombo, 1982). The release and sinusoid parameters for this case had not been optimized, and the post-release tension variations are shown in Figure 5-4 on an expanded scale. (Note that this requires restricting the graph to times greater than 105 seconds after the maneuver starts.) No attempt was made to improve the release time or maneuver. The active damping algorithm was initiated at the moment of release, and several choices of the damping parameters are shown in Figure 5-5, Figure 5-6, and Figure 5-7. Figure 5-5 shows the best damping achieved. Although no effort was made to search fully parameter space for an optimal solution, the behavior is excellent, with a minimum tension of about 76% of the equilibrium value and major variations damping out within 20 or 30 seconds (compare to the natural oscillation period of about 22 seconds in Figure 5-4). Figures 5-6 and 5-7 illustrate how robust the algorithm is: even if the parameters are chosen very poorly, the damping is still effective. In Figure 5-6 the parameters K and β are 1.75 greater than in the best case Figure 5-5 (this was an attempt to use the measured oscillation frequency of the system rather than a

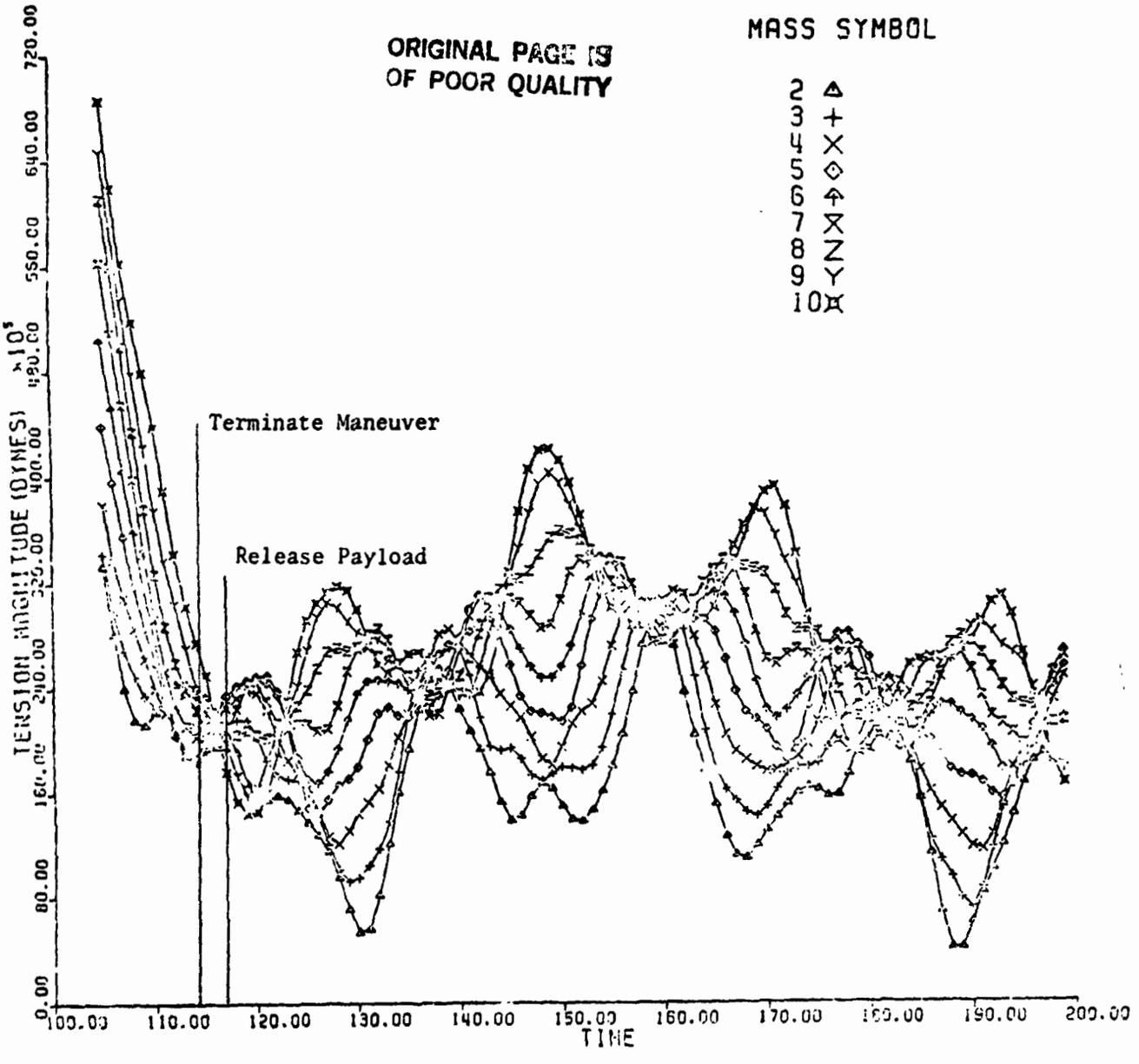

Figure 5-4. Tension oscillations after payload release, with no damping. A reel-in/reel-out sine-law maneuver was used prior to release with amplitude 176 meters, period 114 seconds, phase offset $-\pi/2$. The maneuver terminated at 114 seconds and release was at 117 seconds. We plot only from t = 105 seconds. System: 80-km tether of 0.3-cm Kevlar; 100-metric-ton Shuttle; 9.5-ton payload; 0.5-ton remaining teleoperator.

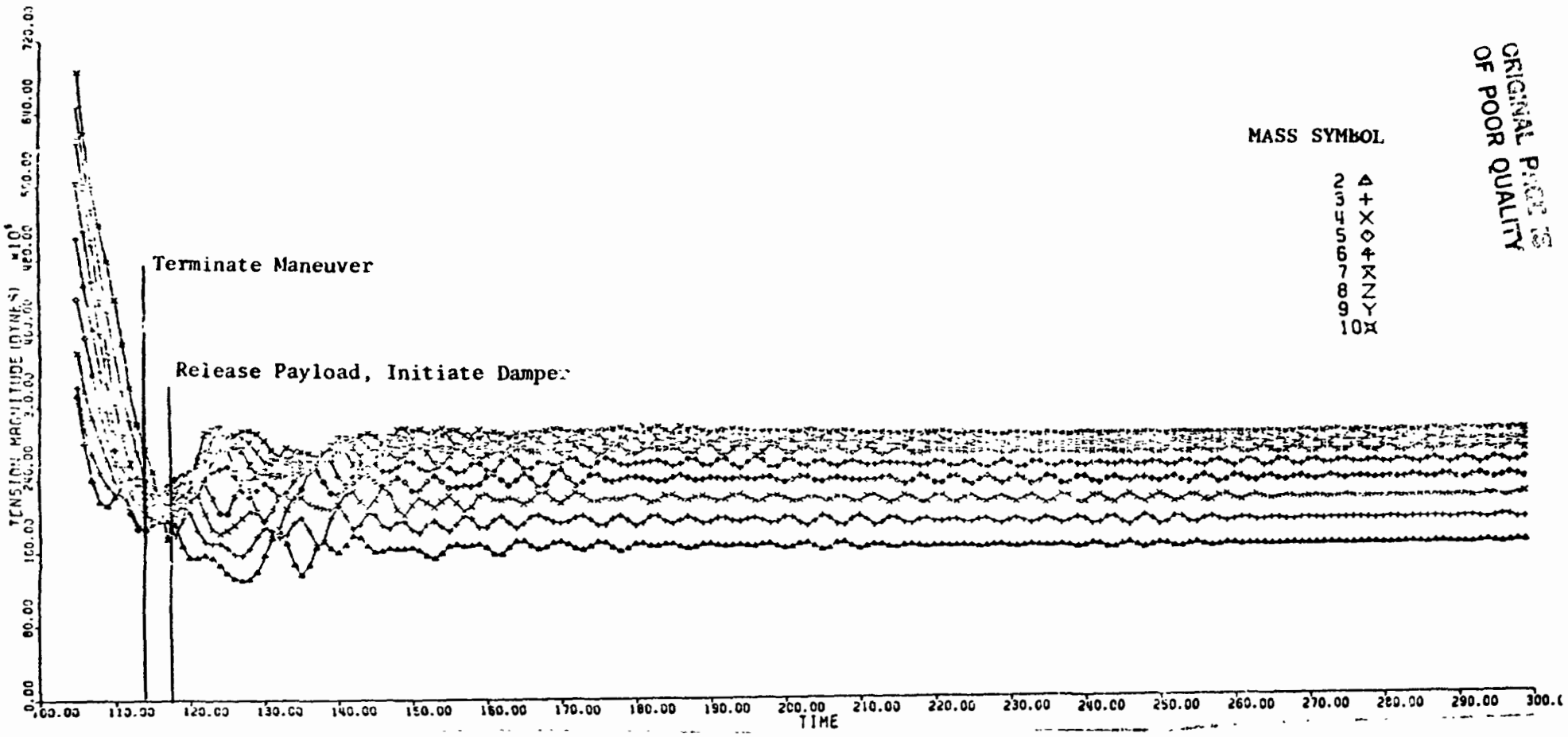

Figure 5-5. Tension oscillations after release, with active damping. The system and pre-release maneuver are the same as for Figure 5-4, and the damper started at release, t = 117 seconds. Damper parameters: $T_o = 2.86 \times 10^7 \times 10^8$ dynes, $K = 1.6 \times 10^{-5}$ cm sec^{-1} dyne^{-1}, $\beta = 0.041$ sec^{-1}.

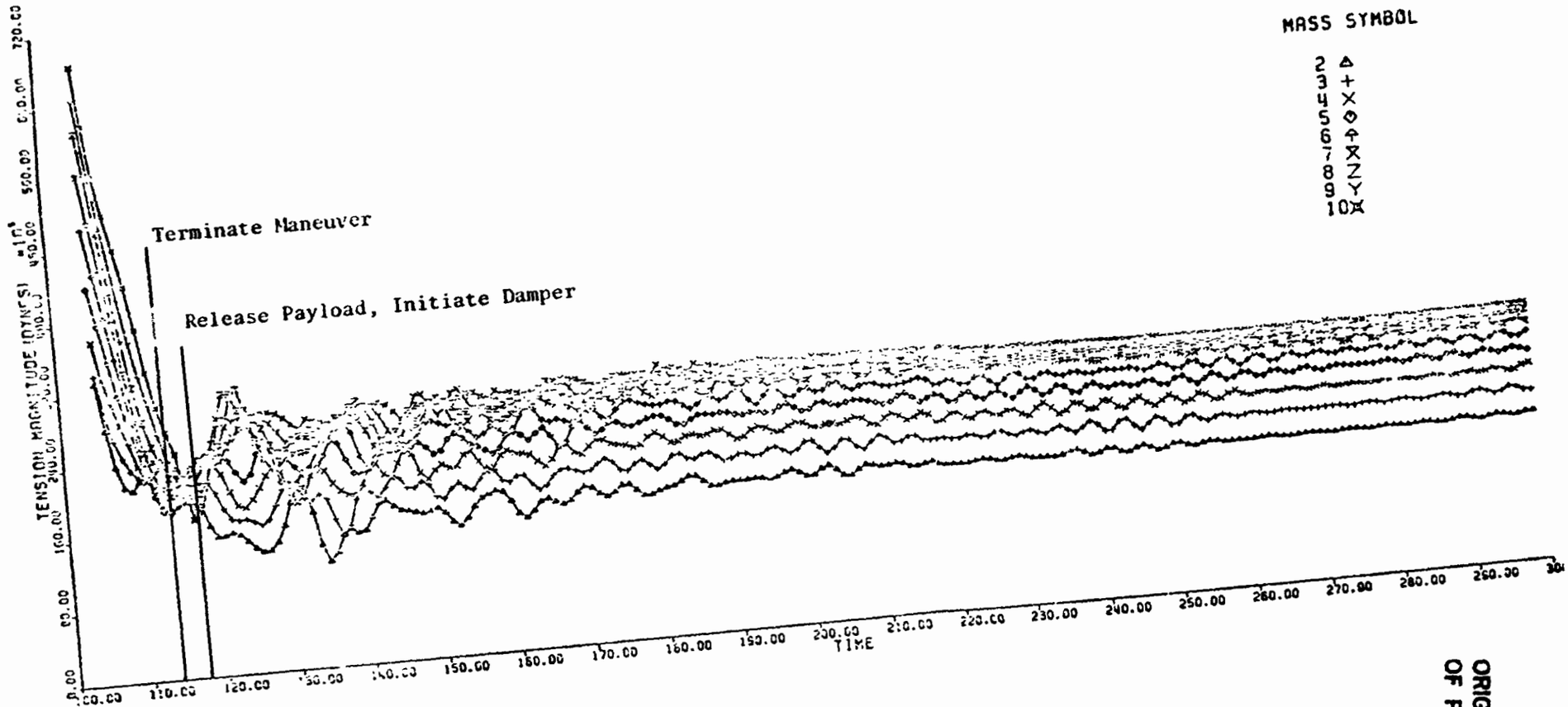

Figure 5-6. The same as Figure 5-5, except that the damper parameter K and β are 75% greater. The response is not significantly altered.

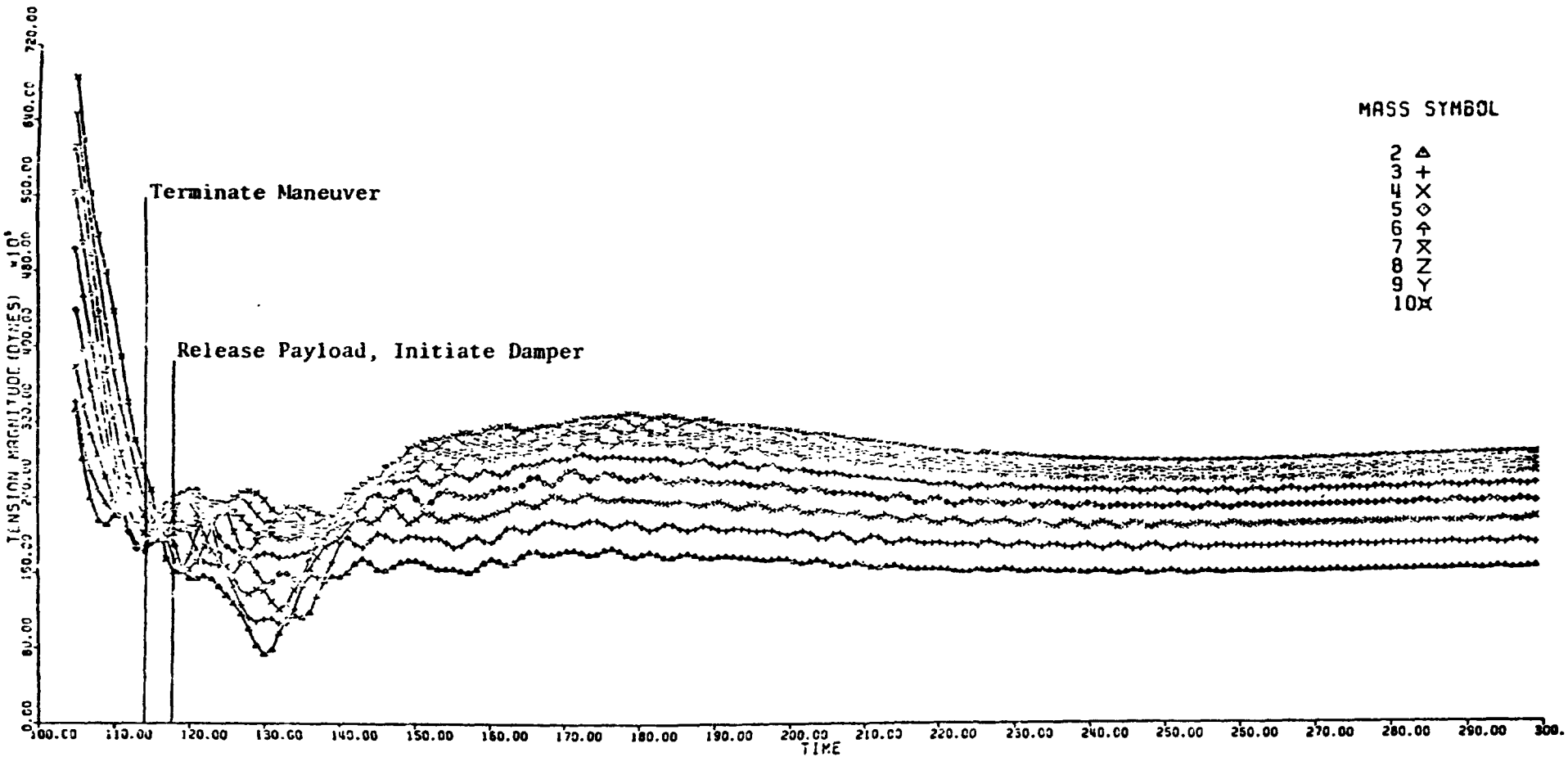

Figure 5-7. The same as Figure 5-5, except that the damper's nominal tension T_o is 63% of that used in Figure 5-5. This figure and Figure 5-6 above illustrate the robustness of the damper algorithm; its success does not depend on choosing optimized parameters.

simple spring/mass derived frequency in computing desired parameters). The difference in the tension plots is barely discernable, though Figure 5-5 is marginally better. In Figure 5-6 the nominal tension T_o was only 63% of the actual equilibrium tension at the Shuttle; though there is an initial excursion toward low tension, the behavior is still quite acceptable.

For the studies of a reel-out pre-release maneuver, we arbitrarily chose a period P for the sinusoid of P = 200 sec. (and stopped the maneuver at t = 100 sec). Varying this parameter would probably allow improvement of the post-release behavior, but did not prove necessary. Given P, simulations were made for various choices of the amplitude A and the tension plotted. Noting that the tension change is closely linear in A, we extrapolated to an amplitude (A = -406 meters) such that the minimum tension (at the subsatellite) reached was the desired post-release tension. The payload was released at the time of this minimum tension (t = 70 sec) and the damping algorithm initiated. The sinusoid maneuver continued until t = 100 sec to avoid an abrupt change in reel velocity. Damper parameters were the same as for the optimal case (Figure 5-5) described above. The resulting tension is shown in Figure 5-8 which plots the complete maneuver. Although the post-release variations are not so impressively damped as in Figure 5-5, the behavior is acceptable and doubtless could be improved with a better choice of parameters (particularly P). This clearly demonstrates the feasibility of a reel-out maneuver combined with an active damping scheme. Note: 1) The tension never goes above the pre-release equilibrium of 300×10^6 dynes; this should allow a thinner, lighter tether. 2) The tension does not fall significantly below the equilibrium value.

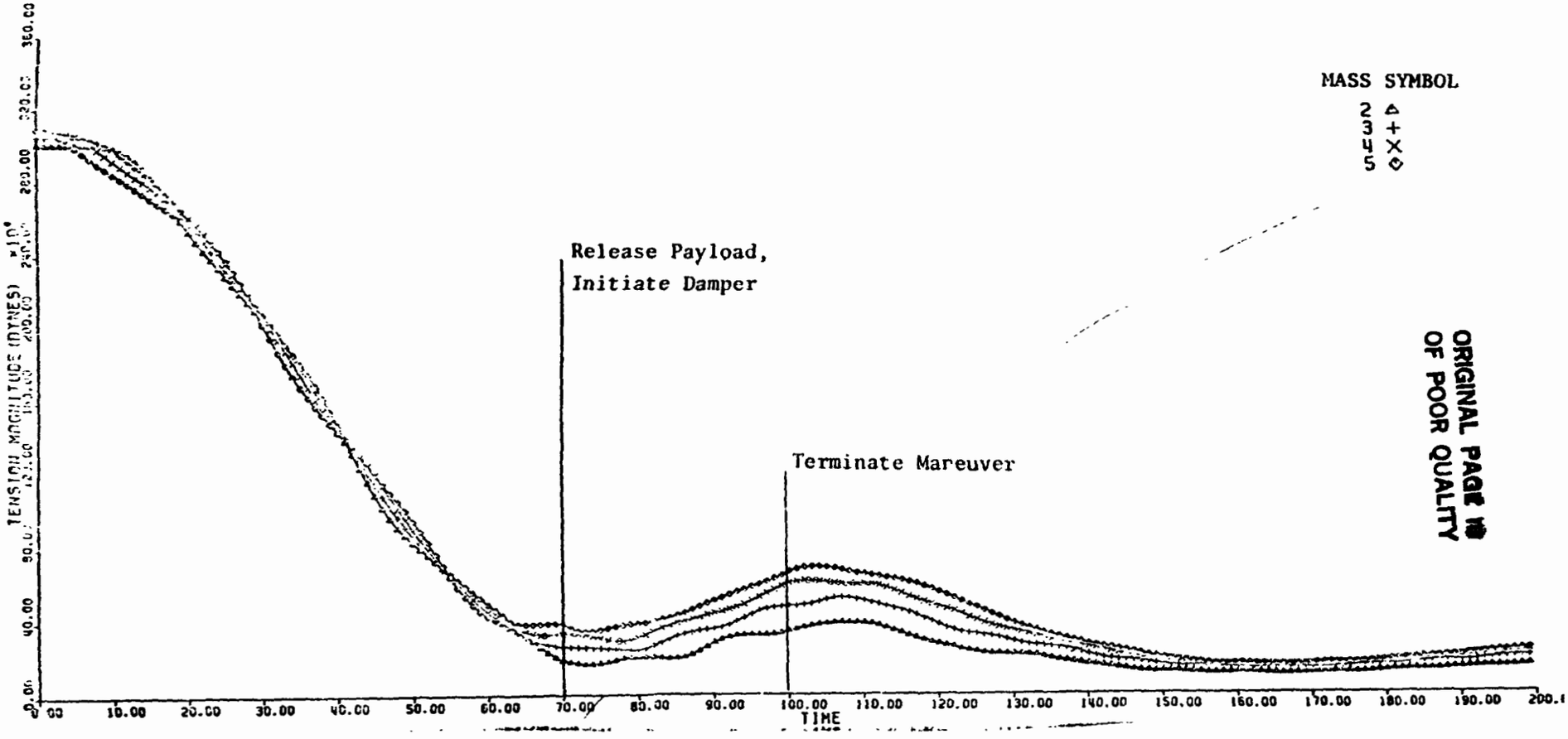

Figure 5-8. Tension variation with a pure reel-out pre-release maneuver and active damping after release. Note that the initial tension increase is avoided. The system configuration is as in Figure 5-4. The pre-release sine-law maneuver had an amplitude of 406 meters, a period of 200 seconds, and a phase offset of $-\pi/2$. Release is at 70 seconds, and the maneuver terminates at 100 seconds (P/2). Active damping begins at release with parameters $T_o = 2.86 \times 10^7$ dynes, $K = 1.6 \times 10^{-5}$ cm sec^{-1} $dynes^{-1}$, $\beta = 0.041$ sec^{-1}.

3) The total time for the maneuver, to a near equilibrium state, is about 150 sec, the same as for the reel-in maneuver.

For the cases plotted in Figures 5-5 and 5-8, the best cases, we computed the deployed length and reel velocity due to both the fixed (sinusoid) reel maneuver and the active damping control. For the case shown in Figure 5-8, these are plotted in Figure 5-9 and Figure 5-10. The maximum reel velocity is largely determined by the fixed reel maneuver, the damping control velocity being relatively smaller and only taking effect when the fixed maneuver has slowed down. The maximum velocity is 12.8 meter/sec. For the case shown in Figure 5-5, these results were not plotted nor computed in detail, but the reel maneuver has maximum velocity 4.9 meter/sec, while the damping control velocity is small, $<<$ 1 meter/sec. These velocities seem reasonable, but one could probably decrease them by varying the period of the reel maneuver. Indeed, if the tension reduction is roughly proportional to the maximum acceleration of the maneuver, we can reason as follows: the maximum velocity of a maneuver $A \sin(2\pi\, t/P)$ is $V = 2\pi A/P$, and the maximum acceleration is

$$a = 4\,\pi^2\, A/P^2,$$

or

$$V = P\, a/(2\pi)$$

$$A = P^2\, a/(4\pi^2)$$

Thus, to reduce the maximum velocity while maintaining the same acceleration a, reduce P by the desired factor and simultaneously reduce A by that factor squared. This analysis is certainly only a crude approximation but should point the way; one would have to

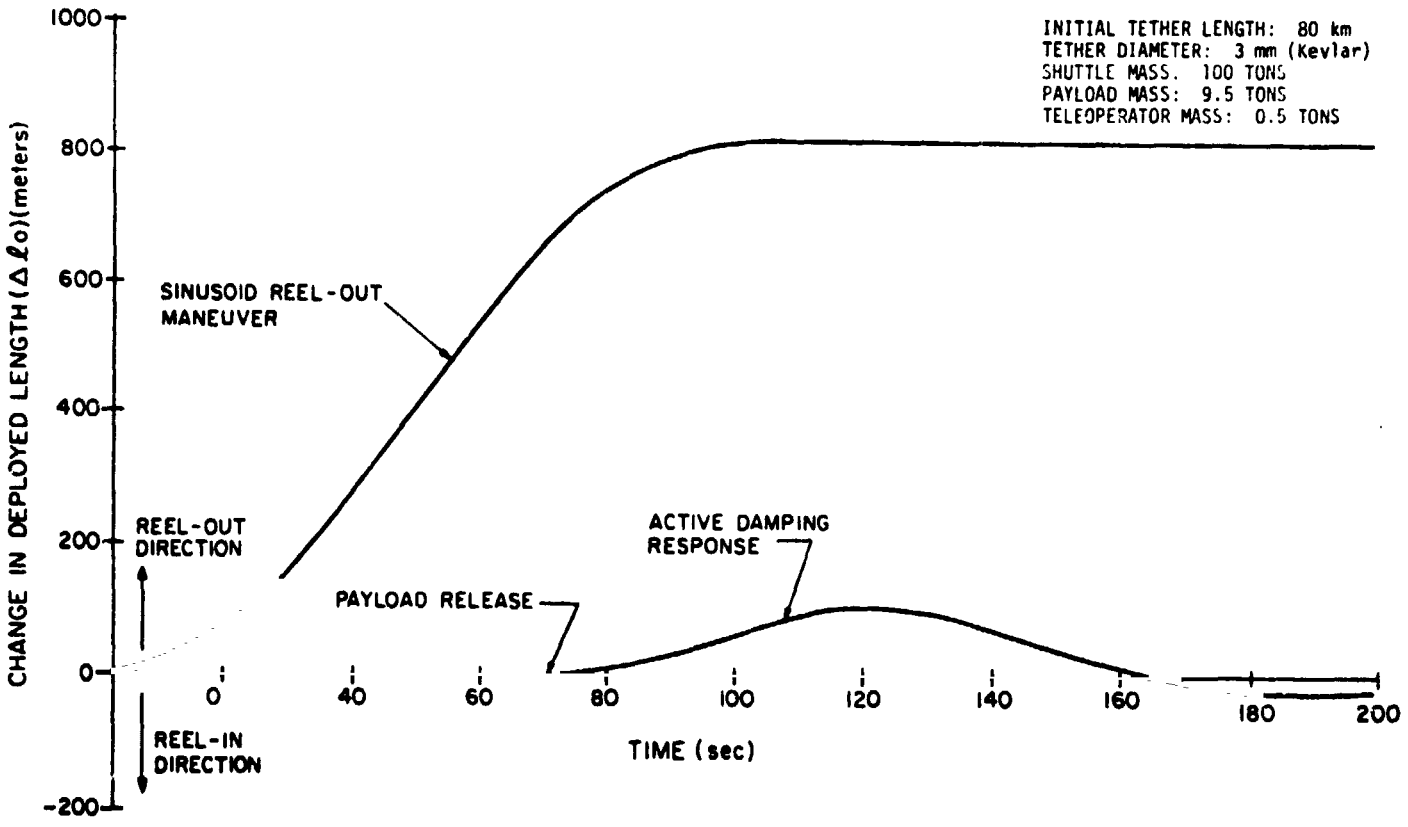

Figure 5-9. Tether deployed length as a function of time. Components due to sinusoid reel-out maneuver and active damping response shown separately.

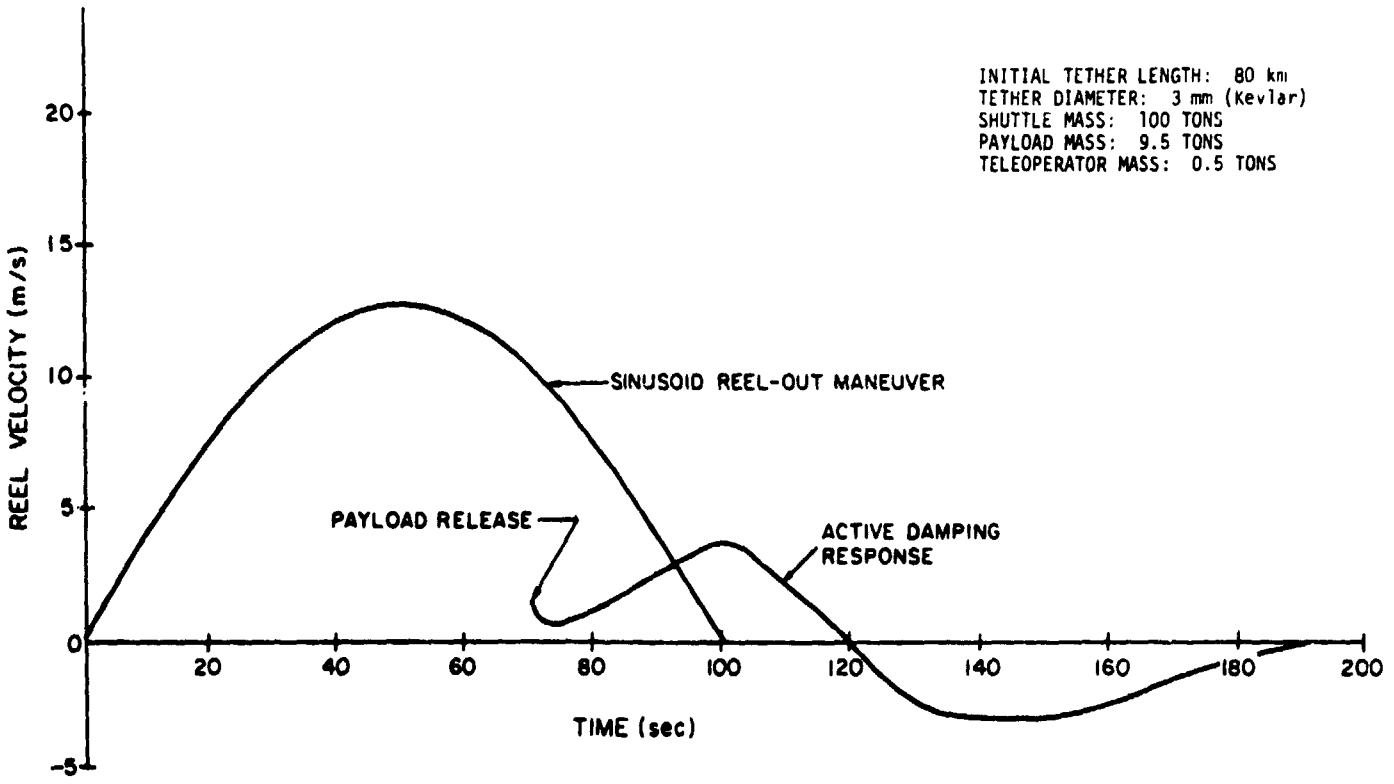

Figure 5-10. Reel velocity as a function of time. Components due to the sinusoid reel-out maneuver and active damping response shown separately.

determine the appropriate A for a chosen P by doing a test case and extrapolating linearly as done above, and possibly iterate on P.

We were only able to make an initial exploration of the release and damping behavior. A number of further possibilities present themselves. As implemented in SKYHOOK, neither the sine-law reel maneuver nor the active damping changes the mass used for the near-Shuttle tether segment. The error is not large (on the order of 10%), but should be accounted for.

There is no a priori reason that the fixed pre-release maneuver should be a sinusoid; this was chosen to give the desired gross properties with a simple two-parameter family. By properly choosing the maneuver function (which need not be a simple analytic expression), one no doubt could reduce the demands on the damping algorithm and on the reel motor, particularly in the reel-out case.

The damping law might also depend on the tension time derivative or include delay terms. The good results achieved with the simple law, however, probably do not justify this complication.

In practice, one would want to initiate the damping law gradually to avoid the sudden shock and resulting oscillations.

One might vary the damping parameters, particularly T_o, to follow the expected behavior during a maneuver such as deployment. The damper would then prevent excursions from the desired maneuver. One could perhaps even create a maneuver by suitably varying T_o between the current and derived states and letting the damper determine the exact trajectory.

5.2 Payload Transfer to Circular Orbit

Here the transfer of a payload to a moderately high circular orbit is demonstrated using an appropriate reel maneuver and the damping algorithm described in Section 5.1 to stabilize the Shuttle/Tether/Teleoperator system after release.

The Shuttle mass was 100 metric tons, the payload mass 9.5 tons, and the teleoperator mass remaining after release, 0.5 tons. The tether used was 0.3 cm diameter Kevlar with a density of 1.5 gm cm^{-3} and elasticity 0.7×10^{12} dyne cm^{-2}. The required tether length is determined by the release conditions and is derived below. This length is 61 km, with a mass of 0.65 tons. All simulations were done with six mass points: the Shuttle, the subsatellite (teleoperator or teleoperator/payload), and four tether sections.

The initial orbit of the Shuttle was a 200 to 520 km altitude ellipse (this orbit could be reached with one burn from a 200 km circular orbit). We assumed that the Shuttle had been injected into this orbit and had then deployed the tether/teleoperator/payload, so that the orbit center of the full system was in the prescribed orbit. The program which generates initial conditions for input to SKYHOOK starts an elliptical orbit at a point 90° forward from the perigee. In this case, this required an initial altitude of 355 km for the orbit center. The integration started at this point with a vertically deployed tether and proceeded until apogee, where it was desired to release the payload. A certain amount of libration was introduced in the simulation by this quarter orbit of integration, resulting in a more realistic case. In an actual, physical situation, the existing

motion due to libration and residual motion from deployment will have to be taken into account in fine tuning the pre-release maneuver and time of release.

Given the elliptic initial orbit for the orbit center, the length of tether must be determined so that when released at apogee the payload will be in an approximately circular orbit. As defined in the "Study of Certain Launching Techniques Using Long Orbiting Tethers" (Final Technical Report for grant NAG-8008, March 1981), the parameters are:

C_1 = apogee of pre-release orbit (for orbit center)

C_2 = perigee of pre-release orbit

S = radius of circular orbit of released payload

z_p = length of tether from orbit center to payload.

The known quantities are:

C_1 = 6898 km

C_2 = 6578 km

and from geometry, $S = C_1 + z_p$; S may be found from an equation on page 11 of the report:

$S^3 = (C_1^4 + C_2 C_1^3)/(2C_2)$ giving

S = 6953.48 km

z_p = 6953.48 - 6898 = 55.48 km.

Approximating the orbit center by the center of mass, recalling the masses of 100 and 10 tons, and neglecting the mass of the tether, the required total tether length is

$$z = (110/100)\ z_p = 61.03 \text{ km.}$$

This example uses a length of 61 km exactly. This is the stretched length of the tether in equilibrium at the initial point on the orbit and is a required for input to the initial condition routine. It would have been more precise to adjust the stretched length of 61 km at apogee back to the length in the gravity gradient at the initial point, but the difference is small compared to other neglected effects such as libration.

The desired elliptical pre-release orbit and the tether length which will allow release into a circular orbit have now been calculated. The final component needed is the reel maneuver and timing of the release. Because of difficulties in renovating the program to generate elliptical initial conditions. the reel maneuver was investigated separately, starting with an initial circular orbit, and later combined with the initial ellipse. This is an acceptable procedure for a first approximation, but care must be taken to operate with an orbit of the same height as the intended release: The tether tension varies as the gravity gradient, which varies as R^{-3}. The tension in a tether at 520 km altitude thus differs from that at 200 km by $(6898/6578)^{-3} = 0.867$, i.e. 13% less. Other effects, especially libration, will effect the tension, but their contribution is minor (the total difference noted when the ellipti. case was run in

fail was 0.856). Since the reel maneuver is designed to reduce the tension by some 95%, a maneuver suitable for 200 km altitude will be most unsuitable for use at 520 km - indeed, it will cause the tether to go slack. With this caution in mind, the following parameters were found to be appropriate:

Reel Maneuver: $A \sin(2\pi t / P + \phi)$

$A = -182.24$ meters

$P = 150$ seconds

$\phi = -\pi/2$ for gradual initiation of maneuver

stoptime = P/2 for gradual termination

Active Damping Algorithm: $\dot{\Delta}(t) = \kappa[T(t)-T_o] - \beta\,\Delta(t)$

$T_o = 0.16 \times 10^8$ dynes

$\kappa = 0.14 \times 10^{-4}$ cm dyne^{-1} sec^{-1}

$\beta = 0.047$ sec^{-1}

The following formulas, based on scaling arguments with coefficients derived from a sample case, provide good starting points for the active damping parameters:

$$\beta = 0.041 \text{ sec}^{-1} [d/0.3 \text{ cm}][z/80 \text{ km}]^{-1/2} [m_s/0.5 \text{ ton}]^{-1/2}$$

$$\kappa = 0.16 \times 10^{-4} \text{ cm dynes}^{-1} \text{ sec}^{-1} [d/0.3 \text{ cm}]^{-1} [z/80 \text{ km}]^{1/2} [m_s/0.5 \text{ ton}]^{-1/2}$$

$$T_o = 0.886 \times 10^8 \text{ dynes } [z/80 \text{ km}] \left[\frac{m_s + 1/2 m_t}{0.924 \text{ ton}}\right]$$

$$m_t = 0.848 \text{ ton} \left[\frac{z}{80 \text{ km}}\right]\left[\frac{d}{0.3 \text{ cm}}\right]$$

although the optimum tension T_o to use is best derived by measuring the actual tension in the damped, released state in a sort of bootstrap procedure. Here, d is the tether diameter, z is length, m_s the subsatellite mass, and m_t the tether mass. The release time was

chosen as the moment when the tension at the subsatellite (payload + teleoperator) was the same as the ultimate equilibrium tension at the teleoperator after release. As with the tension T_o at the Shuttle, a first approximation to this desired tension is

$$T_{subsat} = 0.165 \times 10^8 \text{ dynes } [z/80 \text{ km}] \ [m_s/0.5 \text{ ton}]$$

which must then be iterated to use the actual relaxed tension after a successful, but sub-optimal, release is achieved. The release time derived by this method is 55 seconds. One final point to note: this maneuver uses a strict reel-out control law, without an initial reel-in. This leaves the released payload with a slight outward radial velocity relative to the orbit center; thus, to get a circular orbit (zero radial velocity), the release must occur slightly after apogee, when the system has a net inward velocity.

These components can now be "patched" together. First, an elliptical orbit was generated beginning with a vertically deployed tether 90^o forward from perigee. This orbit was followed until somewhat after apogee (1/4 orbit) with no release. A sample run of the reel maneuver without release was also prepared. Programs were written to read the SKYHOOK simulator output and print tables of various quantities at each output interval, specifically, the radii and velocities in the radial and in-plane directions of the Shuttle and subsatellite, the circular velocity for these radii, and the velocity and position of the subsatellite as perceived in the coordinate system centered on the Shuttle and with axes in the radial and in-plane directions (all out-of-plane components were zero). From these tables, the time at which the system's inward velocity would balance the release velocity relative to the orbit center was

estimated. This is the first approximation to the release time, and by subtracting 55 seconds from this time a start time for the reel maneuver was obtained.

Some details, such as the effects of libration, were neglected in deriving these start and release times. The next step was to refine the estimates. To reduce computation time a SKYHOOK input file was created, on the basis of the SKYHOOK output from the initial elliptical orbit, which allowed the start of the integration shortly before the maneuver start time derived above. Some leeway was left so that this start time could be varied. Several orbits were run with different maneuver start times and no payload release. For each start time, a release time was defined as that time when the total radial velocity of the subsatellite (payload) was zero. Then, by tabulating the release time relative to the start time (this should be 55 seconds for optimal post-release tether behavior) and the difference between the actual in-plane velocity and the circular velocity at the subsatellite radius (which should be zero for a circular release) as a function of time, it was discovered that the first quantity varied much more rapidly than the others, so the relative release time was chosen to determine the start time, and hence the timing of the entire maneuver.

Thus, by beginning with a deployed tether in elliptical orbit, conducting a tension-reducing maneuver and releasing the payload at a time carefully chosen to control the tether's post-release oscillations and to leave the payload with zero radial velocity, the payload orbit was placed in an almost perfectly circular orbit. The final eccentricity was 1.7×10^{-4} which was deemed acceptable.

No attempt was made to analyze the dependence of the final orbit on the other parameters available, nor to modify those parameters to achieve a more nearly circular orbit. The primary parameters available are the initial orbit parameters (say the minimum and maximum heights) and the tether length. The release maneuver has relatively little impact, the velocities involved being small (6 meter/sec) compared to the radial velocity of the elliptical orbit even a minute from apogee (12 m/s). How might these parameters be adjusted to produce a circular orbit if the theoretically derived ones had not been adequate? From a computational standpoint, the simplest way would be to adjust the apogee height, reducing it to increase the payload release velocity relative to circular velocity. The release maneuver would not need to be recomputed, only scaled. In a physical situation, the orbit is more likely to be given and then only the tether length can be varied. This would require recomputing both the initial orbit and the release maneuver. Indeed, an ideal control algorithm for release would also contain a relatively brief (perhaps 5 to 10 minutes) deployment/retrieval phase for minor adjustments to the tether length before starting the tension reducing pre-release maneuver. To achieve circular release at a prescribed height, two of the three parameters (apogee height, perigee height, tether length) must be determined, leaving only one free parameter to meet other mission requirements.

One such mission requirement would be for the final orbit of the system to be high enough after release to avoid re-entry. SKYHOOK was allowed to integrate the system after payload release well past perigee. The Shuttle's lowest altitude was determined to be 165 km,

dangerously low in a practical situation. There was no retrieval of the tether, but this would raise the orbit only slightly. To avoid this situation the initial orbit would need a higher perigee, requiring two shuttle burns for injection.

To summarize:

Shuttle:
100 metric tons

Subsatellite:
9.5-ton payload
0.5-ton teleoperator (remains after release)

Tether:
Length: 61 km
Mass: 0.65 ton
0.3-cm diameter Kevlar

Initial orbit:
Perigee altitude: 199 km
Apogee altitude: 519 km
Eccentricity: 0.0237
Started 90° after perigee, with tether fully deployed

Reel maneuver begins at 1386 seconds after start;
parameters
Amplitude: 182 meters
Period: 150 seconds
Half-period sinusoid maneuver, shifted so that onset and stopping are gradual (a cosinusoid).
Pure reel-out maneuver.

Release payload at 1441 seconds.

Active damping of tether begun at release.

Final orbit of payload:
Eccentricity: 0.00017
Altitude: 575 km

Final orbit of Shuttle:
Perigee altitude: 165 km
Apogee altitude: 514 km

The tension and a side-view of the system are plotted for t = 0 to 2000 seconds in Figures 5-11 and 5-12. The tension behavior near

PAYLOAD RELEASE
TO CIRCULAR ORBIT
TENSION VS. TIME

SHUTTLE MASS:	100 ton
PAYLOAD MASS:	9.5 ton
TELEOPERATOR MASS:	0.5 ton
DEPLOYED TETHER LENGTH:	61 km

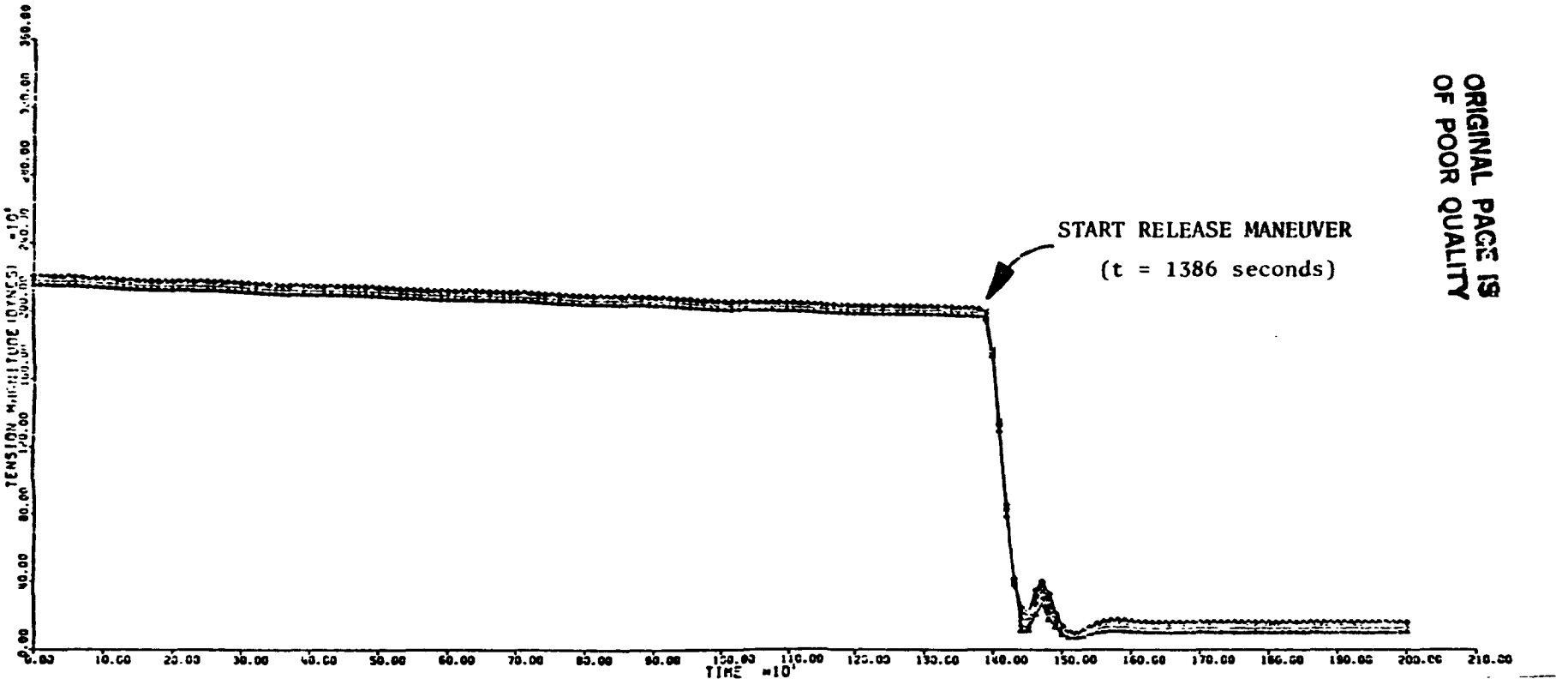

Figure 5-11. Tether tension from the initially deployed configuration (t = 0) through the release and damping (t =1441) until t = 2000 seconds. The detailed mission profile is described in the text.

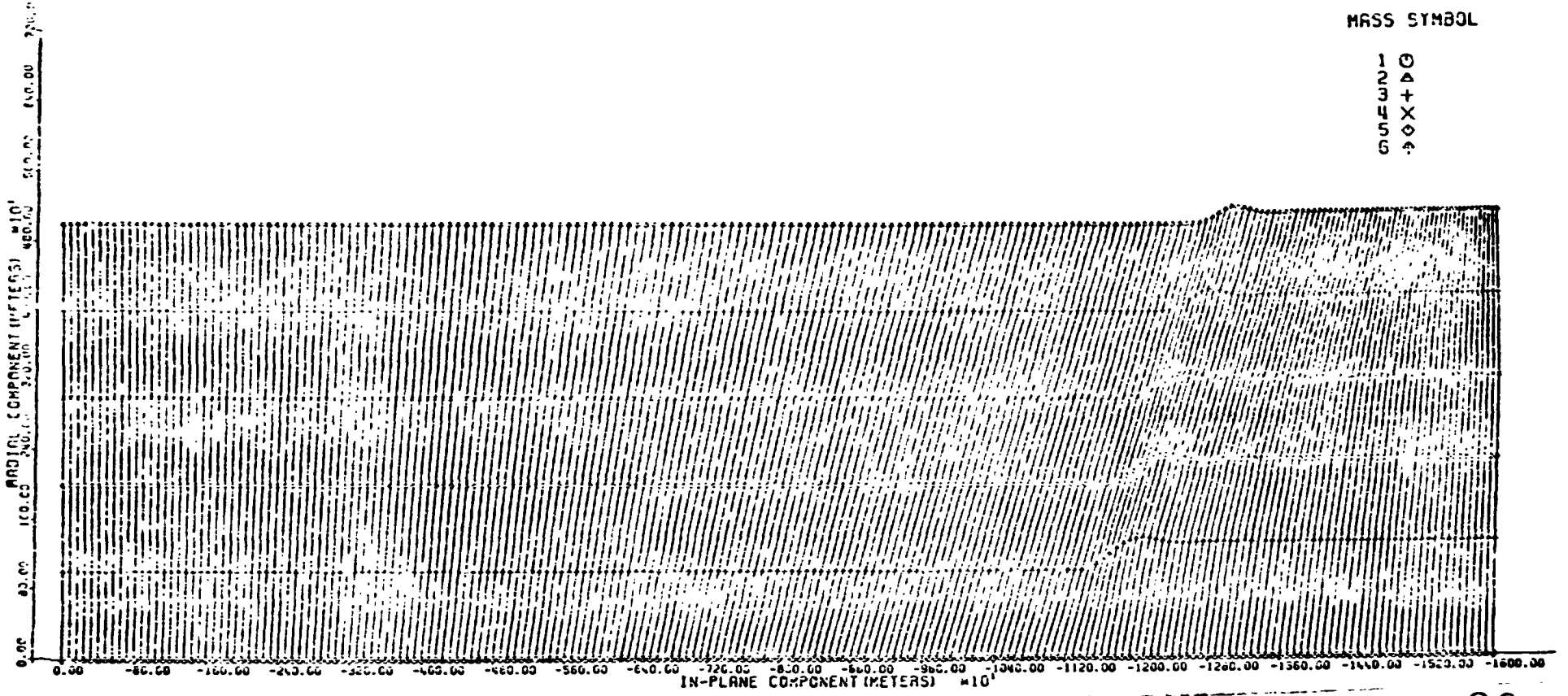

Figure 5-12. For the case in Figure 5-11, the side-view (in-plane vs. radial components) of the system is plotted at 10-second intervals. Each view is arbitrarily displaced in the in-plane direction to avoid overlap, the earliest configurations being at the left. The components are relative to the Shuttle, and uniformly spaced constant vectors have been subtracted from each mass's position (effectively "cutting out" a portion of tether) to expand the resolution in the radial direction.

the time of release is plotted in Figure 5-13. with an expanded time scale. Figure 5-14 gives a schematic representation of the payload orbital transfer.

5.3 Payload Acquisition by a Tether Deployed from a Space Station

The tether behavior when a payload is suddenly acquired by a tether deployed downward from a Space Station in moderately high orbit was investigated.

For this specific case the Space Station was placed in a 500 km altitude circular orbit. The payload was injected from an initial 200 km parking orbit, giving a 200 km perigee for the payload delivery orbit. The tether length and the apogee height of the payload orbit were then adjusted so that 1) at apogee, the payload is at the same height as the teleoperator end of the tether and 2) the velocity of the payload in orbit at apogee is the same as the tethered teleoperator velocity.

If R is the station's orbital radius and L is the tether length then the teleoperator velocity is

$$V_T^2 = [(R-L)/R]^2 \quad GM/R$$

or

$$V_T^2 = (1-\lambda)^2 \ (GM/R)$$

where $\lambda = L/R$ is what we want to find.

The payload orbit's perigee is specified. The small parameter δ is introduced so that the perigee radius is $(1-\delta)R$. The apogee is given by condition (1) as $(1-\lambda)R$ and hence the semimajor axis is $a = [1-(\lambda+\delta)/2]R$. Then, applying $V^2 = GM\,[2/r - 1/a]$ at apogee, $r = (1-\lambda)R$, the payload velocity is $V_p^2 = (GM/R)\,[2/(1-\lambda)-1/(1-(\lambda+\delta)/2)]$.

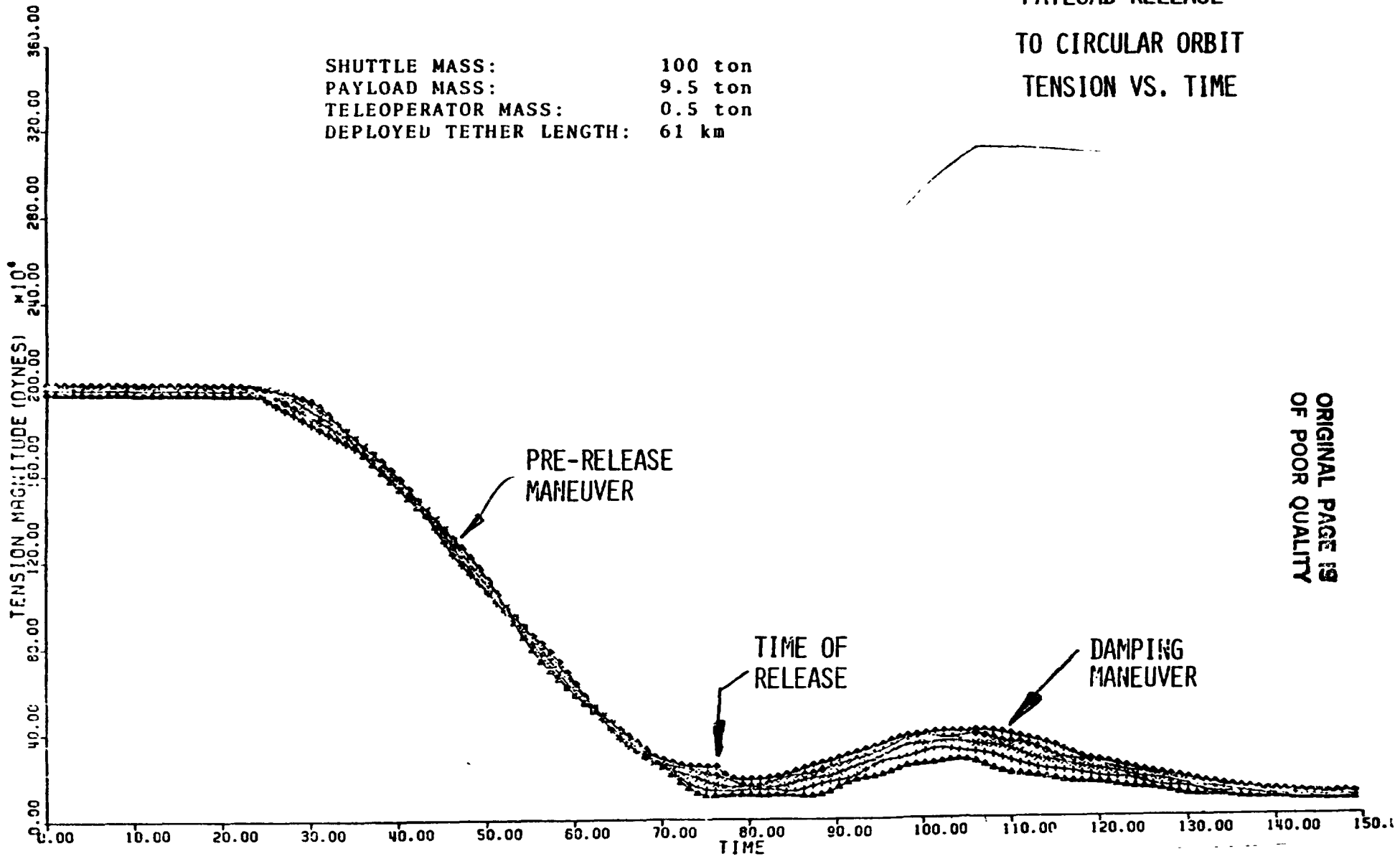

Figure 5-13. The tether tension is plotted near the time of release, with an expanded time scale. The pre-release maneuver and active damping are more readily seen.

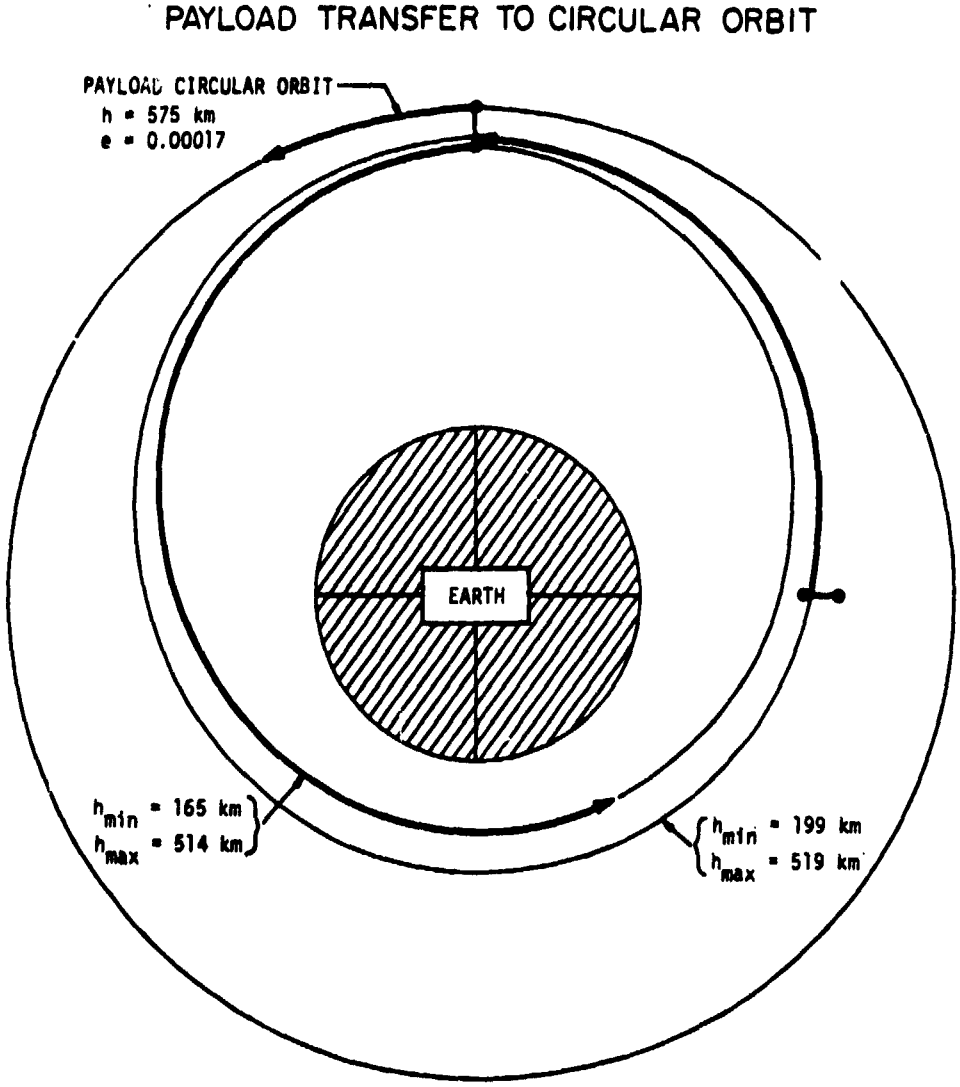

Figure 3-14. A schematic view of the various orbits discussed in the text. The heavily drawn portions represent actual trajectories.

Condition (2) requires equating V_p and V_T, leading after some manipulation to

$$[1-\lambda]^3\ [1-(\lambda+\delta)/2] = 1-\delta$$

This is an equation to be solved for λ, the scaled tether length, given the parameter δ, the scaled difference between the Space Station and payload pre-injection orbital radii. Since λ and δ are small, a first-order solution gives $\lambda=\delta/7$. The equation was solved numerically for $\delta \in [0,1]$ and the ratio $(7\lambda/\delta)$ to the first-order solution is plotted in Figure 5-15. For this case δ = (500-200)/(6378+500) = 0.0436, which is interpolate to $(7\lambda/\delta)$ = 1.0275 giving L = 44.036 km. This is the length from the orbit center to the teleoperator. Using the masses given below and a center-of-mass approximation, a total tether length of 44.07 km is obtained.

In summary, the system parameters are: Space Station orbit, 500 km altitude circular; payload orbits, 200 km perigee and 456 km apogee: Space Station mass, 1000 metric tons:Tether parameters, 44.07 km long, 0.3-cm diameter Kevlar:Teleoperator mass, 0.5 ton:Payload mass, 9.5 ton.

Figure 5-16 shows the tension response when the payload is suddenly acquired at t = 10 seconds. Note the strong tension oscillations with period about 185 seconds, with maximum tension about 3.2×10^8 dynes. By applying the active damping algorithm discussed in Section 5.1 (above) the tension response of Figure 5-17 is achieved. The damper was turned on at the moment of acquisition, with parameters $K = 2.66 \times 10^{-6}$ cm dynes^{-1} sec^{-1}, $\beta = 0.012$ sec^{-1} and $T_o = 1.6 \times 10^8$ dynes (chosen slightly less than the expected past-acquisition equilibrium tension of 1.68×10^8 dynes to reduce the

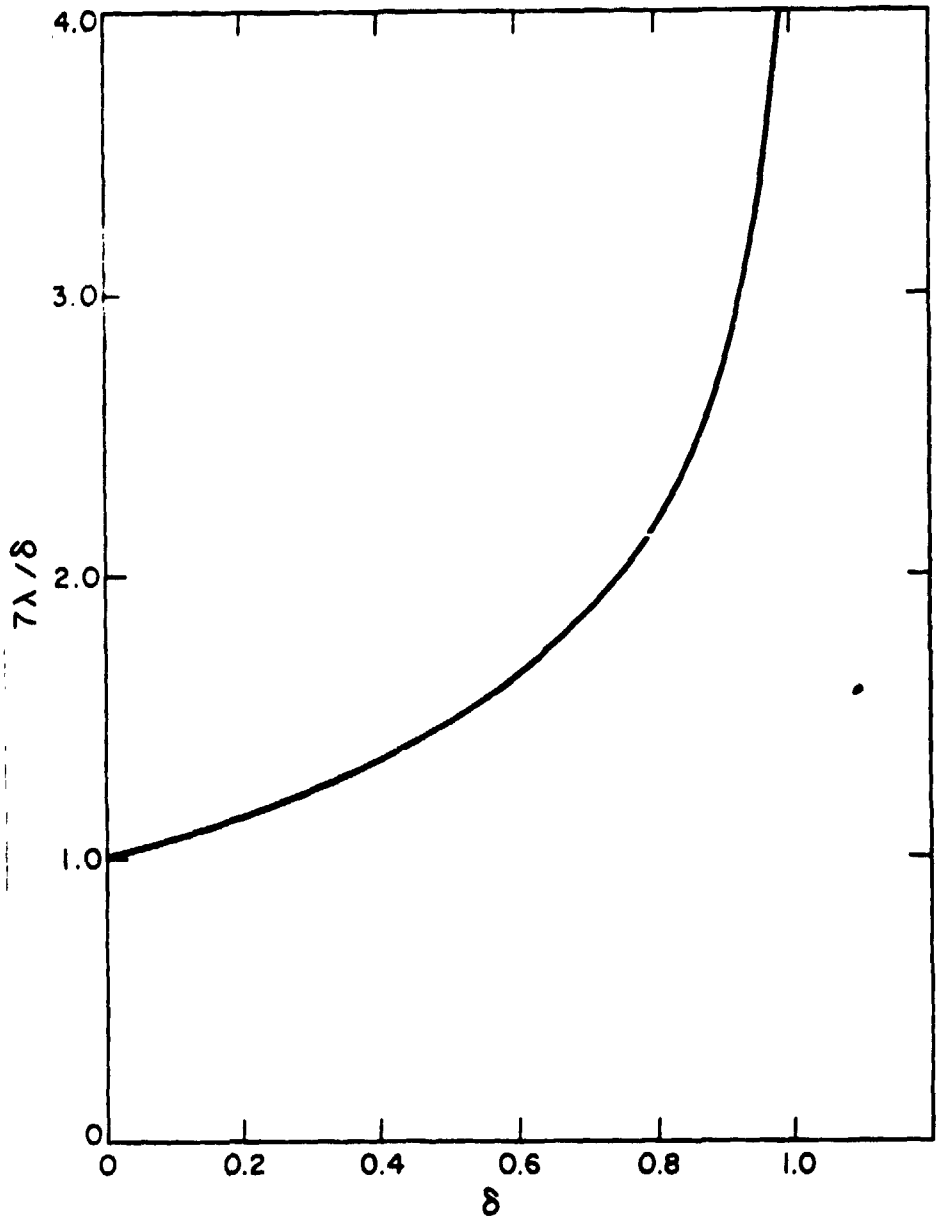

Figure 5-15. λ vs. δ. λ is computed from the equation $[1-\lambda]^3[1-(\lambda+\delta)/2]=1-\delta$ for the parameter δ with range 0 to 1. λ is the scaled tether length (L/R) and δ is the similarly scaled difference in height between the station orbit and the payload parking orbit. The ratio of the actual solution λ to the first-order approximation δ/7 is plotted.

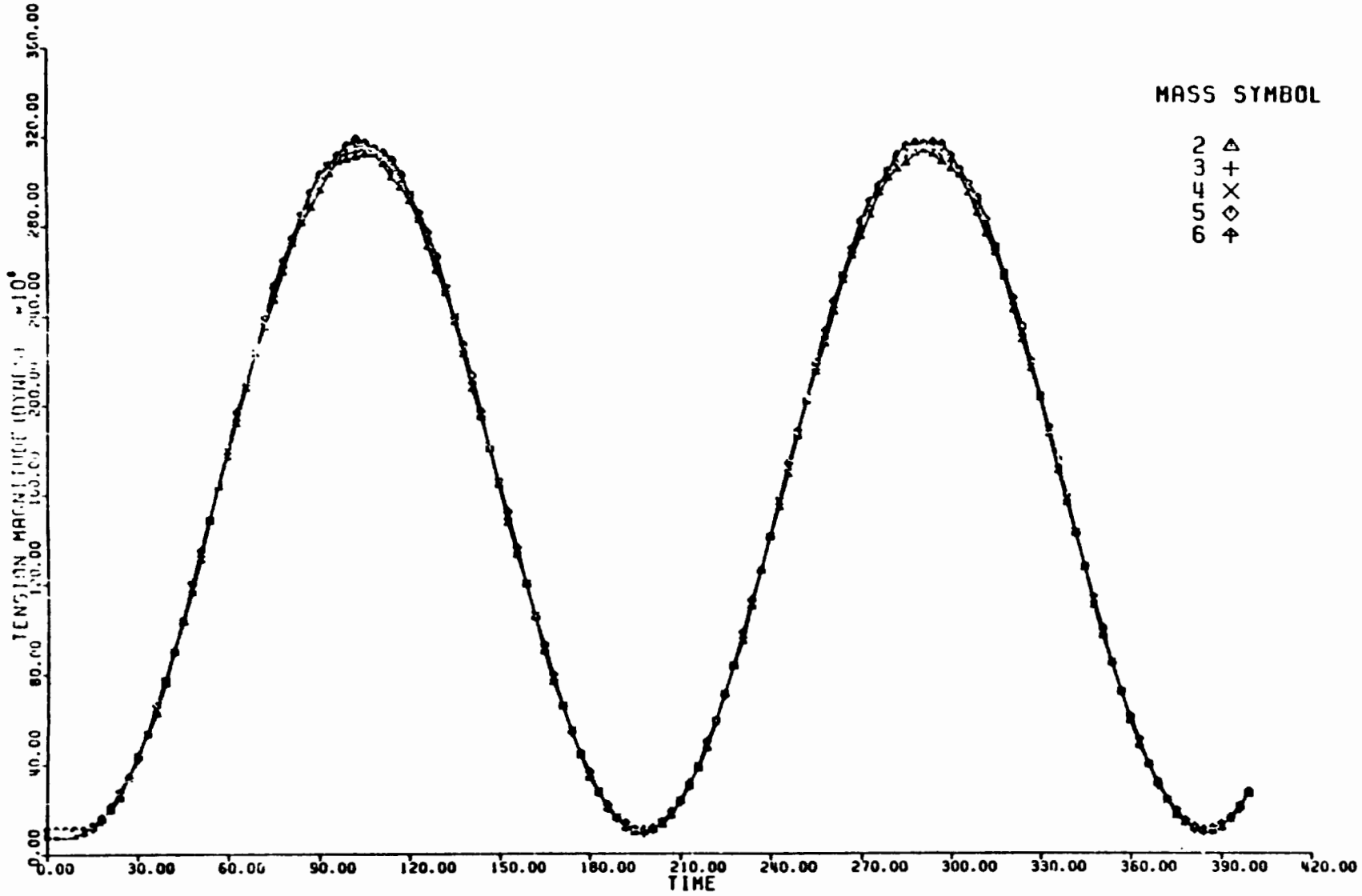

Figure 5-16. Tether tension vs. time for a case in which the payload is acquired with no other maneuver or damping. The system (1000-metric-ton Space Station, 0.5-ton teleoperator, 44 km of 0.3-cm diameter Kevlar tether) was initially in equilibrium in a 500-km circular orbit, with the tether deployed downward. A 9.5-ton payload was acquired with zero relative velocity (payload delivery orbit, 200 to 456 km) at t = 10 sec. Note the oscillation with period about 185 sec.

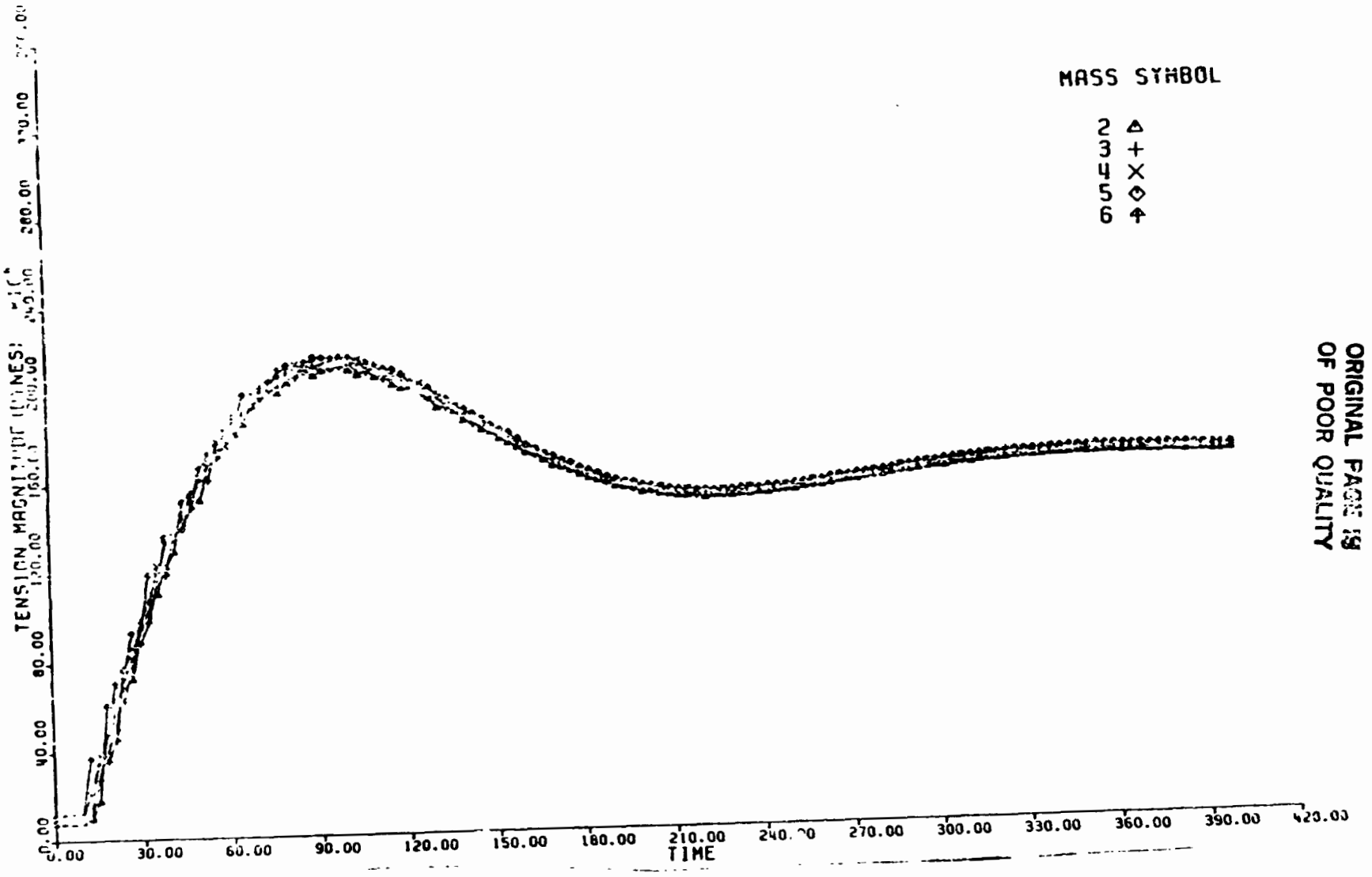

Figure 5-17. Tension vs. time for a case similar to Figure 5-16, except that the active damping mechanism is turned on at acquisition. Damping parameters: $T_{o1} = 1.6 \times 10^{8}$ dynes, $K = 2.66 \times 10^{-6}$ cm dynes^{-1} sec^{-1}, $\beta = 0.012$ sec^{-1}.

first tension maximum). The system reaches a state of virtual equilibrium in about six minutes and the maximum tension reached, about 2.15 x 10^8 dynes, is only about 28% above final equilibrium and 67% of the maximum in the undamped case.

For future comparisons, the damped case of Figure 5-17 is plotted to a different scale in Figure 5-18. Figure 5-18(a) shows the tension vs. time while Figure 5-18(b) is a side-view plot (radial vs. in-plane components) of the tether state at two-second intervals, with the spacing between mass points reduced to 1/2 km to emphasize the motions. Without this scale expansion, Figure 5-18(b) would appear as a motionless "picket fence".

It would be desirable to reduce the tension overshoot from that found for the simple damping-at-acquisition case. As a first approach, the damping algorithm was turned on before acquisition, allowing it to increase the tension somewhat. The tension vs. time plot for such a run, with the damper initialized at t = 0 and the payload acquired at t = 9 seconds, is shown in Figure 5-19. The damping behavior is substantially improved and the maximum tension is only 1.95 x 10^8 dynes, 16% above the equilibrium of 1.68 x 10^8 dynes, compared to 2.15 x 10^8 dynes for the simple damping case. Unfortunately, this method is not very stable: Figure 5-20 shows a case in which acquisition did not occur until 20 seconds after the damper was initialized at t = 5 sec. The tension plummets after about 10 seconds of damping and the tether goes slack soon after acquisition. These two examples show that the peak tension, hence the tether strength needed, can be reduced by suitable pre-acquisition maneuver, but that slight changes in the maneuver can have drastic

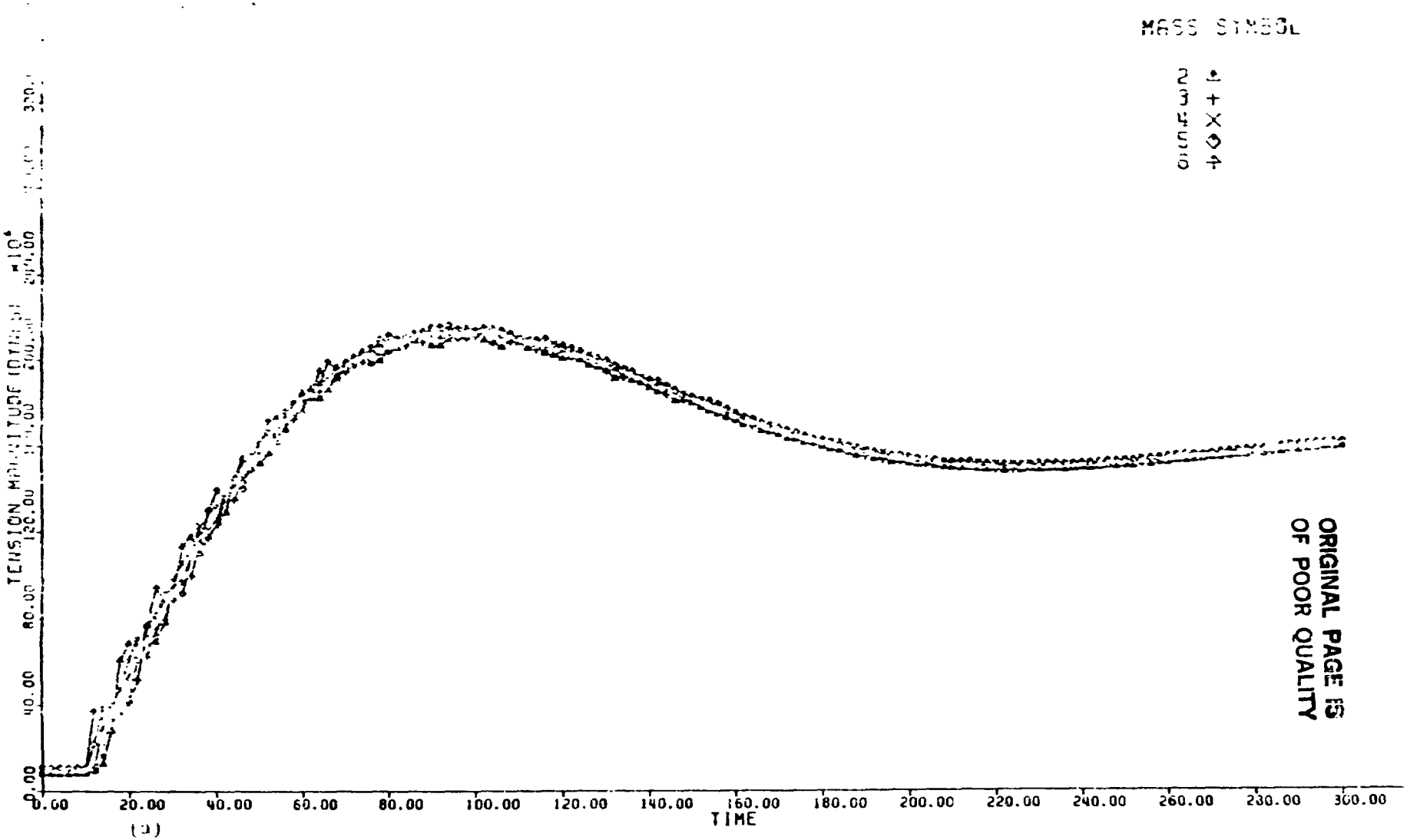

Figure 5-18. Tension vs. time and radial vs. in-plane behavior for the case shown in Figure 5-17, plotted with an expanded time scale for comparison with future runs and with an acquisition time of t = 10 sec. (a) Tension vs. time. (b) A series of radial vs. in-plane plots of the tether system. The successive plots are at two-second intervals, the same as the plotted points in (a), and the station position is arbitrarily shifted to the right at each interval so that the horizontal axis is also, effectively, a time axis with the same scale as (a). A constant (in time) vector is subtracted from the position of each mass to emphasize the displacements. The vectors (one for each mass) are such that at t = 0 the spacing between masses is 1/2 km.

Figure 5-18 (b)

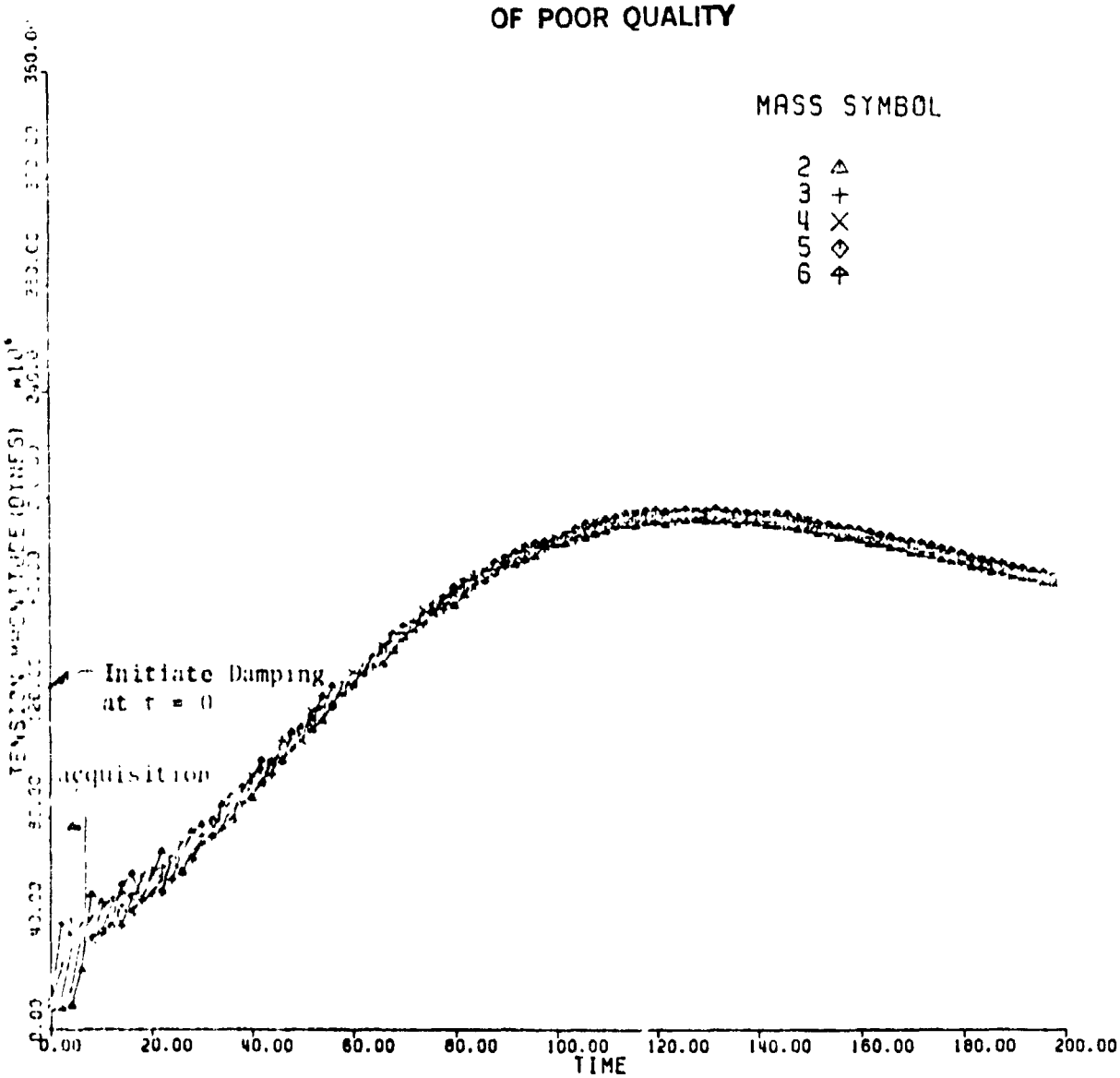

Figure 5-19. Post-acquisition tension variations are reduced by turning on the active damper at t = 0 and delaying acquisition until t = 9 seconds.

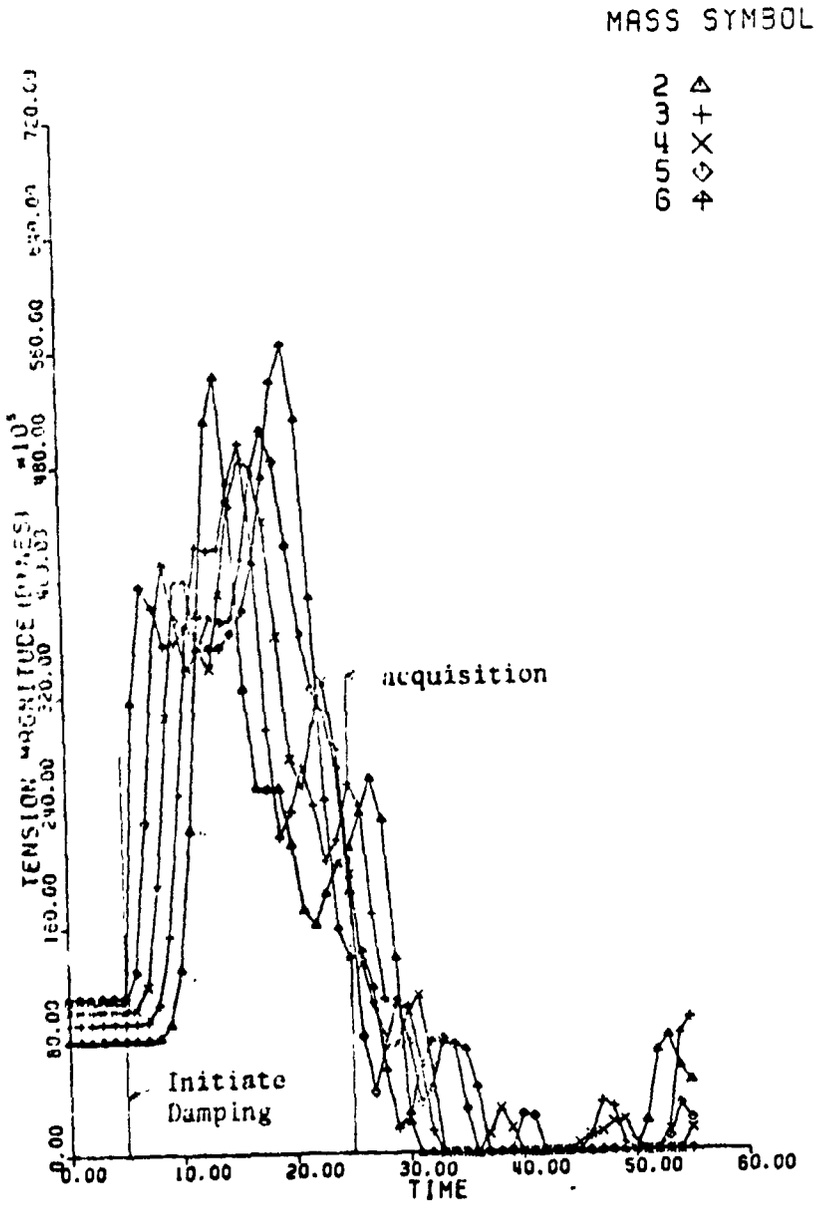

Figure 5-20. Tension vs. time when the payload is not acquired until 20 seconds after the damper is started (at t = 5 seconds). The tension had already begun to decrease when acquisition occurred and went slack at t = 31 seconds. (Note the expanded time scale in this plot.)

effects. Experimentation with a fixed sinusoid maneuver, as used in the previous release studies, would be worthwhile. This situation would probably be less sensitive than the use of the active damping algorithm to generate the maneuver.

The payload transfer orbit is likely to be slightly in error, so that the tether will suffer additional disturbance due either to maneuvering of the teleoperator or to acquisition of the payload with a non-zero velocity. Several cases were run in which the payload had a small residual velocity (3 m sec^{-1}) at acquisition and with the velocity vector in various directions. The tension and side-view plots are given in Figure 5-21 (velocity in-plane) and Figure 5-22 (velocity out-of-plane). We also show the front-view (i.e. radial vs. out-of-plane components) in Figure 5-23 (velocity radial, directed away from the station) and Figure 5-24 (velocity radial, directed toward the station). In all of these cases the payload was acquired and the damper initiated at t = 0. Also, the radial component scales in all cases are expanded by a factor of about 18 to show the motion clearly.

The fundamental lesson of these cases is that the situation is stable and the damping algorithm is able to cope adequately with these disturbances as well as the simple acquisition with zero relative velocity.

The tether response in all cases is much as expected. The tension response in the in-plane and out-of-plane cases, Figures 5-21(a) and 5-22(a), is very close to that in the zero-velocity case, Figure 5-18(a), which is understandable since tension is force along

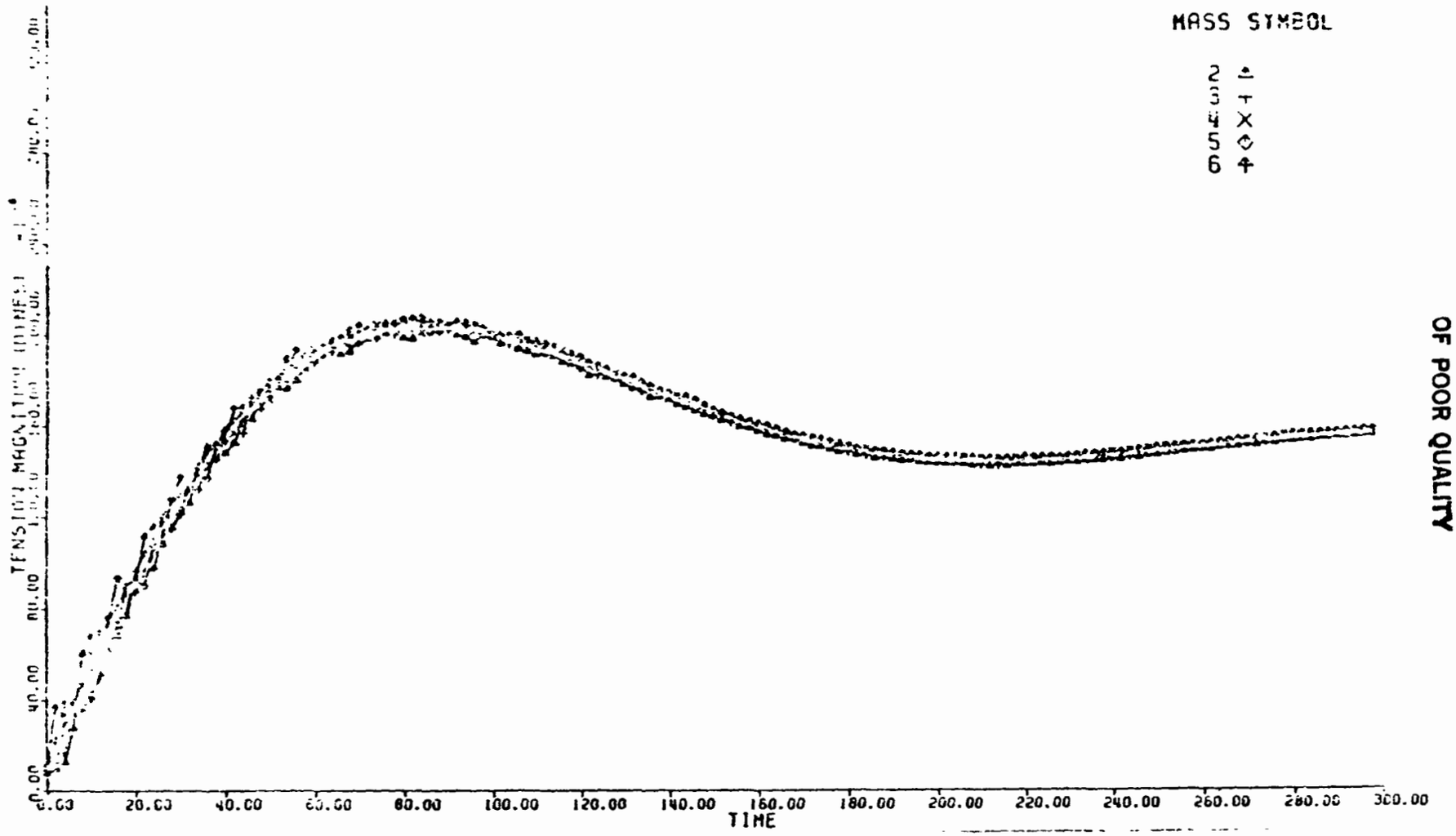

(a)

Figure 5-21. Plots, for the case in Figure 5-18, but with acquisition occurring with a 3 meter/sec relative velocity in the in-plane direction along the orbit. (a) Tension vs. time. (b) Radial vs. in-plane behavior.

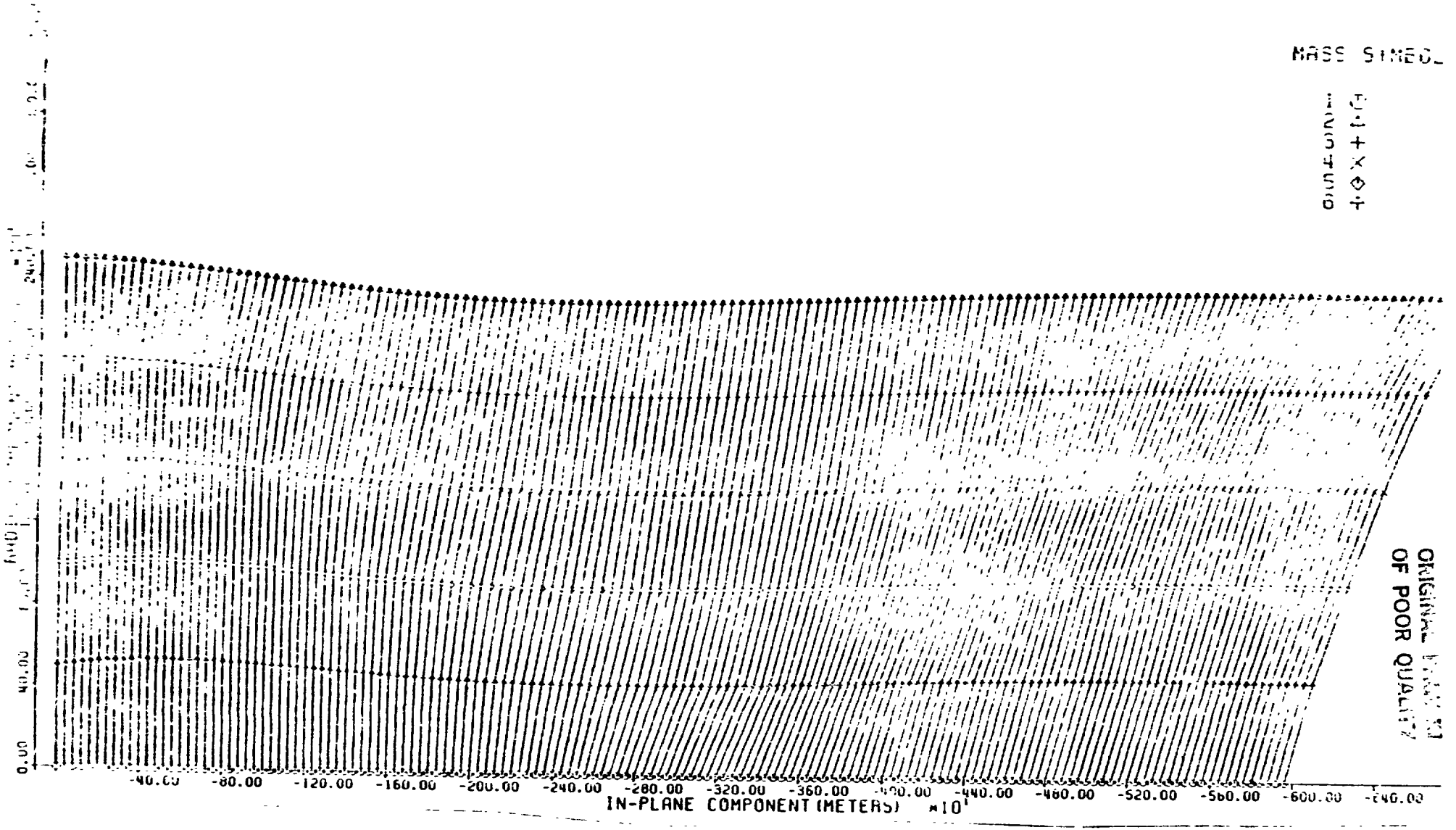
MASS SIMEOL
0.00
-40.00
-80.00
-120.00
-160.00
-200.00
-240.00
-280.00
-320.00
-360.00
-400.00
-440.00
-480.00
-520.00
-560.00
-600.00
IN-PLANE COMPONENT (METERS)
OF POOR QUALITY

Figure 5-21 (b)

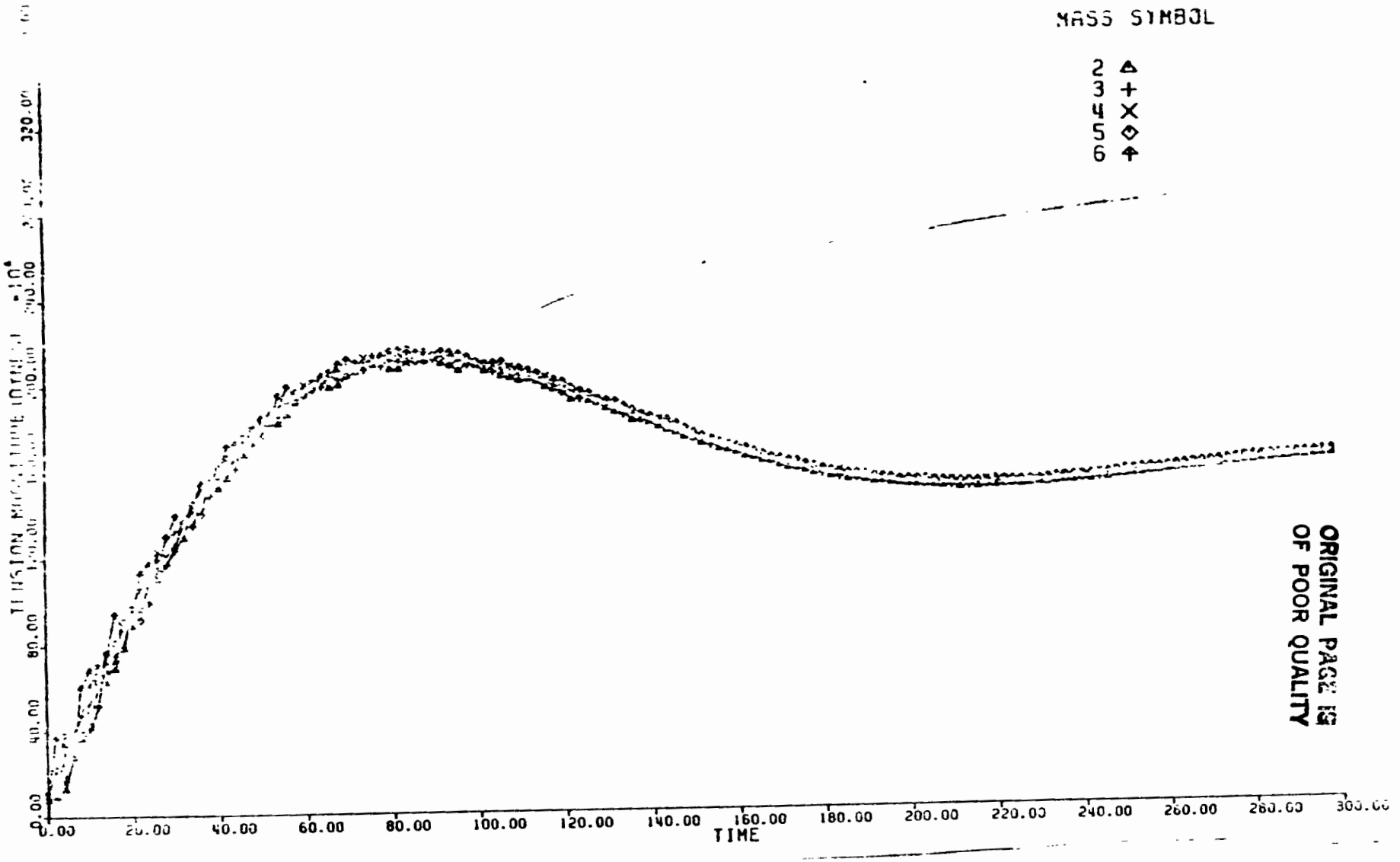

Figure 5-22. As for Figure 5-21, except that the velocity is in the out-of-orbit plane direction. (a) Tension vs. time. (b) Radial vs. in-plane behavior. (c) Radial vs. out-of-plane behavior.

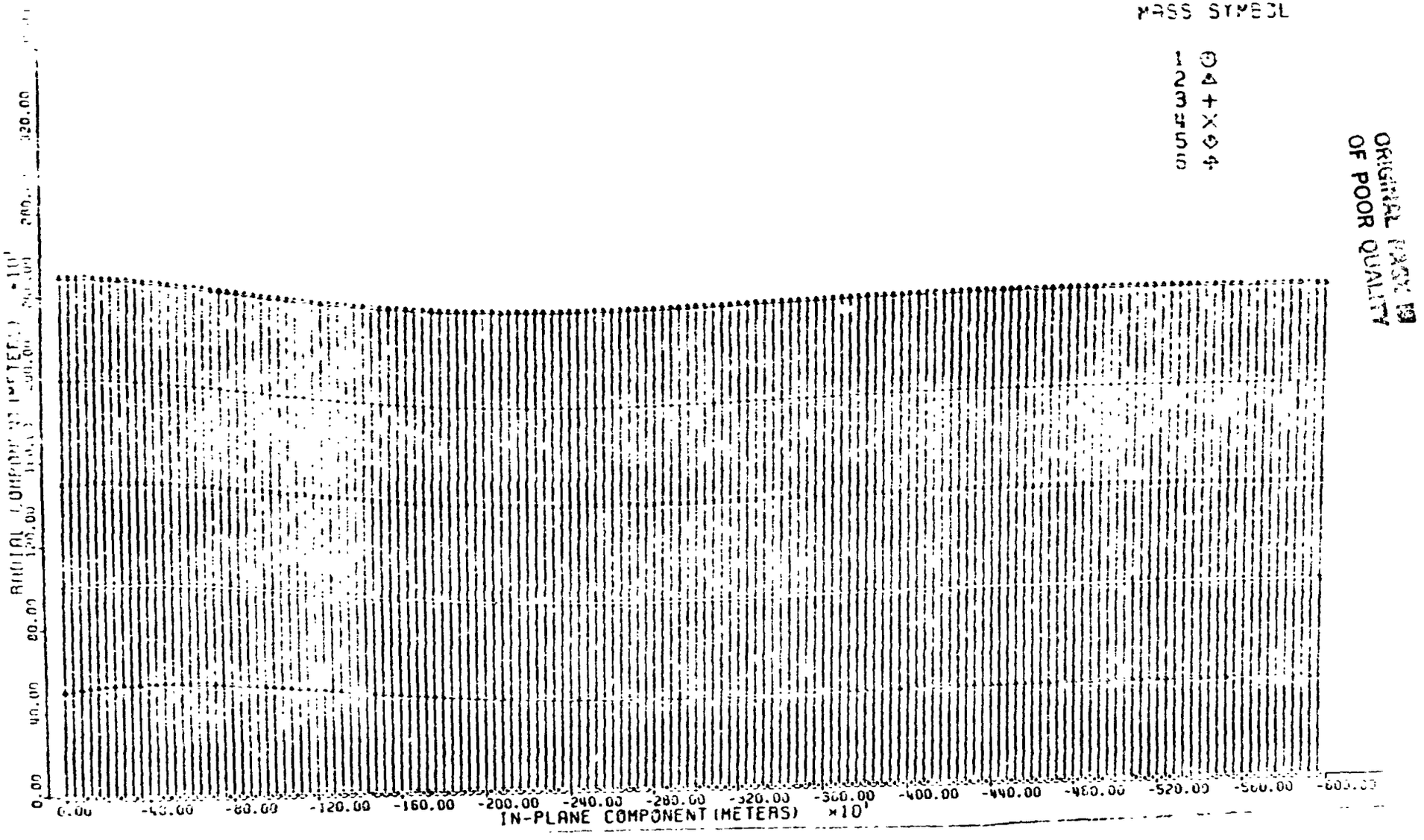

Figure 5-22 (b)

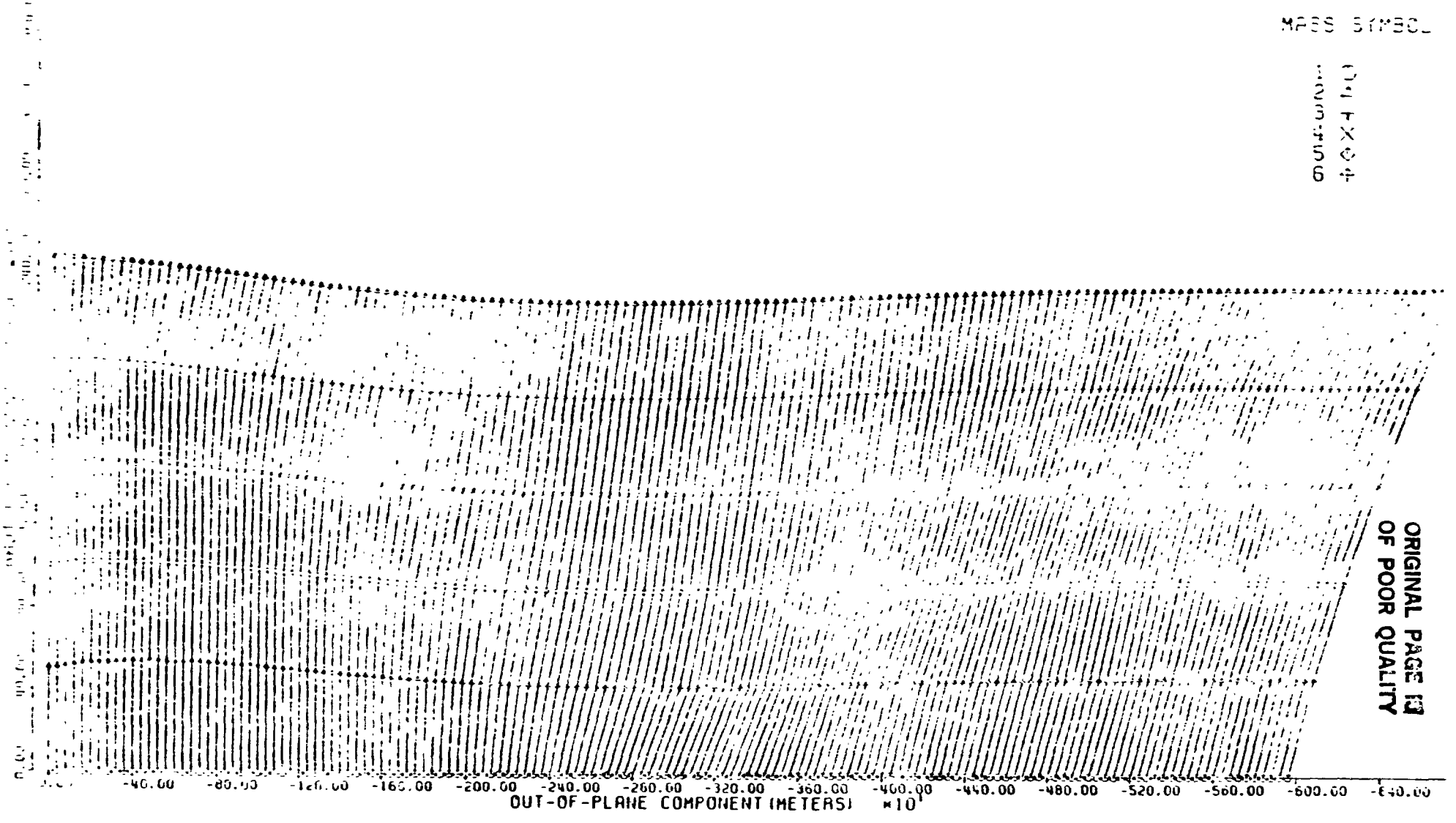
MASS SYMBOL
-40.00
-80.00
-120.00
-160.00
-200.00
-240.00
-280.00
-320.00
-360.00
-400.00
-440.00
-480.00
-520.00
-560.00
-600.00
-640.00
OUT-OF-PLANE COMPONENT (METERS) ×10
ORIGINAL PAGE IS
OF POOR QUALITY

Figure 5-22 (c)

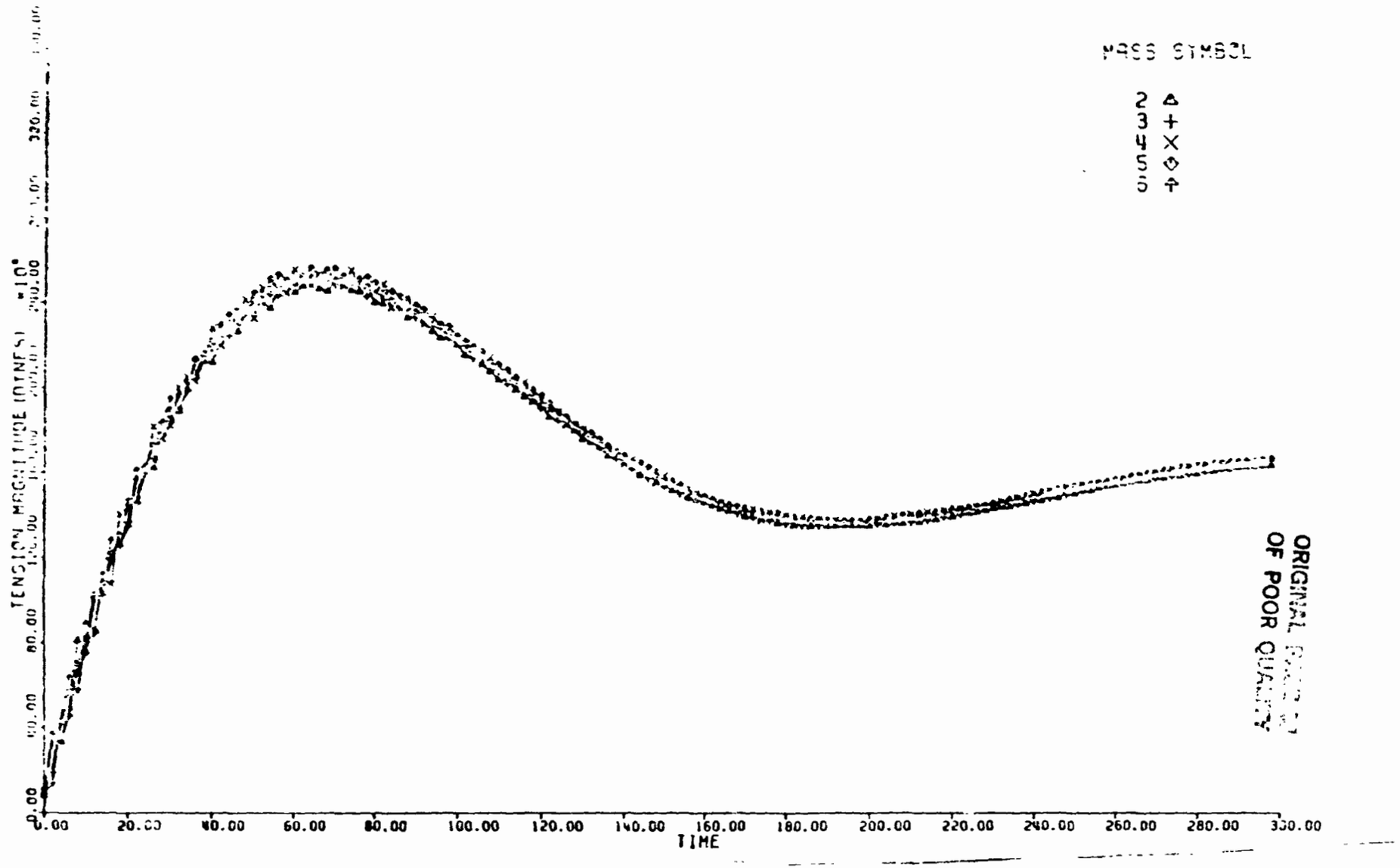

Figure 5-23. As for Figure 5-21, except that the velocity is radial, directed away from the station (downward). (a) Tension vs. time, note the tension variation is greater than the other cases. (b) Radial vs. in-plane behavior.

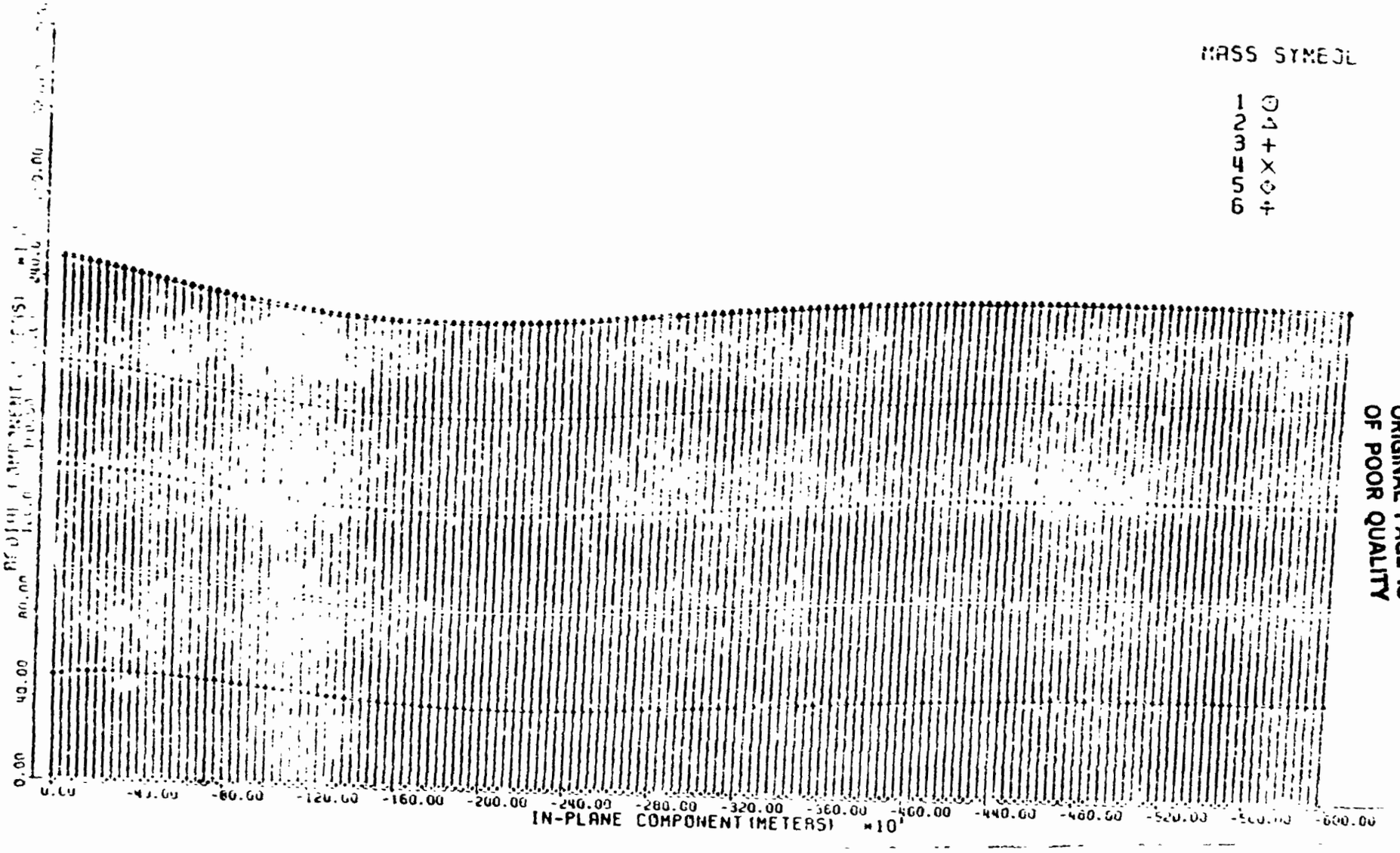
MASS SYMBOL
1
2
3
4
5
6
0.00
40.00
-60.00
-120.00
-160.00
-200.00
-240.00
-280.00
-320.00
-360.00
-400.00
-440.00
-480.00
-520.00
-600.00
IN-PLANE COMPONENT (METERS)
ORIGINAL PAGE IS
OF POOR QUALITY

Figure 5-23 (b)

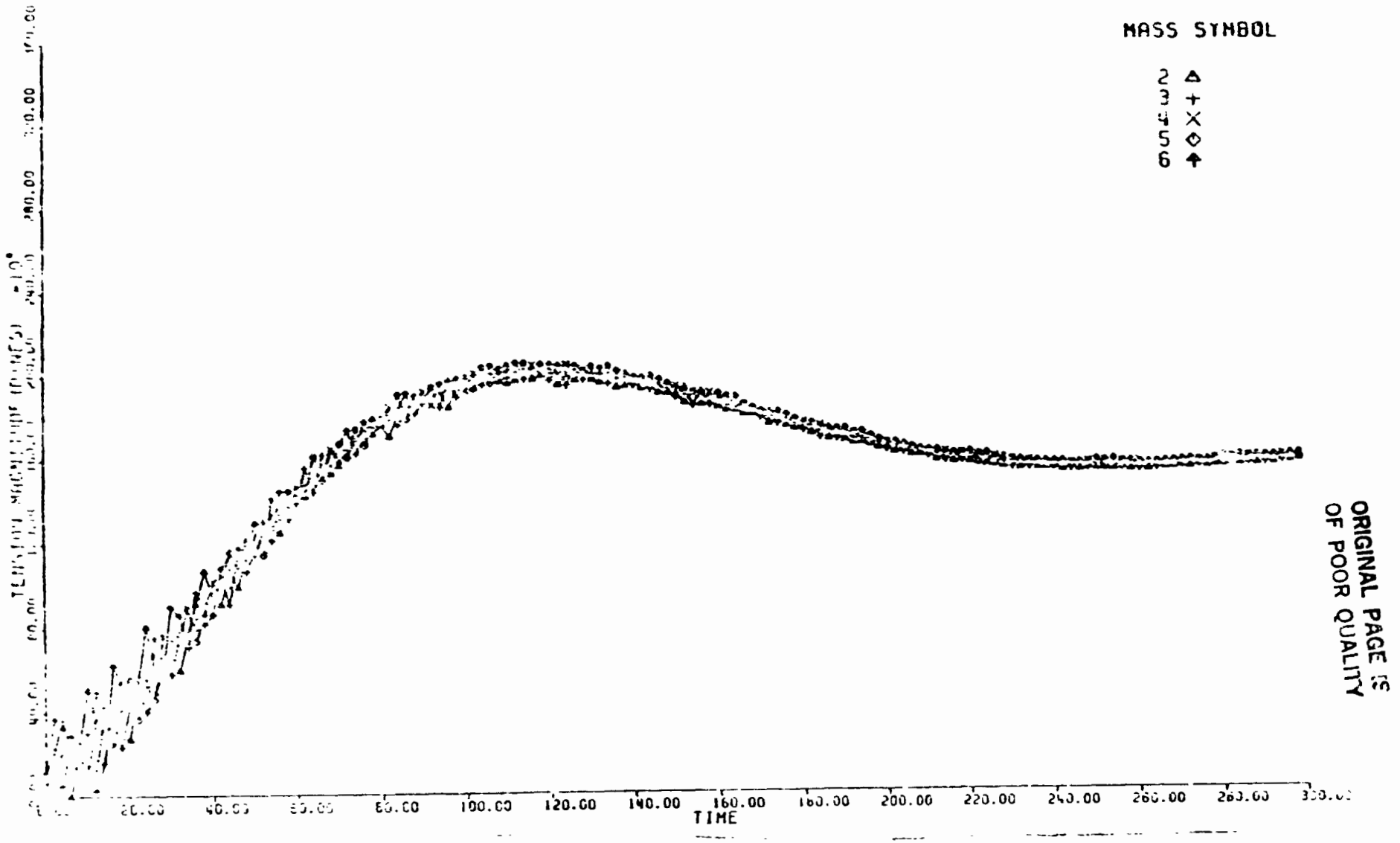

(a)

Figure 5-24. As for Figure 5-21, except that the velocity is radial, directed toward the station (upward). (a) Tension vs. time. Note that the tether segment nearest the payload goes briefly slack. This may be an artifact of the lumped-mass model. (b) Radial vs. in-plane behavior, the dashed lines indicate slack tether segments.

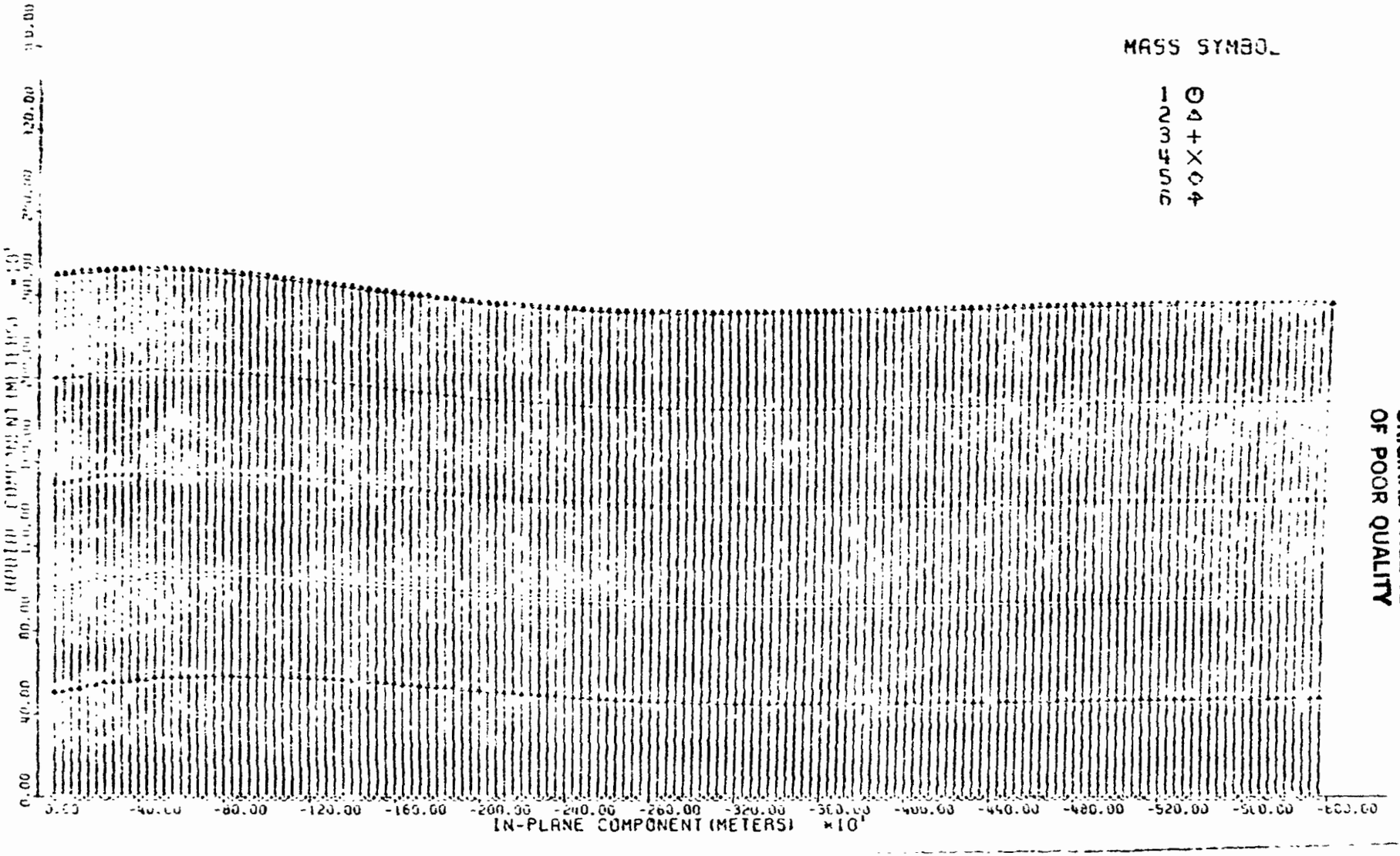

ORIGINAL PAGE IS
OF POOR QUALITY

Figure 5-24 (b)

the tether. In these two cases, substantial swinging of the tether is seen, Figures 5-21(b) and Figure 5-22(b), in the direction expected. When the velocity is radial, little swinging of the tether is seen, Figures 5-23(b) and Figure 5-24(b), but the tension response is substantially different from the zero velocity case. With the velocity away-from-station, the initial bounce is substantially higher (2.55×10^8 dynes, compared to 2.15); while with velocity toward station, the tension peak is somewhat lower (2.05×10^8 dynes). This substantial increase in tension with a 3 m sec^{-1} velocity away-from-station indicates that this direction is clearly less desirable.

The velocity-toward-station case (Figure 5-24) shows a brief initial period of about 6 seconds when the tether segment nearest the payload goes slack. This is rather surprising since tension disturbances propagate through the tether very rapidly compared to the 3 m sec^{-1} acquisition velocity (see Figure 5-20) in which the final segment, at 40 km distance, shows substantial response a mere 5 seconds after the damper is initiated. The slack response is probably an artifact of the lumped mass model used. This should be explored by changing the number of mass points to see if it is only the outermost segment which goes slack in all cases. The impact of a constant-velocity ram on a one-dimensional tether could also be investigated theoretically.

One counter-intuitive response of the tether is illustrated in Figures 5-18(b), Figure 5-23(b), and Figure 5-24(b) for the zero-velocity, away-from-station and toward-station cases, respectively. When the extra mass is attached to the tether,

increasing the tension, the expected response, at least initially, is for the tether length to increase. Instead, it decreases (but note that the mass closest to the station initially moves farther from it). This is even more pronounced in Figure 5-23(b) where the velocity was directed so as to stretch the tether. While when the velocity at acquisition should have compressed the tether (Figure 5-23(b), instead it responded by lengthening. This probably represents an interaction with the active damping mechanism and requires further study to be understood more clearly.

To summarize, these studies have shown that payload acquisition by a tether deployed downward from a Space Station in high orbit is feasible, that the damping algorithm described in previous reports suffices to reduce the initial tension increase and eliminate tension oscillations within a few minutes, and that the procedure is stable against acquisition with non-zero relative velocity. But further investigation is indicated to develop pre-acquisition maneuvers to reduce the tension bounce, to resolve the question of whether the tether actually does go slack if the payload is acquired with a velocity toward the station, and to understand some of the puzzling system responses on a clear and intuitive level.

5.4 Orbital Pumping

5.4.1 Introduction

In this section we consider the general problem of orbit change and control by varying the shape of a spacecraft by internal forces. This does not mean that external forces are not operating. The external field remains Newtonian but the gravity gradient forces

combined with the shape variation of the spacecraft cause a variation of the total force acting on the center-of-mass and, therefore, cause a variation in the orbit. Since the external forces are central, the total angula momentum does not change. What may change is the orbital energy, which may either increase or decrease.

5.4.2 Tether Model for Orbital Pumping Study

Here is a very simple mechanical system for modelling the mechanism we intend to investigate.

Consider two equal masses m at the end of a tether in orbit: a dumbbell (see Figure 5-25). The analytical model of the tether is assumed to have the characteristics of a bar capable of withstanding compression as well as tension. In reality, we are interested only in the tethered "dumbbell" configuration and, therefore, only in one class of its possible movements- those for which the tether is always in tension. If the orbit is equatorial (about an asymmetric primary body) or if the primary is spherical, the external forces on the dumbbell are central and consequently the total angular momentum of the spacecraft is preserved. If a and e are the semimajor axis and eccentricity of the orbit of the center of mass, we have that in any evolutionary motion which does not effect the orbital angular momentum

$$a(1-e^2) = a^* \qquad (1)$$

If by internal control we change the orbital energy, which is to say, the semimajor axis a, we also change e. If a increases, e also increases, and vice versa. From 1) it is clear that a^* is the minimum value of the semimajor axis of the orbit and corresponds to a circular

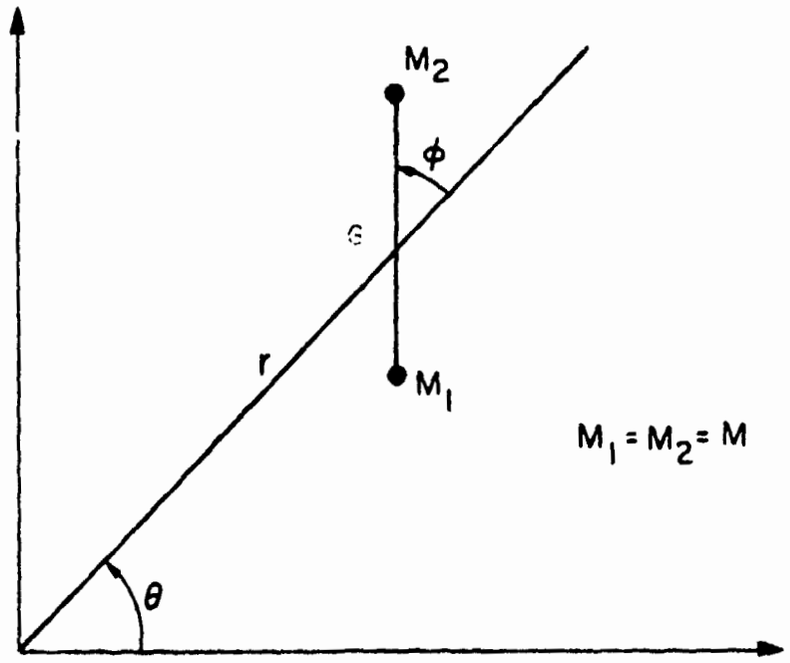

Figure 5-25. Co-ordinate relationship in dumbbell configuration used in orbital pumping study.

orbit. Naturally, a* is the semilatus rectum of any orbit.

Heuristically, when the dumbbell is in orbit, free and forced librations will occur. We assume that the tension in the tether never goes to zero. As an example, let us assume that the orbit has small eccentricity and that the libration amplitudes are small. The tether is almost always aligned with the radial direction. When the system is at perigee, the tension in the tether is roughly given by:

$$\tau_p = 3g_\oplus \frac{R_\oplus^2 z_m}{a^3(1-e)^3} \tag{2}$$

If 2z is the length of the tether, when the system is at apogee the tension is

$$\tau_a = 3g_\oplus \frac{R_\oplus^2 z_m}{a^3(1+e)^3} \tag{3}$$

If we let a segment Δz of tether be pulled out at perigee by the gravity gradient tension against the torque of an electric generator and we pull in with the same motor at apogee exploiting the generator power for recycling the same tether segment, we will have transformed orbital energy into electric energy (for example) or into thermal energy approximately equal to

$$\Delta z(\tau_p - \tau_a) = 18\, e g_\oplus \frac{R_\oplus^2}{a^3} z_m \Delta z \tag{4}$$

which may be written

$$\Delta z\,(\tau_p - \tau_a) = 18\, e\, \frac{\mu}{a}\, m\, \frac{z\Delta z}{a^2} \tag{5}$$

Since the orbital energy is $\mu/2a$, when the eccentricity is passing from 0 to e, while the angular momentum is preserved, the variation of energy is

$$\Delta E_e = -\frac{2\mu m}{2a} + \frac{2\mu m}{2a(1-e^2)} = \frac{\mu m}{a}\frac{e^2}{1-e^2} = \mu m \frac{e^2}{a^*} \tag{6}$$

Therefore, for small eccentricities, the fractional variation per orbit is obtained by dividing 5) by 6). We get

$$\frac{\Delta E/\text{orbit}}{\Delta E_e^o} = 18 \frac{z\Delta z(1-e^2)}{ea^2} \tag{7}$$

In particular for z = 100 km, Δz = 20 km, a = 7000, e = 0.03.

$$\frac{\Delta E/\text{orbit}}{\Delta E_e^o} = 2.4 \times 10^{-2} \tag{8}$$

Notice that this last value corresponds to the value 0.03 of e. Therefore, since the fractional variation of energy per orbit is inversely proportional to e the process is not uniform.

In fact, we may write, from 1)

$$E = \frac{\mu m}{a} = \frac{\mu m}{a^*}(1-e^2) \tag{9}$$

and because of 5)

$$\frac{\Delta E}{\text{orbit}} = -2e\Delta e \frac{\mu m}{a^*}/\text{orbit} = 18\, e \frac{\mu m}{a^{*2}} z\Delta z/\text{orbit} \tag{10}$$

and, therefore,

$$\Delta e/\text{orbit} = 18 \frac{\Delta z.z}{a^{*2}} \tag{11}$$

While other perturbations may give short periodic variations, the atmospheric drag is decreasing the spacecraft orbital energy and angular momentum. As a first approximation, for small eccentricities the variation per orbit of the energy is given by

$$\frac{\Delta E_D}{\text{orbit}} = \frac{C_D}{2} 2\pi a A\rho(a)v^2(a) \tag{12}$$

while the variation of the angular momentum is given by

$$\Delta L/\text{orbit} = \frac{C_D}{2} a A\rho(a)v^2(a)T \tag{13}$$

Since for a circular orbit

$$v^2 = \frac{\mu}{a},\ n^2a^3 = \mu,\ T^2 = \frac{4\pi^2a^3}{\mu} \tag{14}$$

we have

$$\Delta E_D/\text{orbit} = C_D\pi\mu A\rho(a) = 2\ C_D\pi A\rho(a)\ a\ \frac{\mu}{a}$$

$$\Delta L/\text{orbit} = \pi C_D A\ \rho(a)\ a\ \mu a \tag{14'}$$

from 6), and 12') we have

$$\frac{\Delta E_D/\text{orbit}}{\Delta E_e^o} = \frac{2CD\pi A\rho(a)a}{me^2} \tag{15}$$

if we assume $A = 10^6 \sim 10^7$ cm^2, $C_D = 2.2$, $m = 100 \times 10^6$ grams, $a = 7000 \times 10^5$ cm^2, $\rho = 10^{-15}$ grams/cm^3, $e = 0.01$, we have

$$\frac{\Delta E_D/\text{orbit}}{\Delta E_e^o} = 3\pi 10^{-3} \tag{15'}$$

to be compared with 8).

Similarly

$$\frac{\Delta L/\text{orbit}}{L} = 5 \times 10^{-6} \tag{16}$$

For a dumbbell system flying inside the range of 400 to 1000 km, the atmospheric drag is probably negligible for a realistic configuration of the system. The present technique in this situation may therefore be useful in controlling the orbital elements a and e in the presence of small atmospheric drag and any other small perturbations such as radiation pressure.

5.4.3 Analytical Model for Numerical Simulation

A numerical simulation will give all the elements for a precise evaluation of the technique. In the following paragraphs we shall consider a relatively simplified analytical model in order to be able to perform a preliminary system analysis which, however, will eventually require numerical integration in the most interesting cases (large eccentricity).

For establishing the differential equations of motion of the system of Figure 5-25, we introduce the following Lagrangian coordinates θ, r, ϕ (see Figure 5-25). If we also consider as an independent variable the length of the tether 2z we may then consider the four degree of freedom system with coordinates θ, r, ϕ, z.

We first find the kinetic energy

$$\tau = \frac{1}{2} m (\dot{x}_1^2 + \dot{y}_1^2) + \frac{1}{2} m (\dot{x}_2^2 + \dot{y}_2^2) \tag{17}$$

in Cartesian coordinates and in Lagrangian coordinates

$$\tau = m (\dot{r}^2 + r^2\dot{\theta}^2 + z^2(\dot{\theta}+\dot{\phi})^2 + \dot{z}^2 \tag{18}$$

The force function of the central field of gravitational force centered in O is

$$U_g = \frac{\mu m}{(r^2+z^2-2rz\cos\phi)} + \frac{\mu m}{(r^2+z^2+2rz\cos\phi)} \tag{19}$$

If the tether is viscoelastic we have two more forcing functions, the elastic force function:

$$U_C = -\frac{\kappa}{2} (2z-2z_o)^2 \tag{20}$$

and the dissipation function

$$R = -2\ \frac{D\dot{z}^2}{2} \tag{21}$$

Other forces could be applied to the system such as aerodynamic forces, radiation pressure, and possibly electrodynamic forces; however, we will take in consideration in this preliminary model only the forces we have listed above. Naturally the model includes the case of controllable length Δz of the cable. This control will imply internal forces, and related work, and exchange of energy between orbital and rotational energy and internal energy of the system.

Control forces may be also included explicitly. In particular two equal and opposite forces may be applied to P_1 and P_2. The corresponding work may be written

$$\delta = 2f dz + 2\tau z \delta(\theta+\phi) \tag{22}$$

where f is the longitudinal and τ the transversal component. If $\tau = 0$ there is no variation of angular momentum of the system. Limiting ourself to the forces explicitly considered we may write the Lagrangian equation of motion

$$\begin{aligned}
&2m(\ddot{r}-r\dot{\theta}^2) = \frac{\partial \mu}{\partial r} = -2\mu\frac{m}{r} + 3\mu\frac{mz^2}{r} - 9\mu\frac{mz^2}{r}\cos^2\phi \\
&2m\,\frac{d}{dt}[r^2\dot{\theta}+z^2(\dot{\theta}+\dot{\phi})] = 2\tau z \\
&2m\,\frac{d}{dt}\,[z^2(\dot{\theta}+\dot{\phi})] = -6\ \frac{\mu m z^2}{r^3}\sin\phi\cos\phi + 2z\tau \\
&2m[\ddot{z}-z(\dot{\theta}+\dot{\phi})^2] = -2k(z-z_o)-2D\dot{z}\ -2\mu\frac{mz}{r^3}(1-3\cos^2\phi)+2f
\end{aligned} \tag{23}$$

We consider in the present paragraph some specific cases. First we consider the simplest case $\tau = 0$, $k = \infty$ and therefore $z = z_0$ constant. The system 23) becomes

$$\ddot{r} - r\dot{\theta}^2 = \frac{\mu}{r^2} + \frac{3\mu}{2}\frac{z_0^2}{r^2} - \frac{9\mu}{2}\frac{z^2\cos^2\phi}{r^4}$$

$$r^2\dot{\theta} + z^2(\dot{\theta}+\dot{\phi}) = L_0$$

$$z_0^2(\ddot{\theta}+\ddot{\phi}) = -\frac{3\mu z_0^2}{r^3}\sin 2\phi \qquad (23')$$

This differential system models the drag-free rigid dumbbell. In particular, the coupling between libration of the dumbbell and orbital motion of the center of gravity appear explicitly. If $z_0^2 \ll r_0^2$ we may decouple the system and using perturbation techniques study in first approximation how the motion of the dumbbell about its center-of-gravity effects the motion of c.g. and vice versa. In the second case, we control ϕ to the value $\phi = 0$, applying two opposite forces, given by

$$\tau = (z\ddot{\theta} + 2\dot{z}\dot{\theta})m \qquad (24)$$

It is evident in this case that the total angular momentum is not preserved (see equation 23.2). We treat this case here incidentally; but it is natural that even though the total external force is zero, the external torque is not.

The force 24) is small only if $\dot{z}$ and $\dot{\theta}$, $\ddot{\theta}$ are small. Now for a low orbit the order of $\dot{\theta} = 10^{-3}$ rad/sec, the order of $\ddot{\theta}$ is $2e\dot{\theta}^2$. Assuming $\dot{z} = 10\text{~}20$ m/sec and $e = 10^{-2}$ the acceleration is of the order of $10^{-3}g$, which means that τ may reach value of 10^{-3} mg, a quite large force in particular if the system has to be operated for long periods

of time while the length of the tether z is controlled.

In this case the equations of motion become

$$r^2\dot{\theta} = L_o$$

$$\ddot{r} - r\dot{\theta}^2 = -\frac{\mu}{r^2} - 3\mu\frac{z^2}{r^4}$$

$$\ddot{z} - z\dot{\theta}^2 = -\frac{k}{m}(z-z_o) - D\frac{\dot{z}}{m} + 4\frac{\mu z}{r^3} + f \qquad (25)$$

and following the Binet formula,

$$\frac{d^2 1/r}{d\theta^2} + 1/r = \frac{\mu}{L_o^2} + 3\frac{\mu z^2}{L_o^2 r^3} \qquad (26)$$

Since z is a control function (of θ) the problem may be solved only numerically in the case of large eccentricity of the reference orbit. For small eccentricity one may use a perturbation technique. We assume

$$1/r = \frac{1+e\cos(\theta-\tilde{\omega})}{a(1-e^2)} + \varepsilon x \qquad (27)$$

and 26) becomes

$$\frac{d^2 x}{d\theta^2} + x = \frac{3\mu^3 z^2}{L_o^6}[1+e\cos(\theta-\tilde{\omega}] \qquad (28)$$

If we assume

$$z = z_o[1+\alpha\cos(\theta-\theta^*)] \qquad (29)$$

Equation 29) becomes

$$\frac{d^2 x}{d\theta^2} + x = \frac{3\mu^3 z^2}{L_o^6}[1+\alpha\cos(\theta-\theta^*)][1+e\cos(\theta-\tilde{\omega})] \qquad (30)$$

and

$$\frac{d^2x}{d\theta^2} + x = k[1 + a\cos(\theta-\theta^*) + e\cos(\theta-\tilde{\omega})$$

$$+ \frac{ae}{2}\cos(\theta^*-\tilde{\omega}) + \frac{ae}{2}\cos(2\theta - \theta^* - \tilde{\omega})] \qquad (31)$$

A general solution of this equation contains (a) a constant term

$$x_1 = k[\frac{ae}{2}\cos(\theta^*-\tilde{\omega}) + 1] \qquad (31')$$

(b) secular terms

$$x_2 = \frac{ka}{2}\theta\sin(\theta-\theta^*),\ x_3 = k\frac{ke}{2}\theta\sin(\theta-\tilde{\omega}) \qquad (31'')$$

(c) higher frequency term

$$x_4 = -k\ \frac{ae}{6}\cos(2\theta-\theta^*-\tilde{\omega}) \qquad (31''')$$

The correction on $\dot{\theta}$ should be done a posteriori considering 25), $r^2\dot{\theta} = L_o$ the constant a, θ^*, x_o are part of the control function.

The third more natural and realistic case is to have $\tau=0$, $f=0$. In this case, the equations become more complex and the model resembles a satellite in orbit affected by tides raised by the primary on the dumbbell. The dynamical equations are practically 23) where $\tau=0$ and $f=0$. For enhancing the tidal effects, the elastic constant k is made very small and a critical damping constant is selected.

More complex is the fourth case where length changes are controlled by reeling operations in addition to being due to viscoelastic behavior.

5.4.4 Comments on System Behavior

For all four models considered above, only numerical integration will give interesting results in the case of high eccentricity which appears to possibly provide some new techniques for modifying the orbital elements of the c.g. by internal forces. For small eccentricity orbits, when the atmospheric drag is negligible, the third case $\tau=0$, $f=0$ has been dealt with in a number of papers, the most important one is the paper by P. Goldreich, "On the Eccentricity of Satellite Orbits in the Solar System" (G.R. of Royal Astronomy Society, vol. 126, 1963, p. 357). In that paper it is shown that for a non-spinning satellite, in our case for a librating dumbbell, the tide raised on the satellite may overcome the effect of the tide raised by the satellite on the primary. While the former tends to decrease the eccentricity, the latter tend to increase it. For a large dumbbell, even one of the size of a large space station, when the dissipation factor is made large enough, the eccentricity will certainly decrease if no control system is operated on the dumbbell. The equation of motion will be equation 23) where we put $\tau = f = 0$ and let the orbit evolve under natural forces. If the dissipative tide raised by the Earth on the dumbbell is large (small rigidity and low quality factor of the tether, or the insertion of a spring-dashpot system with properly designed characteristics) we will get circularization of the orbit.

For more clarification, we will consider resonant spin-orbital coupling different from one-to-one ratio (which means a motion different from the dumbbell making one rotation and libration during one revolution). The constant angular momentum is related to the sum of both the orbital and the spin angular momentum. The tide raised on

the satellite by the planet will dissipate both rotational energy and orbital energy. Since the rotational energy is much smaller than the orbital energy the process will lead to resonance first, because in this state, rotational energy dissipation will go to zero or to a small value related to the changing of orbital period. Therefore, starting with an eccentric orbit the dumbbell will first settle down on a resonant orbit and thereafter the orbital energy will decrease by enhanced tidal dissipation on the satellite. When the eccentricity and semi-major axis decreases, the system may shift from a higher to a lower resonance. The system will rapidly evolve if the enhanced dissipation is operating. A numerical integration example is given below. The numerical example will be limited to relatively small eccentricity for technical reasons.

In principle, a dumbbell may be injected on a high eccentricity orbit. Eventually it will lose the rotational angular momentum and will stabilize on a spin-orbital coupling regime as does the planet Mercury (see Figure 5-26) and as do all satellites. After being launched in an eccentric orbit, the dumbbell will settle in a regime where it will make, during one orbital period, an integer number of half rotations about an axis close to the normal to the orbital plane (or coinciding with the normal to the orbital plane if the orbit is equatorial or polar). Thereafter, the tidal evolution will cause the eccentricity and the semimajor axis to decrease while the eccentricity is decreasing. The system may go through other spin orbital coupling resonances ending in a final stage with the dumbbell always aligned radially and moving in a circular orbit.

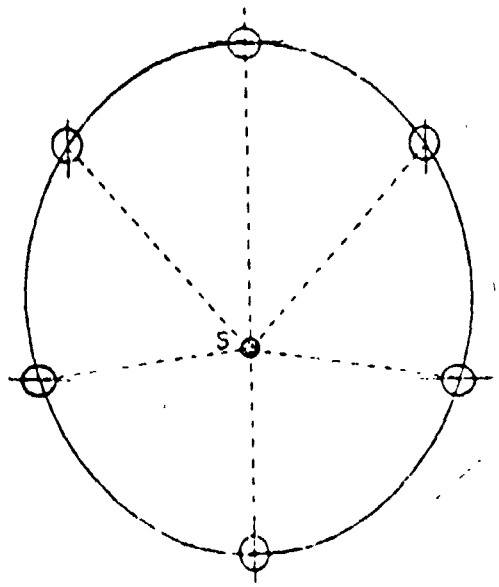

Figure 5-26. A rough plannar sketch of the orientation of Mercury's axis of minimum moment of inertia, at different points along its orbit, given that the rotational period is two-thirds of the orbital period and that this axis is aligned with the Sun-planet vector at perihelion.

5.4.5 Applications of System Behavior to Orbital Transfer

In principle, the process just described could be efficiently mechanized in a spacecraft on a highly eccentric orbit. In particular, two examples come to mind. The first one concerns the transfer orbit of an OTV (see Figure 5-27). One should examine if transfer from GEO to low Earth orbit might be accomplished by the technique of tidal interaction combined perhaps with atmospheric drag. Starting with a transfer orbit (6800 - 42000 km) the eccentricity being (2a = 24400 km) e = 0.72, and a* = 24.400 (1-0.53) = 11.460. Without drag dissipation, this will be the radius of the circular final orbit after removal of energy from the orbit by tidal effects. The exploitation of relatively low atmospheric drag which would not require heavy thermal protection may drastically reduce the initial semimajor axis and speed up the process of circularizing at low altitude in the OTV parking orbit.

The second example may be given by the capture in geostationary orbit of a spacecraft from a high eccentricity orbit. Naturally, if a* = 42000 km, $a(1-e^2)$ has to be 42000 km also; and, since this is the semilatus rectum of the orbit, the perigee altitude of the starting orbit should be larger than 21000 km, that is, one-half of the minimum semilatus rectum.

In particular, if the perigee of the orbit is 24000 km, the eccentricity and the semimajor axis should be

a = 96,000 km e = 0.75 a(1+e) = 158,000 km

If the perigee is at 23,000 km

a = 132,000 km e = 0.83 a(1+e) = 241,000 km

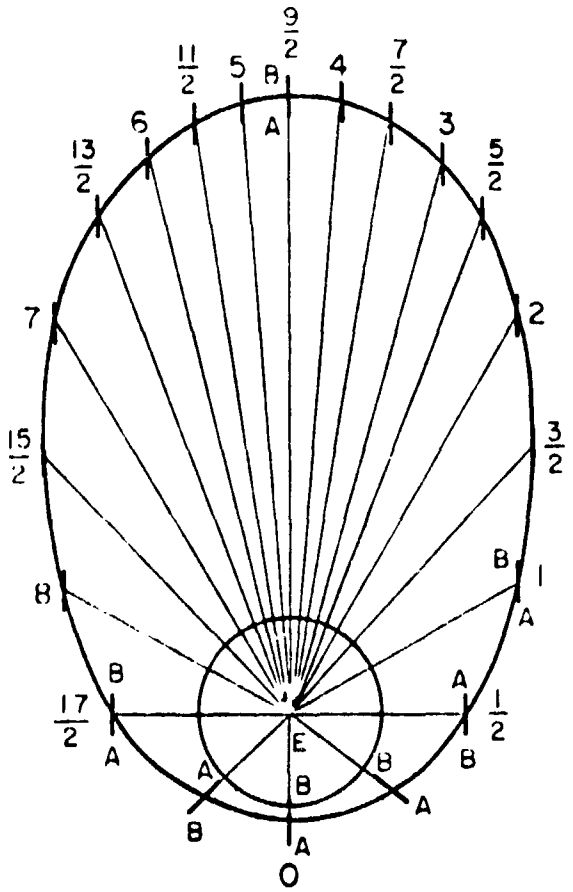

Figure 5-27. Orbital transfer from GEO to LEO of a dumbbell OTV. Initially, the system may synchronize in a 9:1 resonance due to spin orbital coupling as shown. During the decay, or even from the beginning if the characteristics of the dumbbell and initial conditions are correct, the dumbbell may low order resonances - 8.5:1, 8:1,-------1:1. It will finally synchronize in the 1:1 spin orbital coupling in the final LEO orbit where the retrieval to compact configuration will be performed.

If the perigee is at 22,500

$$a = 168{,}750 \quad e = 0.87 \quad a(1+e) = 315{,}000 \text{ km}$$

It is apparent that, if the apogee should be at the Moon distance for transfer from the Moon to geostationary orbit, the perigee should be around 22500-22600 km.

Finally, in principle, it may be possible to insert a dumbbell system in geostationary orbit by launching the complete system in a highly eccentric orbit, and either by exploitation of the Moon's gravity field or by a small (<200m/sec) Δv, raise the perigee to the wanted value and bring the orbit into the equatorial plane.

We computed that without Moon assistance we still gain ~600~700m/sec Δv for inserting the spacecraft in a geostationary orbit, comparing a classical launch from the Eastern Test Range (ETR) with the technique outlined above. It has to be noticed that a large part of the energy will be recovered during the circularization. This may supply electrical energy for the operation. Naturally one should be careful in considering the time required for dissipating the energy. It strongly depends on the design of the spring-dashpot system and/or of the length of the tether reeled out at perigee and reeled in at apogee.

As a technique for transferring a spacecraft from LEO to GEO with the aim of saving energy with respect to the energy involved in the actual launch procedure from the ETR, this technique is valid when the mass of the system is very large. The basic element of the transfer is a dissipation mechanism which absorbs energy from the orbit which may be recovered as electric power. In line with what we have written above we want to use the enhanced effect of the tide raised by the

Earth on the spacecraft to decrease its energy. This can be done passively or actively by proper design of a spring-dashpot system and by properly controlling the tension on the tether connecting the two masses and, therefore, its length.

Let us start with a spacecraft in a circular parking orbit at an altitude a_o (typically a_o = 220 km + R_0 (equatorial) with an inclination of 28° (E.T.R.) and a velocity v_o close to 7.8 km/sec with an incremental velocity

$$\Delta_1 v = v_o \quad \frac{2\bar{a}}{a_o+\bar{a}} - 1 \tag{32}$$

The spacecraft is inserted in a transfer orbit with apogee $\bar{a}$. The velocity at apogee $\bar{a}$ in this Hohman transfer is

$$v_a = v_o \quad \frac{a_o}{\bar{a}} \quad \frac{2\bar{a}}{a_o+\bar{a}} \tag{33}$$

At apogee distance $\bar{a}$ the circular velocity is

$$v_{c\bar{a}} = v_o \quad \frac{a_o}{\bar{a}} \tag{34}$$

Suppose we want to raise the perigee of the Hohman transfer orbit and change the inclination from 28° to 0°. We need to bring the magnitude of the velocity vector to the value

$$v_1 = v_o \quad \frac{a_o}{\bar{a}} \quad \frac{2\bar{p}}{\bar{p}+\bar{a}} \tag{35}$$

and its orientation in the equatorial plane (see Figure 5-28).

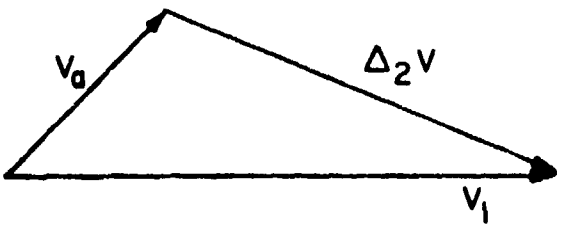

Figure 5-28. Vector relationships.

By trivial computation we have

$$\Delta_2 v = \frac{2a_o^2}{\bar{a}(a_o+\bar{a})} + \frac{2a_o\bar{p}}{\bar{a}(\bar{p}+\bar{a})}$$

$$-4\frac{a_o}{\bar{a}}\cos 28^o \left(\frac{\bar{p}a_o}{(p+\bar{a})(a_o+\bar{a})}\right)^{1/2} v_o \qquad (36)$$

If we call a^* the radius of the GEO orbit and we want to transfer the spacecraft by tidal effect from the orbit with perigee $\bar{p}$ and apogee $\bar{a}$ to GEO since the angular momentum is preserved $\bar{a}$, and $\bar{p}$ have to satisfy the following condition

$$a^* = \frac{2\bar{a}\bar{p}}{\bar{a}+\bar{p}} = \frac{2\bar{p}}{1+\bar{p}/\bar{a}} \qquad (37)$$

which means

$$\bar{p} > \frac{a^*}{2} \qquad (38)$$

The relation 37) is directly deduced from

$$a(1-e^2)=a^*,\ a(1-e)=\bar{p},\ a(1+e)=\bar{a} \qquad (39)$$

Transferring the spacecraft from the orbit $(\bar{a},\bar{p})$ to GEO implies a dissipation of energy

$$\Delta E = \frac{M\mu}{2a^*} - \frac{\mu M}{\bar{a}+\bar{p}} \qquad (40)$$

Here μ is the Earth gravitational constant and M is the mass of the spacecraft. If $\bar{a} + \bar{p} \sim 4a^*$) as we have shown, when we reduce the magnitude of $\Delta v_1 + \Delta v_2$ or to exploit the Moon gravity assistance ($\bar{a} + \bar{p} \sim 9a^*$), the amount of energy to be dissipated is more than one-half of the total energy of the spacecraft in GEO. Now the total orbital energy in GEO of a spacecraft of mass M is given by $M\mu/2a^*$ and, therefore, the order of magnitude of energy to be dissipated ranges between $M\mu/4a^*$ and $M\mu/2a^*$. A rough evaluation gives in the case of $\bar{a} + \bar{p} = 4a^*$

$$\Delta E/M = 23000 \text{ joule/kg} \tag{41}$$

From these figures it is clear that it may be difficult to imagine practical system which could do the job in a reasonable time interval. For example, assuming a Moon-assisted transfer orbit as a starting orbit for exploitation of enhanced tidal dissipation for circularization to GEO: the period of the first orbit will be of the order of 8-9 days. Since the initial perigee $\bar{p}$ of the orbit will be at roughly 4 earth radii, at perigee passage we may depend upon some amount of energy dissipation generated by the tide raised at 4 earth radii.

In fact, suppose we start with a spacecraft of the following general shape (see Figure 5-29): a main spacecraft of mass M connected with a secondary spacecraft with a mass of the same order of magnitude with a tether of length 2z. We leave for the moment the problem of stabilization of the dumbbell on a spin orbital coupling mode and try to estimate the maximum work which can be done by the gravity gradient force. Suppose $\bar{p}=4R_0$, the gravity field at $\bar{p}$ will be

$$g_{\bar{p}} = g_\oplus \frac{1}{16} \tag{42}$$

while the gravity gradient force will be

$$\Delta f_g = M\, 2\, \frac{g_\oplus}{16}\, \frac{z}{4R_\oplus} = \frac{1}{32} M g_\oplus \frac{z}{R_\oplus} \tag{43}$$

Since the orbit is very eccentric and the dumbbell is very elongated we may assume that the angular velocity of the dumbbell is close to the orbital angular velocity $\dot{\theta}$ at perigee when the tide of the earth will keep the system oriented toward it.

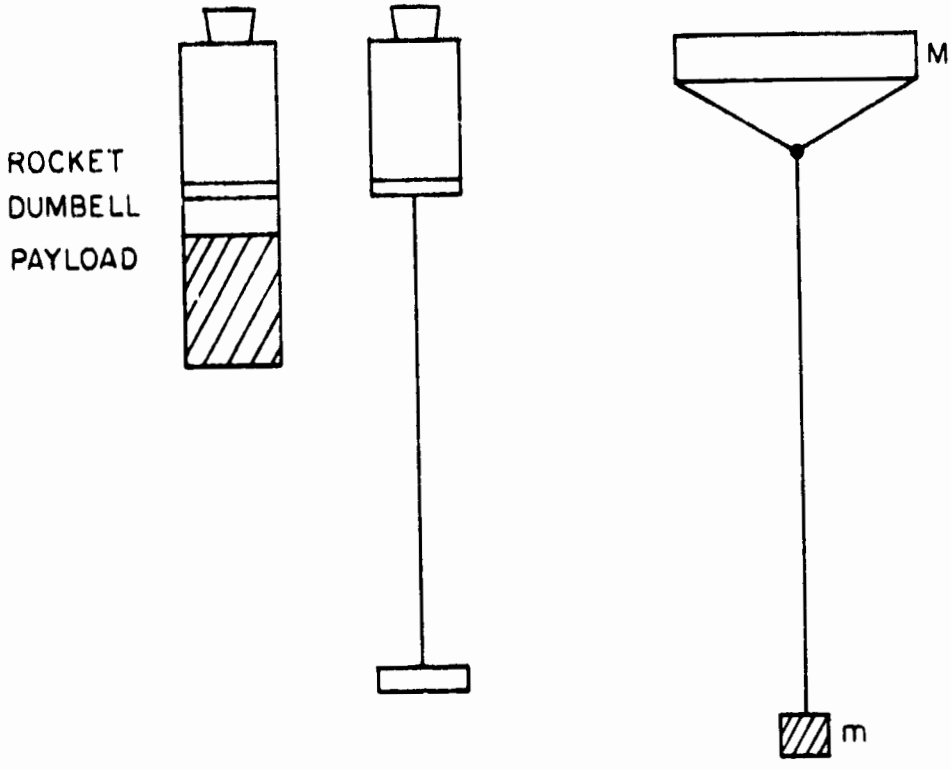

Figure 5-29. Spacecraft configurations for orbital pumping.

If n is the mean motion of the c.g. of the dumbbell the orbital angular velocity at perigee is

$$\dot{\theta}_p = n \frac{(1+e)^{1/2}}{(1-e)^{3/2}} \tag{44}$$

which in the case of the OTV-S/C is roughly 9n and in the case considered of a lunar assisted orbit is of the order of 30n~31n. At perigee passage the tension in the tether will be given by the sum of the gravity gradient force (43) and the differential centrifugal force

$$\Delta f_c = M \dot{\theta}_p^2 z = M n^2 \frac{(1+e)z}{(1-e)^3} = M g_o \frac{R_\oplus^2 (1+e) z}{a^3 (1-e)^3} \tag{46}$$

and since e is close to 1 the tension will be close to

$$\tau^* = \frac{1}{16} M g_\oplus \frac{z}{R_\oplus} \tag{47}$$

This tension is reduced to roughly 1/2 of the value (47) very rapidly when the gravity gradient is no longer operating and only the centrifugal force is keeping the system in tension.

The work which can be done by the gravity gradient per orbit is equal to the elongation Δz of the tether at perigee multiplied by $1/2\tau^*$ as given by (47). In fact, the work to retrieve the same height of tether at perigee is done against the centrifugal force (due to the rotational motion of the dumbbell) with an angular velocity which remains almost constant from perigee to apogee. The maximum value of the work dissipated per orbit is given by:

$$\Delta = \frac{1}{32} M g_\oplus \frac{z}{R_\oplus} \Delta z \tag{48}$$

or

$$\frac{\Delta}{M} = 1/32 \, g_\oplus \frac{z \Delta z}{R_\oplus} \tag{49}$$

On the other hand, the amount of energy dissipated in tranferring the system from the eccentric orbit to the GEO orbit is almost twice the value given by (41) that is 40000 joule/kg. An evaluation of (49) gives 10^3 joule/kg, not an unreasonable value when compared with the total energy to be dissipated.

This example shows that the process may work. In particular it may be most applicable to a system of huge linear dimension and if a relatively long time scale of the process can be accepted.

In conclusion, probably the most interesting practical applications of these orbital pumping techniques will be for circularizing small eccentricity orbits and for helping to circularize an orbit prior to reentry of an OTV in parking orbit from Hohman transfer. These two cases seem to deserve particular attention. But we should not exclude the possibility that further study of these phenomena would not lead to other useful orbital transfer techniques.

5.4.6 Numerical Simulation Results

Two cases were simulated using SKYHOOK, one with a low eccentricity (e = 0.036 initially) and moderate altitude (400 to 900 km), the second with high eccentricity (e = 0.72) and high altitude (6800 km to 42000 km).

Two equal masses were used, initially separated by 100 km; the SKYHOOK model used only these two masses and no discretization of the tether. In order to use existing software for generating initial conditions, the simulations were begun 90° along orbit from perigee and in neutral libration, that is, straight up and rotating at the same rate as the orbital radius vector.

The tether characteristics were determined so that (1) the natural frequency of the longitudinal tether/mass vibrations were the same as the orbital period (i.e. resonant) and (2) the tether/mass system was critically damped to enhance energy transfer.

The results in the high eccentricity orbit, although containing features expected from the theory, were confusing and due to time and funding constraints, we were unable to fully investigate the causes for these inconsistent results. Most likely, the problem lies in the way this run was set up since the agreement between the theory and the model was excellent in the low eccentricity case.

The results of the low eccentricity study, which ran for about 22 orbits, are consistent with the theory outlined above. From the SKYHOOK output, a variety of parameters of the center-of-mass orbit, as well as the tether length and libration angle of the system, were computed and printed.

The eccentricity and semi-major axis showed the expected behavior; a periodic (at the orbital period) component superimposed on a secular decrease. The eccentricity is shown in Figure 5-30, where both the periodic and secular terms are clear.

For a more quantitative discussion, consider the results for one particular orbit. Apply equation 11) above, $\Delta e/\text{orbit} = -9\ \Delta z.z/a^2$, and compare this to the observed change in eccentricity. For orbit 5, the tether length (separation of masses) is shown in Figure 5-31a, the minimum and maximum are 89.86 and 108.22 km. The eccentricity at successive peaks are 0.035142 and 0.034994, giving $\Delta e = -1.48 \times 10^{-4}$. To apply 11), recall that z is <u>half</u> the tether length while Δz is the <u>full</u> amount of the increase or decrease. Thus we use the average $2z = (89.86 + 108.22)/2$ or $z = 49.52$ km, and $\Delta z = 108.22 - 89.86 = 18.36$

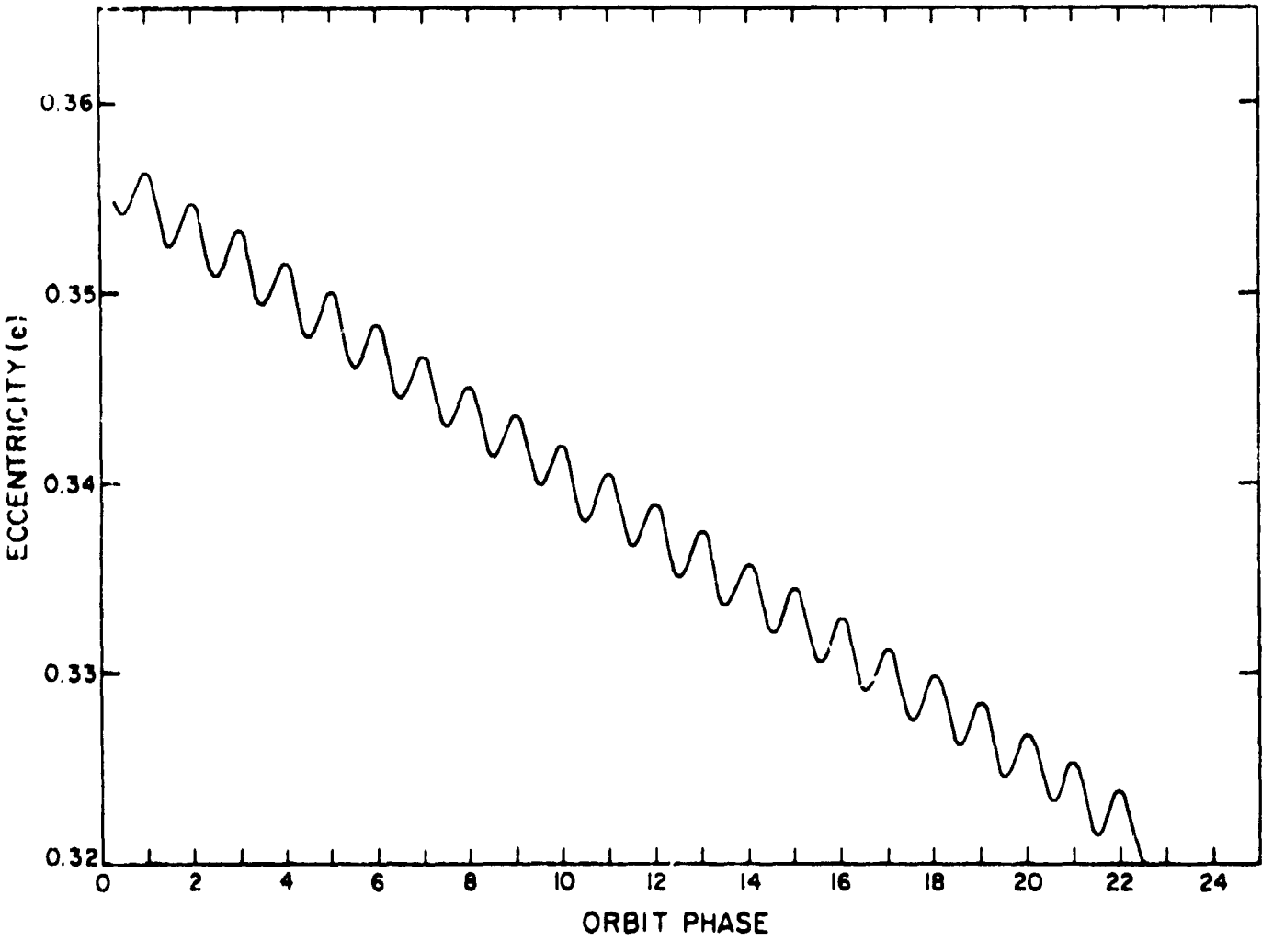

Figure 5-30. Eccentricity of the center-of-mass orbit vs. the orbital phase (true anomaly/2π). A critically damped dumbbell configuration, with oscillatory frequency tuned to the orbit, is allowed to evolve, converting orbital energy to internal (e.g. thermal) energy, circularizing the orbit. The numerical simulation was made with SKYHOOK.

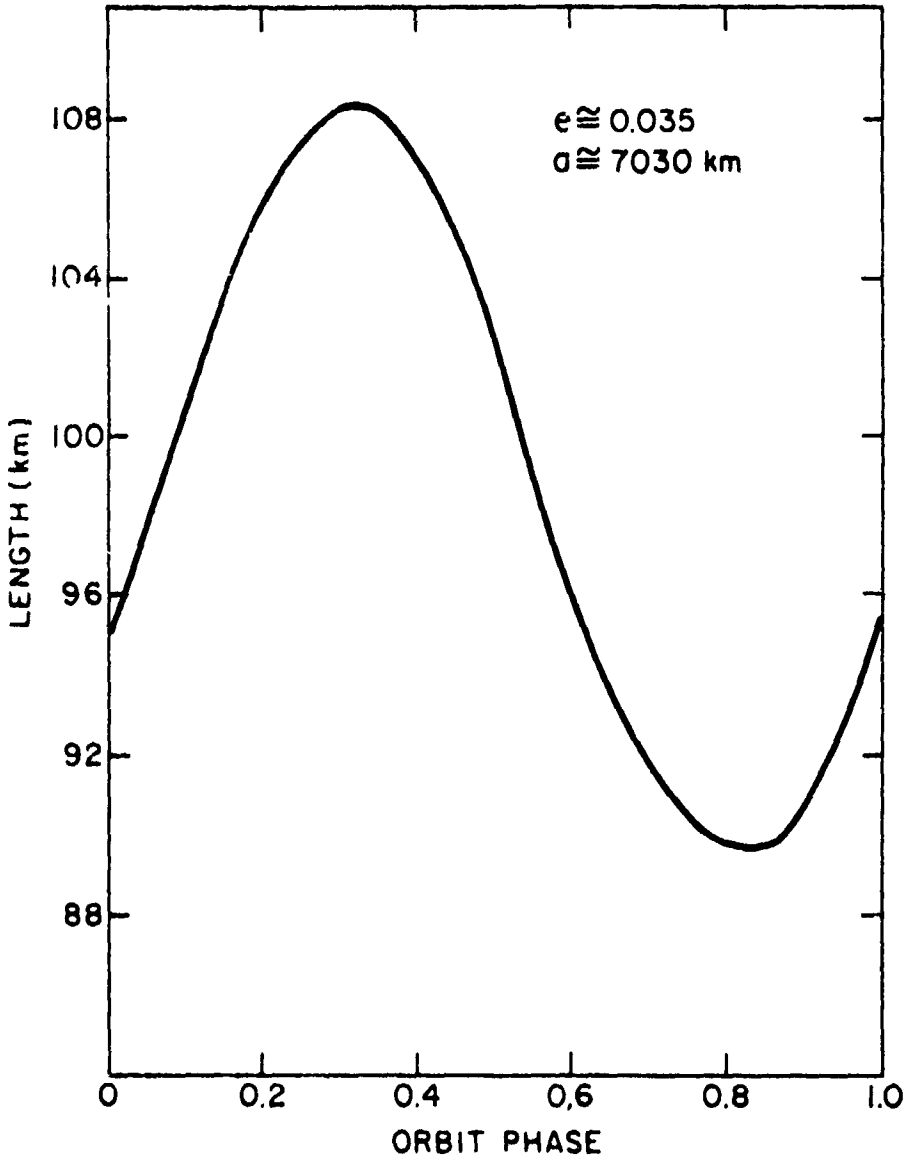

Figure 5-31(a). Tether length vs. orbital phase for one particular orbit of the study shown in Figure 5-30. (b) The derivative of the curve shown in (a), together with the gravity gradient forcing function. These are nearly in phase and their product (the work done by the orbit on the dumbbell) is nearly maximal. (c) A plot similar to (b) for a case with zero time lag in tether response. The work is shown as well, and obviously integrates to zero over an orbit.

ORIGINAL PAGE IS
OF POOR QUALITY

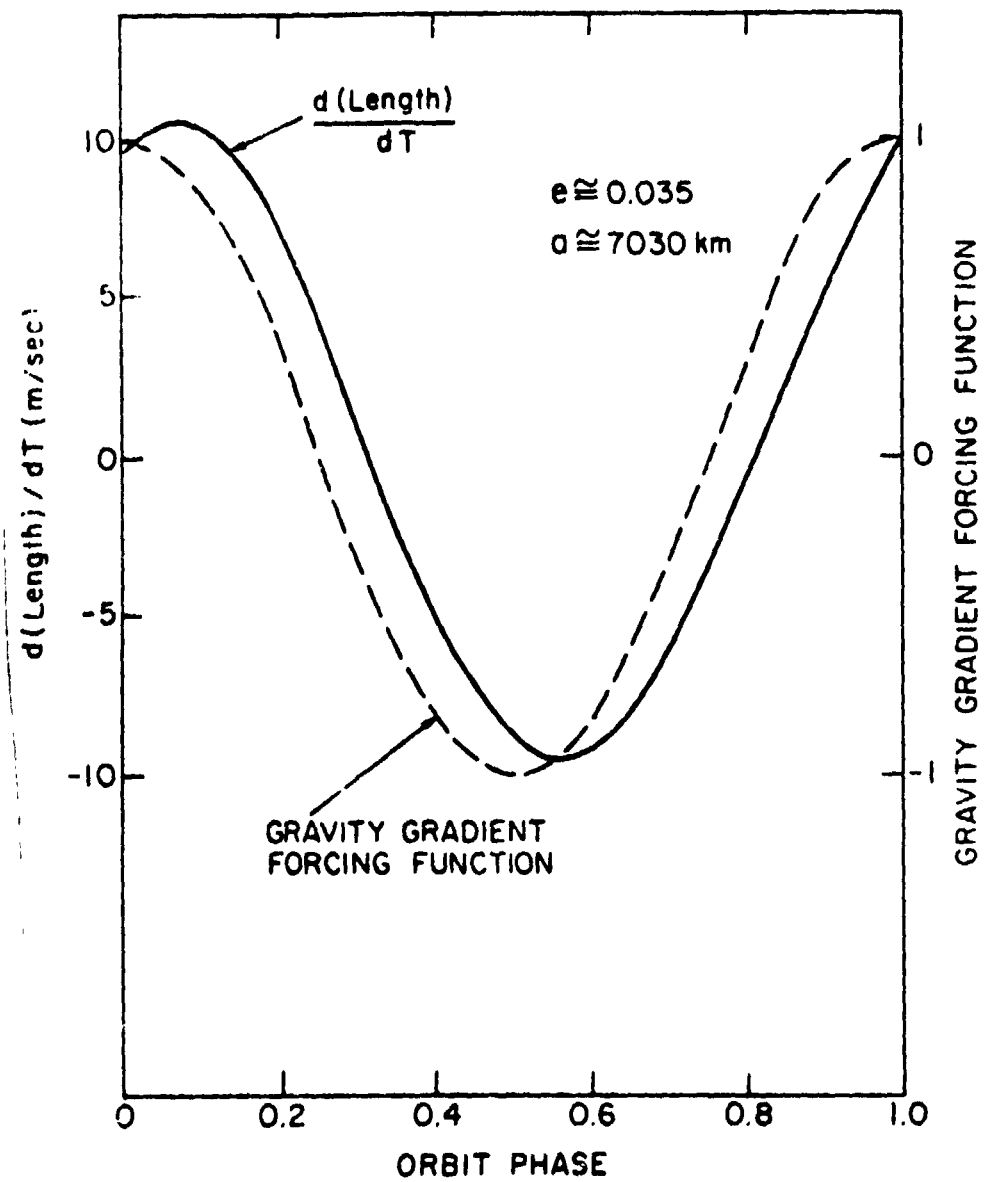

Figure 5-31(b)

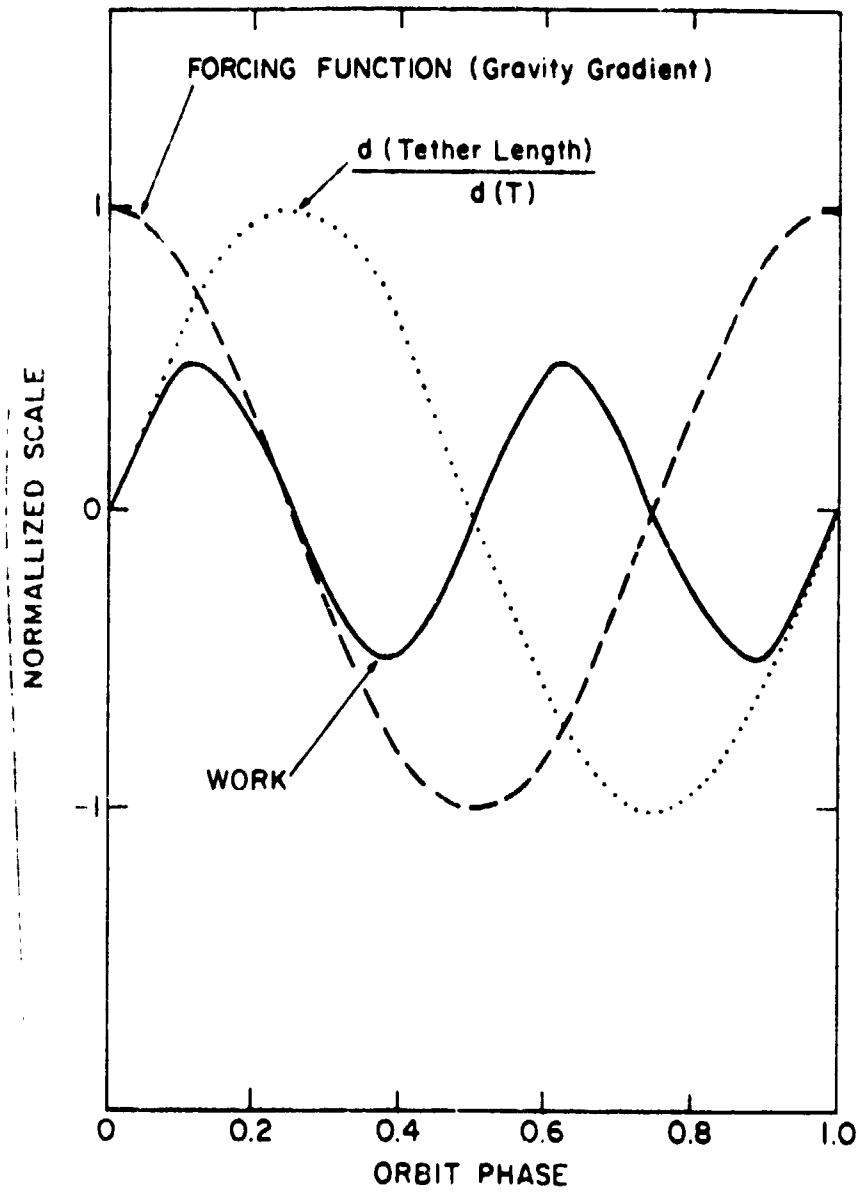

Figure 5-31(c)

km. With a semi-major axis of 7028.75 km (the mean of the maximum and minimum for the orbit), this gives an expected Δe/orbit of 1.66×10^{-4}.

This agreement is quite good, indeed surprisingly good considering that the predicted value is for a maximally efficient system in which all the work is done on or by the system at moments of maximal or minimal tension. However, in some sense the critical damping causes the dumbbell to behave "well": the work done over an orbit is more properly $\int \frac{d(2z)}{dt}$. (Force) dt. Figure 5-31(b) shows the gravity gradient forcing function (arbitrarily normalized and with the d.c. component, which integrates to zero, removed) together with the observed d(2z)/dt. These two are nearly in phase, so their product is (almost) always positive and the integral, hence the work done by the orbit, is (nearly) optimal with respect to the tether's response lag. A zero-lag idealized case is shown in Figure 5-31(c); the integral over an orbit is seen to be zero.

We can compute, to first order, the time required to circularize the orbit as follows. Since Δe/orbit is small, we may write 11) as $de/dN = -9\% \Delta z/a^2$, where N is the orbit number. If we assume that, even allowing for the phase lag, Δz is proportional to the gravity gradient forcing function (g.g.f.), then (to first order) Δz $\propto$ [max-min] g.g.f. $\propto$ [max-min]$(1/r^3)$ $\propto$ [max-min]$1/(1+e\cos\theta)^3$ $\propto$ [max-min]$(1-3e\cos\theta) \propto e$. Hence $\Delta z = \Delta z_o\,(e/e_o)$ where $\Delta z_o, e_o$ and z_o are the values at N = 0, say. Then $de/dN = [-9z_o\Delta z_o/(a^2 e_o)]e = [(de/dN)_o(1/e_o)]e$, and $e(N) = e_o \exp(-N/\tau)$ where $\tau = e_o/(de/dN)_o$ is a "time" scale for decay. In the low eccentricity case, from the observed Δe/orbit, we have $\tau = 3.5 \times 10^{-2}/1.5 \times 10^{-4} = 230$ orbits, or about 15 days. To circularize an orbit from, say, 5% to 1%

eccentricity would thus take about log (0.05/0.01)$\tau \approx 25$ days, a practical and useful length of time for such an operation.

The numerical simulation results therefore confirm the theory, at least in the low eccentricity case, and the usefulness of orbital pumping for orbit circularization is demonstrated in a practical sense.

APPENDIX I - TETHER SOFTWARE DATA

APPENDIX II- REFERENCES

1. Boyce, W.E. and DiPrima, R.C., 1977. Elementary Differential Equations and Boundary Value Problems, John Wiley and Sons, New York, Chapter 7.

2. Jacchia, L.G., 1971. Revised static model of thermosphere and exosphere with empirical temperature profiles. Smithsonian Astrophys. Obs. Spec. Rep. No. 332.

3. Goldreich, P., 1963. On the Eccentricity of Satellite Orbits in the Solar System (G.R. of Royal Astronomy Society, vol. 126, p. 357).

4. Colombo, G., Arnold, D.A., Taylor, R.S., 1982. "Investigation of Electrodynamic Stabilization and Control of Long Orbiting Tethers." Final Report on Contract NAS8-33691.